AD-A121 456 MATERIAL OPTIMIZATION FOR HIGH ELECTRIC CURRENT HIGH 1/3
SPEED APPLICATIONS(U) MASSACHUSETTS INST OF TECH
CAMBRIDGE DEPT OF MECHANICAL ENGIN..
UNCLASSIFIED E RABINOWICZ ET AL. 30 SEP 82 F/G 20/3 NL

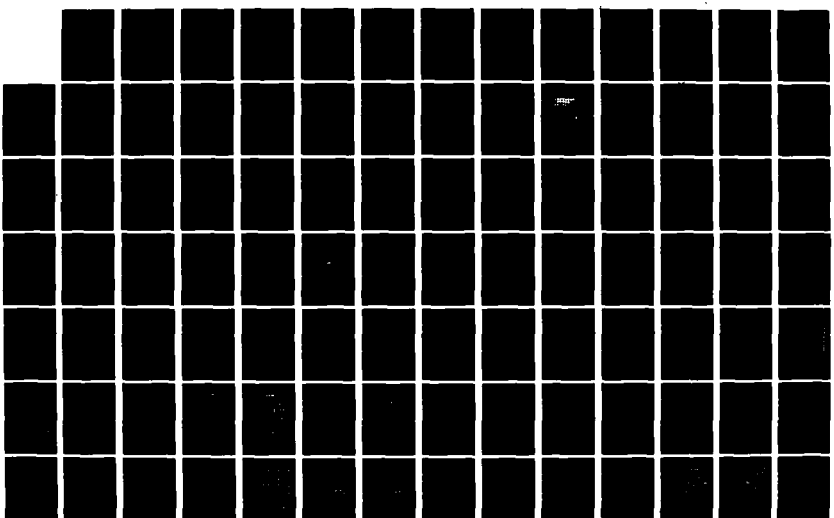

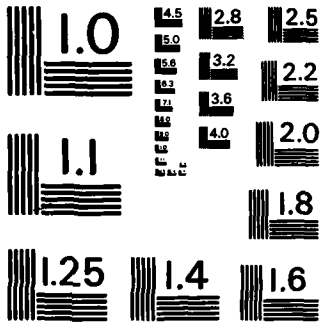

MICROCOPY RESOLUTION TEST CHART
NATIONAL BUREAU OF STANDARDS - 1963 - A

12

MATERIAL OPTIMIZATION FOR HIGH ELECTRIC CURRENT, HIGH SPEED APPLICATIONS

Ernest Rabinowicz, Alan Rozenfeld and
Jeanne M. Tanner

Final Report
January 1, 1980-December 31, 1981
Contract No. N00014-80-C-0316

SECURITY CLASSIFICATION OF THIS PAGE (When Data Entered)

REPORT DOCUMENTATION PAGE		READ INSTRUCTIONS BEFORE COMPLETING FORM
1. REPORT NUMBER	2. GOVT ACCESSION NO. AD-A121456	3. RECIPIENT'S CATALOG NUMBER
4. TITLE (and Subtitle) MATERIAL OPTIMIZATION FOR HIGH ELECTRIC CURRENT, HIGH SPEED APPLICATIONS		5. TYPE OF REPORT & PERIOD COVERED Final Report Jan. 1, 1980 - Dec. 31, 1981
		6. PERFORMING ORG. REPORT NUMBER
7. AUTHOR(s) Ernest Rabinowicz, Alan Rozenfeld and Jeanne M. Tanner		8. CONTRACT OR GRANT NUMBER(s) N00014-80-C-0316
9. PERFORMING ORGANIZATION NAME AND ADDRESS Department of Mechanical Engineering Massachusetts Institute of Technology Cambridge, MA 02139		10. PROGRAM ELEMENT, PROJECT, TASK AREA & WORK UNIT NUMBERS
11. CONTROLLING OFFICE NAME AND ADDRESS Naval Research Laboratory MRL Code 2627 (DODAAD Code N00173) Washington, DC 20375		12. REPORT DATE September 30, 1982
		13. NUMBER OF PAGES
14. MONITORING AGENCY NAME & ADDRESS (if different from Controlling Office)		15. SECURITY CLASS. (of this report) Unclassified
		15a. DECLASSIFICATION/DOWNGRADING SCHEDULE

16. DISTRIBUTION STATEMENT (of this Report)

Approved for public release; distribution unlimited.

17. DISTRIBUTION STATEMENT (of the abstract entered in Block 20, if different from Report)

NA

18. SUPPLEMENTARY NOTES

19. KEY WORDS (Continue on reverse side if necessary and identify by block number)

20. ABSTRACT (Continue on reverse side if necessary and identify by block number)

Studies of electrical contacts carrying high currents have been carried out at speeds in the range 1.5 to 13m/sec, and current densities in the range 1 to 3 amp/mm^2. As regards the wear of graphite brushes, it was shown that the wear rates were low when the ring metals were metallurgically incompatible with graphite. When silver-graphite brushes were used, low wear was associated with ring materials that were incompatible both with silver and with carbon.

An expression was developed for the temperature rise at the interface

DD FORM 1 JAN 73 1473 EDITION OF 1 NOV 65 IS OBSOLETE
S/N 0102-014-6601

SECURITY CLASSIFICATION OF THIS PAGE (When Data Entered)

between sliding electrical contacts. This equation was tested indirectly using wear measurements and directly using a thermocouple technique. The agreement between theory and practice was reasonable, but more work is needed to define one key variable, namely the number of junctions formed at any one time.

Table of Contents

Introduction

This research project was carried out during the period January 1, 1980 to December 31, 1981. The aim has been to answer a number of questions regarding the performance of high current, high speed electrical contacts. Renewed interest in such contacts is related in part to the requirements of novel devices like homopolar machines, in part to the realization that if current densities of sliding contacts can be increased, then overall machine size and weight can be reduced.

Compatibility effects of graphite sliding against noble metals

The first problem investigated dealt with the question of compatibility. Earlier work (1,2) using silver-graphite brushes (Ag 50, graphite 50) indicated that the wear was low when the ring metal was incompatible against carbon, but not when the ring material was incompatible against silver. In tests carried out during the first year of the project, two other brush materials were used, namely pure graphite and silver-graphite (Ag 75, graphite 25).

It was found that when graphite brushes were used, wear was low when the ring metal has low compatibility against carbon, not otherwise. This, by the way, constitutes perhaps the first clear-cut demonstration that compatibility effects exist in sliding systems involving non-metals; previous studies of compatibility have used pairs of metals (3-8).

When the silver-graphite brushes were used, the wear was determined by the compatibility of both silver and carbon against the ring material. This work is described in detail in appendix A.

Temperature rise of current-carrying sliding contacts

The second study was a determination of the maximum speed and current density that could be carried at a brush-cylinder interface before a heavy wear regime was encountered. A theoretical model suggested, surprisingly, that higher sliding speeds could give lower interfacial temperatures and thus lower wear rates, and experimental tests confirmed this prediction. This work has been published, and is shown as appendix B.

Measurement of the interfacial temperature of sliding contacts

The third investigation dealt with more detailed consideration of the temperatures existing at sliding interfaces transmitting high electrical currents. A new experimental method for studying such temperatures was devised. It consisted of rapidly switching off the high current at the brush-ring interface, measuring the intrinsic thermoelectric voltage at the interface as it decayed away, and then extrapolating back to the time of switching to determine the interface temperature which existed while the current was being transmitted. This research is described in detail in appendix C.

Discussion

It will be seen that the research carried out under this contract, combined with the work carried out in prior years, provides a firm basis for incorporating compatibility effects into the selection of slip-ring materials. However, further work in the temperature modelling study will be needed, to refine the model so as to make it possible to incorporate theoretical considerations into the selection of speeds and current densities which will allow sliding contacts to operate with minimal wear.

References

1. P. C. Chan 'Materials for advanced electrical current collecting techniques', MS Thesis in Mechanical Engineering, MIT, May 1979.

2. E. Rabinowicz and P. Chan "Wear of silver-graphite brushes against various ring materials at high current densities", pp. 123-127 of 'Electric Contacts, 1979', Illinois Institute of Technology, Chicago, 1979.

3. H. Ernst and M. E. Merchant 'Surface friction of clean metals - a basic factor in the metal cutting process' Special Summer Conference on Friction and Surface Finish, MIT Press, Cambridge, pp. 76-101, 1940.

4. L. F. Coffin 'A Study of sliding metals, with particular reference to atmosphere', Lubrication Engineering, 12, 50-58, 1956.

5. C. L. Goodzeit 'The seizure of metal pairs during boundary lubrication', pp. 67-81 of 'Friction and Wear', ed. R. Davies, Elsevier, Amsterdam, 1959.

6. E. Rabinowicz 'Compatibility criteria for sliding metals', 'Friction and Wear in Deformation Processing', New York, pp. 90-101, 1966.

7. E. Rabinowicz 'The determination of the compatibility of metals through static friction tests' ASLL Trans., 14, 198-205, 1971.

8. E. Rabinowicz and S. P. Loutrel 'Compatibility effects involving soft metals used as solid lubricants', Proc. Int. Solid Lubrication Symposium, Tokyo, pp. 84-89, 1975.

TRIBOLOGICAL PROPERTIES OF HIGH SPEED SLIP RING SYSTEMS

by

Zinovi Rozenfeld

Submitted to the Department of Mechanical Engineering on May 16, 1980 in partial fulfillment of the requirements for the Degree of Master of Science in Mechanical Engineering.

ABSTRACT

A series of tests have been performed to study wear, friction and electrical contact resistance of pure graphite and silver graphite (75% w/o Ag) electrical brushes, sliding against copper, nickel, cobalt and noble metals (silver, gold, iridium, palladium, platinum, rhenium, rhodium and ruthenium. The tests were performed at sliding speeds of 4 m/sec and 8 m/sec. The test atmospheres were: dry ambient winter air, wet CO_2, or air with 1-Bromo-Pentane vapors. The current for the experiment was 50 A per brush (160 A/cm^2).

The results from the tests showed a high positive correlation between the wear of the slip rings and the compatibility of the slip ring metal against the brush material. In the case of silver graphite brushes, both constituents were involved for in the compatibility relationship. There is a negative correlation between the wear and the friction of the slip rings. Increased current level increases wear, while changing the sliding speed does not significantly change wear. The silver graphite brushes showed less wear and less contact resistance than the pure graphite brushes by a factor of four. The noble metals usually performed better than the oxide forming metals.

Thesis Supervisor: Dr. Ernest Rabinowicz
Title: Professor of Mechanical Engineering

ACKNOWLEDGEMENTS

I would like to sincerely thank my future wife, Eleonora for her indispensable support and patience throughout this research.

I am grateful to my thesis advisor, Professor Ernest Rabinowicz, for his encouragement and invaluable advice during the experiment. Appreciation is also extended to Scott Webber, Sankar Sankaran, Joseph Boustani, Ping Chan and other students and staff of the Laboratory for Manufacturing and Productivity for their good humor and directions. Special thanks to Fred Anderson, Ralph Whittemore, Fred Cote and Bob Kane for helping me to build the experimental set up.

This work has been sponsored by the Office of Naval Research under contract number N00014-80-C-0316.

TABLE OF CONTENTS

LIST OF FIGURES

LIST OF TABLES

I. INTRODUCTION

Recently much interest has been directed toward brush systems which can operate under high current densities and high sliding speeds. Some of the interest is due to the realization that decreasing the brush size and increasing the speeds would lead to smaller, more compact motors and generators. Another use for high current density brushes is in homopolar generators, which are cyclic motor-generators used for repetitive pulsed power applications. Homopolar machines usually run at speeds in excess of 200 m/sec with pulses of 30 ms carrying 12 MA or more. The proper brush operation plays a significant role in the efficiency of these machines[1].

Some of the current collecting techniques proposed for high speed, high current applications include liquid metals[2], multi-segmented fiber brushes, and graphite or metal graphite brushes. Liquid metals that have been proposed for high current operations include mercury and mercury-indium alloys, a gallium-indium eutectic alloy, and a sodium-potassium eutectic alloy. However there are many difficulties involved in using liquid metals, including their toxicity their metal compatibility, and their reactivity with potential machine environments. The basic problem with fiber brushes is their poor wear and friction characteristics in dry air environments. Solid monolithic brushes have been extensively studied and several conclusions have been reached regarding their performance, including their ability to follow the unevenness of the commutator surface, low friction characteristics, and high electrical conductivity. The solid brushes are the subject of investigation of this paper.

1.1 CRITERIA FOR A SUCCESSFUL BRUSH

The main purpose of slip ring systems is to transfer currents from a stationary brush to a rotating slip ring, or vice versa. In order to achieve high levels of performance, certain requirements have to be met. These include:

a. low wear
b. low friction
c. low contact resistance
d. the ability to absorb, without damage, high current pulses or mechanical loads
e. chemical inertness
f. high electrical conductivity
g. the ability to withstand different environments

During specific operations some of these characteristics are more important than others. However low wear is important in almost all applications, especially where minimal or no maintenance is required or when the down time of a machine must be minimized. High friction and high contact resistance produce excessive mechanical and electrical power losses, which are to be avoided during all operations.

1.2 THE SCOPE OF THE RESEARCH

Most of the research done on graphite brushes under high speed and high current conditions was performed on copper or copper-plated surfaces [1,3,4] and in a few instances steel and nickel surfaces were used[5]. During sliding in most atmospheres an oxide film develops on the metal surfaces.

This film is generally insulating or at best semi-conducting. It is also abrasive when disturbed, thus reducing the brush life and increasing the contact resistance. Noble metals form very little or no oxide films, so they serve as potential candidates for high speed, high current slip ring systems. The noble metals are ruthenium, rhodium, palladium, silver, rhenium, osmium, iridium, platinum, and gold. They occupy adjacent positions in two rows of the periodic table of the elements as shown in Figure 1.1. They share a number of physical and mechanical properties. These metals are characterized by chemical inertness, particularly low or no oxidation, high densities, high melting temperatures, high mechanical strengths, high thermal conductivities, and high electrical conductivities. In order to study how the absence of oxides would influence the brush performance, all the noble metals except osmium, which was unavailable in an extended surface form, were chosen for this investigation.

Ohmae and Rabinowicz[6], in a study of the tribological properties of noble metals, concluded that the friction and wear behavior of these metals sliding against each other are governed largely by two metallurgical considerations:

a. Metallurgically compatible combinations (a high degree of solid solubility, one liquid phase when molten give high friction and wear, while metallurgically incompatible combinations (very little solid solubility, two liquid phases) give low friction and wear. Combinations which are intermediate (forming just one liquid phase, but exhibiting low solid solubility) give intermediate friction and wear behavior.

FIGURE 1.1: THE RELATIVE POSITION OF THE NOBLE METALS IN THE PERIODIC TABLE

THE PERIODIC TABLE OF THE ELEMENTS. The number above the symbol of each element is its atomic number, and that below is its atomic mass in u. The elements whose atomic masses are given in parentheses do not occur in nature, but have been prepared artificially in nuclear reactions. The atomic mass in such a case is the mass number of the most long-lived radioactive isotope of the element.

Period	Group I	Group II											Group III	Group IV	Group V	Group VI	Group VII	Group VIII
1	1 H 1.00																	2 He 4.00
2	3 Li 6.94	4 Be 9.01											5 B 10.81	6 C 12.01	7 N 14.01	8 O 16.00	9 F 19.00	10 Ne 20.18
3	11 Na 22.99	12 Mg 24.31											13 Al 26.98	14 Si 28.09	15 P 30.98	16 S 32.07	17 Cl 35.46	18 Ar 39.94
4	19 K 39.10	20 Ca 40.08	21 Sc 44.96	22 Ti 47.90	23 V 50.94	24 Cr 52.00	25 Mn 54.94	26 Fe 55.85	27 Co 58.93	28 Ni 58.71	29 Cu 63.54	30 Zn 65.37	31 Ga 69.72	32 Ge 72.59	33 As 74.92	34 Se 78.96	35 Br 79.91	36 Kr 83.8
5	37 Rb 85.47	38 Sr 87.66	39 Y 88.91	40 Zr 91.22	41 Nb 92.91	42 Mo 95.94	43 Tc (99)	44 Ru 101.1	45 Rh 102.91	46 Pd 106.4	47 Ag 107.87	48 Cd 112.40	49 In 114.82	50 Sn 118.69	51 Sb 121.75	52 Te 127.60	53 I 126.90	54 Xe 131.30
6	55 Cs 132.91	56 Ba 137.34	57-71 *	72 Hf 178.49	73 Ta 180.95	74 W 183.85	75 Re 186.2	76 Os 190.2	77 Ir 192.2	78 Pt 195.09	79 Au 197.0	80 Hg 200.59	81 Tl 204.37	82 Pb 207.19	83 Bi 208.98	84 Po (210)	85 At (210)	86 Rn 222
7	87 Fr (223)	88 Ra 226.05	89-103 **															

*Rare earths	57 La 138.91	58 Ce 140.12	59 Pr 140.91	60 Nd 144.24	61 Pm (145)	62 Sm 150.35	63 Eu 152.0	64 Gd 157.25	65 Tb 158.92	66 Dy 162.50	67 Ho 164.92	68 Er 167.26	69 Tm 168.93	70 Yb 173.04	71 Lu 174.97
**Actinides	89 Ac 227	90 Th 232.04	91 Pa 231	92 U 238.03	93 Np (237)	94 Pu (242)	95 Am (243)	96 Cm (247)	97 Bk (249)	98 Cf (251)	99 Es (254)	100 Fm (253)	101 Md (256)	102 No (254)	103 Lw (257)

b. Combinations in which at least one of the surfaces has a hexagonal structure (i.e. ruthenium, rhenium, osmium and cobalt) give low wear irrespective of the compatibility of the sliding system.

Rabinowicz[7] in a similar study of non-noble metals obtained the same results. However the statistical scatter in friction and wear was higher than with noble metals due to the complications which arise due to oxide layers.

To further investigate the effect of compatibility and crystal structure on friction and wear behavior, the noble metals tests were supplemented with tests on copper, nickel and cobalt. The compatibility chart for those metals and that of carbon is shown in Figure 1.2. The chart is based on the binary phase diagrams[8-11].

In an earlier research by Johnson and Moberly[5] it was concluded that addition of metal powders to the graphite brushes significantly decreases the voltage drop across the contact without a large increase in wear or friction. In order to study the effect of metal content on the brush performance, two different types of brushes have been used in this experiment: (a) pure graphite brushes and (b) silver graphite brushes containing 75% by weight silver and 25% graphite.

In another study by Savage[12] it was shown that in order for graphite to behave as a solid lubricant a critical minimum level of humidity has to be reached. Furthermore many investigators[13,14,15] found that by running the slip rings in a carbon dioxide environment the friction and wear can be kept to a minimum. Savage and Schafer[25] showed that some condensible organic vapors can be used instead of water vapors and at much lower

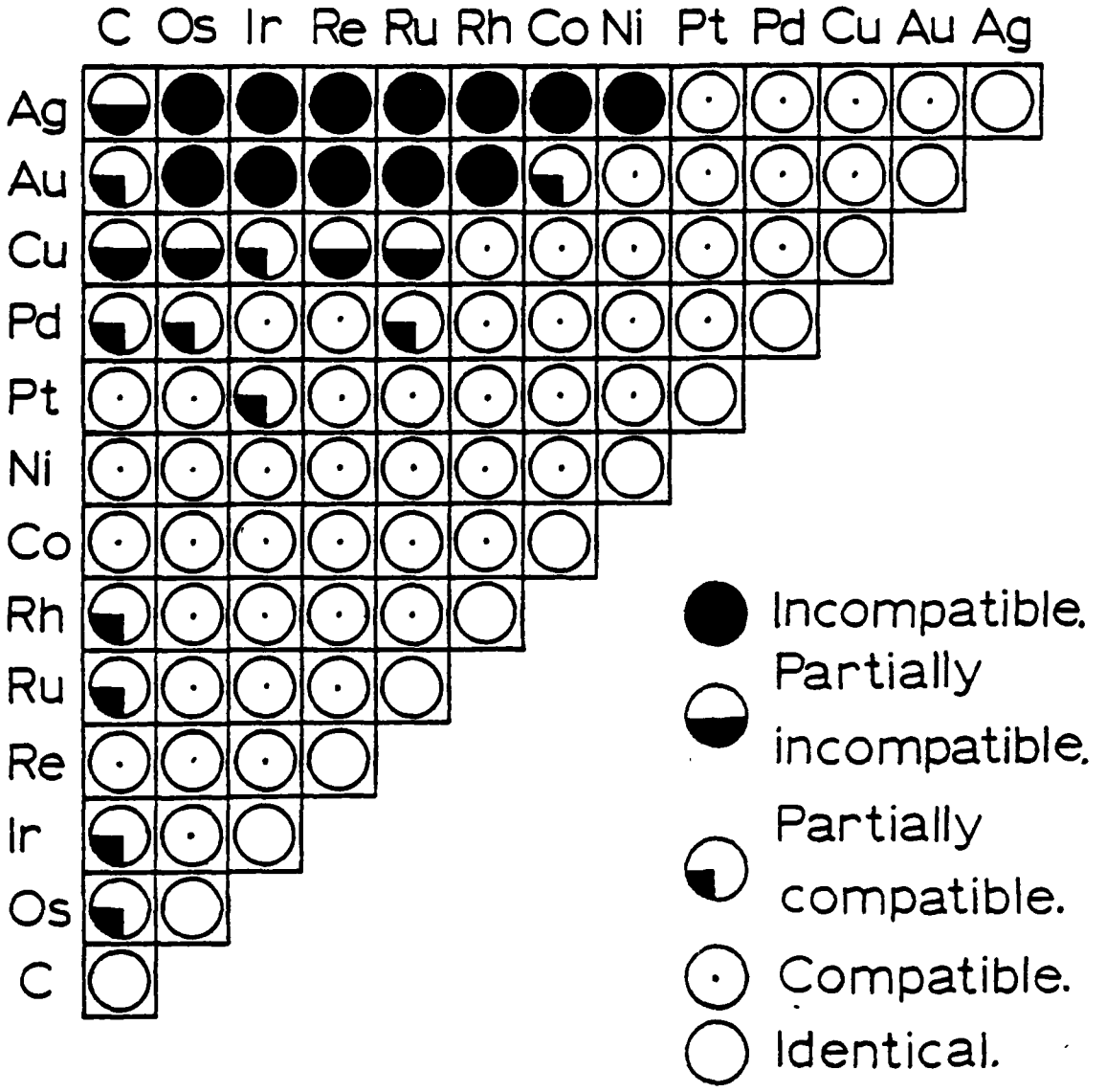

FIGURE 1.2: THE COMPATIBILITY DIAGRAM FOR THE ELEMENTS EVALUATED

humidity levels.

The tests in this investigation were run under three different atmospheric conditions in order to determine the effect of the atmosphere on the tribological properties of slip rings. These atmospheres are: a) ambient, dry winter air, b) humidified carbon dioxide, and c) dry air with 1-bromo-pentane vapors. The effect of speed was studied by running the tests at 4 m/sec and 8m/sec. The effect of current density was studied by performing tests at 160 A/cm^2 current density and at no current. In addition a set of tests was performed using a silver graphite brush and an iridium flat at different current levels.

1.3 REVIEW OF CHAPTERS

This chapter serves as a general introduction to the thesis report. The second chapter will review the theories of friction, wear and contact resistance, and in addition will discuss the different parameters that influence brush performance. The apparatus, the procedure, and the materials used in the tests will be covered in the third chapter. Chapter four will present the results of the tests. The detailed discussion of the results will follow in chapter five. The summary of conclusions will appear in chapter six and finally recommendations for further research are contained in chapter seven.

II. WEAR, FRICTION AND CONTACT RESISTANCE OF SLIP RINGS

The actual processes which occur at the brush and slip ring interface are not clearly understood. Many investigators present different explanations as to the nature of the wear, friction and electrical contact resistance at the sliding interface. However, the magnitude of these parameters can reflect the actual processes and provide some insight as to the nature of the processes. This chapter will provide the basic theories of wear, friction and contact resistance for graphite and metal graphite brushes. After the theories, the different parameters influencing brush performance will be examined. These parameters include the compatibility and the molecular structure of the sliding pair, the speed of sliding, the atmospheric conditions, the current density, the presence of surface films formed at the interface, the composition of the brush, and finally the mechanics of the sliding system.

2.1 THE WEAR MECHANISM

The wear process proceeds by removal of small particles from the sliding surfaces. The particle size is in the order of 10^{-4} cm under conditions of very high wear rates[16], but it is usually smaller under normal wear conditions[17]. Three different wear mechanisms were proposed for the wear process: abrasive wear, surface fatigue wear, and adhesive wear.

The abrasive wear mechanism requires the presence of a hard rough surface or hard abrasive particles at the sliding interface. However in sliding electrical contacts the commutator surface is usually polished, so the abrasion must be due to formation of hard oxide particles or other hard

compounds. Aluminum is a bad slip ring surface, because aluminum oxide particles are very hard and cause abrasion of the brush[18]. Noble metals, on the other hand, do not form oxides or other chemical compounds at any significant amount, thus abrasion is absent.

The surface fatigue wear process is a result of a succession of repeated elastic stresses over the localized regions of true contact[19].

Adhesive wear is due to pulling of fragments off one surface to adhere to another[20], eventually resulting in a loose particle.

It is possible that all three forms of wear are present under some sliding conditions. However, for a noble metal substrate, the adhesive wear mechanism is likely to be the dominant form of wear. The adhesive wear process is discussed in more detail in the following sub-section.

2.1.1 MECHANISM OF ADHESIVE WEAR. Adhesive wear arises from the strong adhesive forces between atoms. In sliding the surfaces have a finite roughness, which means that the actual area of contact will be only a fraction of the apparent area of contact. At the points of actual contact the stresses will be very high, forcing the individual atoms to come close together and building up the interatomic forces. These forces can be due to formation of metallic bonds, Van der Wall forces, or hydrogen bonds. During sliding there is a finite probability that the contact will break at an interface other than the original, thus forming a transferred particle. This process can occur in both the hard and the soft material, due to the presence of small local regions of low strength. The transferred particle can be transferred back to the original material or it may be detached

forming a loose wear particle. The ratio of the rates of wear for two materials is inversely proportional to the ratio of the square of the penetration hardnesses of two materials[7]. This means that a softer brush will wear more rapidly than the harder slip ring.

The amount of adhesive wear can be given by the Archard's wear equation[21]:

$$V = \frac{kLx}{3p}$$

where k is a non-dimensional constant (the wear coefficient), L is the normal load, x is the distance of sliding, and p is the penetration hardness of the material being worn. The formula applies for a single contact or multiple contacts.

K is the probability, that, at a contact, the adhesive forces will be large enough to tear out a wear particle. Provided that k is independent of the load and the hardness, which are present in the equation, it is mainly influenced by R, the ratio of the interfacial surface energy of adhesion to the sum of the surface energies of the two materials in contact[7]:

$$R = \frac{Wab}{\gamma_a + \gamma_b}$$

The dependency is close to $k \alpha R^2$. Values of k vary from about 10^{-2} to 10^{-7} or less[10]. The small values of k mean that the formation of a wear particle is an unlikely phenomenon, and during most of the contact between the asperities of the two sliding materials no damage is produced[22].

The particles produced are of a finite size and not single atoms or molecules[20]. Later in this chapter the parameters influencing the adhesive wear will be discussed.

2.2 THE FRICTION MECHANISM

The friction coefficient is the ratio of the normal force to the tangential force in a sliding contact. The tangential force arises from the shear forces needed to break the junction created between the two sliding materials[23]. Thus the friction process is very similar to the process of adhesive wear. The friction coefficient can be expressed simply by[20]

$$f = \frac{s}{p}$$

where f is the friction coefficient, s is the shear strength of the weaker material and p is the hardness of the softer material. However, the equation must be modified by ratio of the work of adhesion to the hardness $\frac{Wab}{p}$, in order to give more accurate results. High $\frac{Wab}{p}$ ratios result in high friction coefficients. Friction is independent of the apparent area of contact, but is directly proportional to the real area of contact.

The friction process involving graphite is further complicated by the solid lubrication phenomena. Graphite has a layered structure, which results in solid lubrication. The friction of graphite is discussed in the following sub-section.

2.2.1 FRICTION OF GRAPHITE.

A large portion of graphite brushes consist of carbon black particles, about 200 Å in diameter which have an "onion-like" structure with graphic layers oriented parallel to the surface[24]. The

distance between atoms inside the layers is much smaller than the distances between two layers, resulting in high interatomic forces within the layers, but weak forces between them. During sliding platelets of graphite detach from the graphite brush and are deposited parallel to the slip ring surface. This creates low friction coefficients.

However the process is largely dependent on the presence of moisture or organic vapors in the atmosphere[12,25,26] as will be discussed later in this chapter.

2.3 CONTACT RESISTANCE

The contact resistance between two surfaces can be given by the following equation[27]:

$$R_T = R_C + R_B + R_F$$

where R_T is the total contact resistance, R_C is the constriction resistance at the brush rotor interface, and R_B is the bulk resistance of the brush, and R_F is the film resistance. There are two basic theories of resistance at a contact: resistance due to fritting[18], and the "thermal mound"[27] phenomenon.

The fritting process can be described as follows. Initially an insulating film of oxides or sulfides separates the two surfaces. When a voltage is applied a voltage gradient exists across the film. In a few places, where the film is thinner or the film is more conductive, a little current is conducted by tunneling[16]. The current is sufficient to heat a very small region of the film and the adjacent metal. The film break down is believed to be by the injection of electrons into the film by the

Zener effect[18]. The cohesion of the film is diminished as the result of heating and some molten metal is attracted into the channel forming a small conducting column. These metal to metal contacts are called a-spots, and the fritting process is called A-fritting. The column may increase in size into a larger conducting spot. The increase of the area of the contact is called B-fritting.

There are probably five to twenty[16] separate, simultaneously conducting a-spots at any one time. The resistance due to the current flow being channeled through these conducting spots is called the constriction resistance, and it can be expressed by[18]:

$$R_C = \frac{0.4(\rho_B+\rho_S)}{(n\ A_T)^{1/2}}$$

where ρ_B and ρ_S are the resistivities of the brush and the slip ring respectively, n is the number of contact spots and A_T is the area of mechanical contact. The area of contact can be given by[18]:

$$A_T = \frac{L}{\xi p}$$

where L is the applied normal force, p is the brush indentation hardness and ξ a constant approximately equal to 1/3 for a graphite brush.

The film resistance R_f can be given by[18]:

$$R_F = \frac{\rho_F}{A_T}$$

where ρ_F is the film resistivity.

The expression for R_C was obtained by assuming circular contacts and a large separation and can be modified for other geometries[23,28].

At high current levels (> 1000 A per brush) the thermal mound phenomenon occurs[3]. The thermal mound phenomenon can be explained as follows[27]. At sufficiently large current levels the rate of heat input into the brush is great enough to cause the brush material to expand at a rate greater than the material is worn away, causing a "thermal mound". If the brush is free to move in a direction normal to sliding, but is restricted from tilting or the ability to realign itself on the slip ring surface, the formation of the mound will lift the remainder of the brush off the surface, thus making of the mound the sole conducting spot. The mound will continue to carry current until it is worn flat and a new thermal mound will form on a different part of the brush. Meanwhile the "old" mound will cease to carry current and the brush material behind will cool and shrink leaving a shallow hollow in its place. The process is repeated and multiple dark spots will be seen on the face of the brush. This process is macroscopic in scale, and at a microscopic scale the conduction still proceeds by fritting.

2.4 PARAMETERS INFLUENCING BRUSH PERFORMANCE

Wear, friction and contact resistance are influenced to a large degree by the conditions of sliding. Some of the parameters which influence the brush performance are discussed in this section.

2.4.1 EFFECT OF COMPATIBILITY. Rabinowicz[7] suggests that the wear coefficient k, and the friction coefficient f are both proportional to the square of the interfacial surface energy of adhesion W_{ab}, which can be given by[6]:

$$W_{ab} = c\,(\gamma_a + \gamma_b)$$

where γ_a and γ_b are the surface energies of the two materials a and b, and c is a constant. The constant c depends on the compatibility of the two materials. A compatible pair is evidenced by high mutual solubility or the formation of intermetallic compounds. For a highly compatible pair of material c has a high value of 0.5 and c is about 1 for an identical pair. An incompatible pair is one in which the materials are insoluble, and form two liquid phases when molten. For an incompatible pair c is usually 0.125.

A high value of W_{ab}, which represents a compatible pair of materials, gives rise to higher wear and friction. A low value of W_{ab}, which represents an incompatible pair of materials, will produce low wear and friction.

Based on the binary phase diagrams, a compatibility rating diagram can be obtained. Such a diagram is shown in Figure 1.2. This diagram contains the materials studied in this experiment. An open circle in the diagram represents an identical combination. An open circle with a dot in the center represents a metallurgically compatible combination. A black circle represents an incompatible pair, while the partially colored circles represent different degrees of partial compatibility, the lighter the circle, the more compatible is the combination. The compatibility ratings, particularly those involving carbon, iridium and rhenium are based on very limited metallurgical data, and could be changed later, should better information be available.

In experiments performed by Ohmae and Rabinowicz[6], the effect of compatibility of metals on their wear and friction have been studied. The

materials used in the experiments were all noble metals. The authors concluded, that both the wear and the friction are significantly lower for an incompatible combination of metals. For example the wear coefficients for a silver pin sliding on a silver disk were 7.0×10^{-4} for both the pin and the disk, and the friction coefficient was 0.72. On the other hand for a silver pin riding on a rhenium disk, which is an incompatible combination, the wear coefficients were 0.38×10^{-4} and 0.31×10^{-4} for the pin and the disk respectively, and the friction coefficient was 0.36. In another investigation by Rabinowicz[7], the same general trend is observed for other metals, with the wear coefficient proportional to the fifth power of the friction coefficient.

Rabinowicz and Chan[29] performed pin on disk experiments using silver graphite brushes (50% w/o) at 25 A current per brush. They concluded, that for these brushes the compatibility of the slip ring metals against graphite is more important than the compatibility against silver. The wear coefficients of brushes sliding on a metal compatible to graphite had a mean value of 7.2×10^{-7}, and the wear coefficient for a partially compatible metal-graphite combination had a mean value of 1.5×10^{-7}. The friction coefficient was negatively correlated with wear.

2.4.2 EFFECT OF MOLECULAR STRUCTURE. As was pointed out before, graphite has a laminar crystal structure with weak bonds between it's basal planes. In sliding applications platelets of graphite are detached from the brush, thus making graphite self-lubricating. It will be shown later, that presence of moisture plays a big role in graphite lubrication.

Rabinowicz[7,20] showed that in a combination of two metals in which at

least one metal, possesses a hexagonal crystalline structure, the wear and friction are low. In the experiment on noble metals[6] the advantage of using a metal of hexagonal crystalline structure showed for both compatible and incompatible pairs. However the effects due to crystalline structure and compatibility were not additive. In Rabinowicz and Chan[29] experiments the effect of using a hexagonal structured metal did not show, due to the complication resulting from a graphite film on the slip ring metal.

2.4.3 EFFECT OF BRUSH MATERIAL. Johnson and Moberly[5] studied the effect on brush performance of introducing metal powder into the graphite brush. They used silver graphite and copper graphite brushes sliding on a copper slip ring. The experiments showed that the addition of metal powder into the graphite brush significantly decreases the electrical contact resistance, with an optimum amount being 75% (w/o) of metal in a brush. The friction was constant from 0% to 75% (w/o) of metal, and both friction losses and electrical losses drastically increased at above about 80% (w/o) of metal in a brush.

The wear rate of the metal-graphite brushes steadily increased as the proportion of metal increased. The slope of the wear vs. metal content graph increased drastically when more than 75% (w/o) of metal powder was present. Based on their results, the investigators concluded that a brush with 75% by weight of silver would provide optimum performance. Rabinowicz and Chan[29] found very little difference in wear between graphite brushes and 50% (w/o) silver-graphite brushes, with a current of 25A per brush.

The brush conductivity ρ_b for a silver graphite brush can be expressed

by[30]:

$$\rho_b = 224\ \phi_v^{3.56}$$

where ϕ_v, the volume fraction of silver can be calculated from:

$$\phi_v = \frac{\delta_{app}}{\delta_{Ag}} \cdot \phi_m$$

where ϕ_m is the mass fraction of silver, δ_{app} is the apparent brush density, and δ_{Ag} is silver density. For the silver graphite brush used in this thesis (75% w/o) the brush conductivity is:

$$\rho_b = 224\ \left(\frac{4.9\ g/cm^3}{10.5\ g/cm^3} \cdot 0.75\right)^{3.56} = 5.33\ Mmho/m$$

Silver does not form an appreciable oxide layer, however it forms silver-sulfide films. Silver-sulfide films are much softer than copper oxide films and are usually very thin. Their resistivity is roughly the same as for copper oxide films. Because silver-sulfide films are soft, they are not abrasive, and can even provide some lubrication, reducing friction and wear at the expense of increasing contact resistance.

2.4.4 EFFECT OF SLIDING SPEED. Many experiments performed at very high speeds using metal graphite brushes[4,31,32] (100m/sec to 300m/sec) produced wear rates the same order of magnitude as low speed commutation (< 5m/sec). Archard[21] concluded in his paper that the wear coefficient k is independent of speed. However the experiments reported by Cassteven's et al[1] suggest that wear increases with an increase in velocity for most graphite and

metal graphite brushes. The friction coefficient remained constant or showed very little increase or decrease in the same experiments. Brennan et al[32] also reported increase in wear and a small increase in friction with an increase in speed.

In most experiments[1,4,32] where speed was varied the contact resistance remained constant. Marshall and Slepian[31] found however that the contact resistance increases with increasing speed.

Increasing the speed of a sliding contact has the effect of disturbing the lubricating graphite layer and the oxide layer on the slip ring surface in addition to raising the temperature of the contact. Dillich and Kuhlmann-Wissdorf[33] explain that at high speeds the lubricating graphite films tends to be disturbed and finally ruptures increasing wear and friction of the contact for a silver graphite brush on a copper surface. On the other hand, Lancaster[19] reports that at high speeds and heavy loads a continuous layer of transferred graphite is formed and the rate of wear per unit load is relatively high. At low speeds and light loads, a surface film of cuprous oxide develops which prevents transfer of graphite and reduces the rate of wear.

Probably the more important influence of higher speeds is the increase of temperature. Most of the experiments performed on homopolar generators are pulsed, with pulses of about 30ms. The pulses are short enough to prevent significant temperature rise, however continuous operation experiments show a significant temperature rise due to increased speed. The increase in temperature has the effect of decreasing the local shear strength of the brush material. This would correspond to a decrease in

friction coefficient but an increase in total wear. The high temperature will also lower the humidity level around the contact, thus further increasing the wear.

2.4.5 EFFECT OF CURRENT

In an experiment performed by McNab[4] on metal graphite brushes the wear rate at a current of 600 A per brush was found to be of the same order of magnitude as at zero current. The passage of a high current through a sliding contact has the effect of raising the temperature of the contact and disturbing the surface films on the slip ring.

At low current levels the commutation proceeds by fritting. The conducting tunnels are formed through the oxide layer or other films on the slip ring surface. Betz[34] reports that as the current is increased the temperature becomes higher, the oxide layer becomes more conductive and the electrical field strength is reduced. This reduces the formation of channels and the oxide layer can itself carry a greater part or even the whole of the current. However at high temperatures the conditions for a wear reducing film are unfavorable and the wear increases. Brennan et al[3] explains the higher wear rate as due to increased area of the conducting spots, B-fritting effect[18], thus the real area of contact is increased which corresponds to the increase in wear. Lancaster[19] supports the idea of film breakage, which leads to more graphite transfer, increasing wear but decreasing friction.

At high current levels two different mechanisms may be present. One is removal of the surface films, which would generate abrasive particles

and also increase contact between the slip ring metal and the brush. The second mechanism is the formation of the "thermal mound". Brennan et al[3] points out that as the current level is increased for a given brush size, the power input to the mound is increased. The localized temperature increases and thus decreases the localized shear strength of the brush material. The decrease in strength would make it easier to remove graphite particles corresponding to a decrease in friction but an increase in the total wear rate.

Most investigators[1,5,26] found an increase in wear and a decrease in friction for an increasing current density. However there is some disagreement as to the influence the current has on the contact resistance. Betz[34] reports that the contact resistance drops with an increased current and in effect the voltage drop across the sliding contact is constant. Most other investigators[1,4,31,35,36] found that at higher currents the voltage drop increases linearly with current thus keeping the contact resistance constant.

2.4.6 EFFECT OF ATMOSPHERE

Probably one of the greatest effects on the brush performance is due to the atmospheric conditions present during sliding. The atmospheric conditions at the time of sliding influence both the ability of graphite to perform as a solid lubricant, and the nature of surface films formed at the brush-slipping interface. Savage[12] showed that in vacuum graphite brushes seize upon the moving slip ring surface and wear away as fine dust at a rate of about 0.1 mm^3/second. The friction coefficient under these sliding conditions is about 1.0. However a small addition of moisture to the

atmosphere reduces friction and wear[38,20]. Savage[35] postulates that the lubricating characteristics of graphite are not intrinsic in the graphite crystal alone but depend on the absorption films. Vapor molecules tend to cover the exposed graphite surface by forming transient monolayers, and thus lowering the free surface energy. Moberly and Johnson[39] point out, that a critical humidity level has to be maintained in order to have the low friction films and long brush life. The critical humidity level may vary with current density, brush and ring temperature, sliding speed and particularly with the type and amount of the atmosphere and the condensible vapors in the atmosphere. For operation in air for most brush-ring applications the ideal humidity level seems to be in the order of 2 grams of water per cubic foot of air.

Brush dusting occurs in most atmospheres (helium, hydrogen, argon, nitrogen, carbon monoxide) if the humidity level is sufficiently low[38]. However, Johnson and Moberly[15] found that wear is SF_6 and CO_2 is lower than air and is unaffected by moisture level. Pardee[13] found that the wear of silver graphite brushes sliding on copper slip rings in CO_2 gas does not depend on moisture at least down to -62°C dew point, for nondusting operation. However dusting does occur at elevated temperatures of over 200°C. This is due to desorption of moisture from the contact counterface graphite sites[5].

Low wear and friction can also be achieved by additions of a few parts per million of the larger organic molecules, as was shown by Savage and Schaefer[25]. For example the minimum lubricating relative humidity level for water vapor at 30°C is 0.10. The minimum lubricating relative humidity

for 1-Bromo-Pentane is 2.1×10^{-5} (from Savage and Schaefer[25]).

The contact resistance is usually higher as the moisture level is increased or in carbon dioxide[14]. The increase in contact resistance is probably due to the additional film resistance. Marshall and Slepian[31] point out that it is unlikely that the atmosphere plays part in fixing either the number or the average size of the contact spots.

In the absence of oxygen or water, the oxidation process is suppressed. Active chemical gases such as SO_2, CL_2, and H_2S cause the oxidation rates to increase appreciably, points out Shoebert[16]. Oil vapors may cause a lower oxidation rate of copper, and organic vapors may act either as filming agents or as corrosive materials, depending upon the composition. Shoebert suggests that with most of these special gases and chemicals, a little is good, but a lot is harmful.

The effect of surface films on brush performance is discussed in more detail in the next section.

2.4.7 EFFECT OF SURFACE FILMS FORMED AT THE INTERFACE. The films present at the brush-slip ring interface contribute a significant part to the total wear, friction and contact resistance. According to Dillich[33], the interface film can be divided into two basic components:

1. The film due to the graphite platelets transferred from the brush. The graphite layer, with absorbed layers of water and gas vapor in it, may reduce brush to metal contact at the interface causing the brushes to slide along a film layer with relatively high film resistance.

2. The films formed under atmospheric conditions, oxides, sulfides, H_2O

vapors absorbed on the bare metal surfaces, and which presumably persist regardless of the presence or absence of the lubricating film.

The first film is usually relatively thick, and the second film is very thin, or as with most noble metals, non-existent. Schreurs et al[17] found that with silver graphite brushes sliding on copper the deposits from the brush are about 300 mm thick, while the films due to CU_2O-H_2O complexes are from 0.5 mm to 1.5 mm thick. Silver forms silver-sulfide films. Silver sulfide films are much softer than copper oxide films and are usually much thinner[31].

Lancaster[19] found that when the cuprous oxide is present the wear is mild, but when a transferred layer of graphite is present the wear is severe. The cuprous oxide film prevents transfer of graphite and reduces the rate of wear.

Generally the presence of films increase the electrical resistance of the contact, which in turn can raise the temperature of the interface. On the other hand the films may lubricate the sliding process, thus reducing wear and friction.

2.4.8 EFFECT OF THE MECHANICS OF SLIDING CONTACTS. Graphite has a very fast rate of response to sudden elastic deformations due to a high modulus of elasticity and low density[16]. A brush containing graphite is less susceptible to small topological variations of the sliding surfaces. These variations are induced by the slip ring eccentricities or vibrations in the machine. However excessive waviness of the sliding surface can produce instability which gives rise to bounce and sparking. Taylor and Reichner[40] point out that the irregularities in the moving surface produce forces such

as brush inertia and holder friction which alter the contact force. Furthermore the brush power loss is higher for a fluctuating contact force than that which would occur for a steady force equal to the average value.

III. EXPERIMENTAL APPARATUS AND PROCEDURE

This chapter will describe the apparatus used for running the experiments and the experimental procedure and materials used.

3.1 APPARATUS

The apparatus used for these experiments are two pin-on-disk testers, similar to those used in many previous studies at M.I.T. However, the sliding speeds of 4 m/s and 8 m/s are much higher than those used to perform other tests. In order to provide increased mechanical stability, the brushes are loaded by leaf springs rather than dead weights. The spring force is adjusted by a micrometer, and balanced against counterweights over a pulley system. A schematic illustration of one of the testers is shown in Figure 3.1.

The basic difference between the two testers is that the lower speed tester has a friction measuring transducer, but the higher speed tester does not. The friction transducer consists of a strain gage ring[41] designed for the forces achieved during these tests. The output of the strain gages is fed into a Sanborn preamplifier and is recorded by a strip chart recorder.

In order to provide for tests at high current levels, a flexible battery cable is connected to the free arm of the tester and to the positive terminal of a D.C. power supply, making the test brush anodic. Three large copper brushes, sliding on the copper shaft of the rotating disk, are used to collect the current from the disk to the negative terminal of the power supply, as shown in Figure 3.2. The D.C. voltage has a ripple of

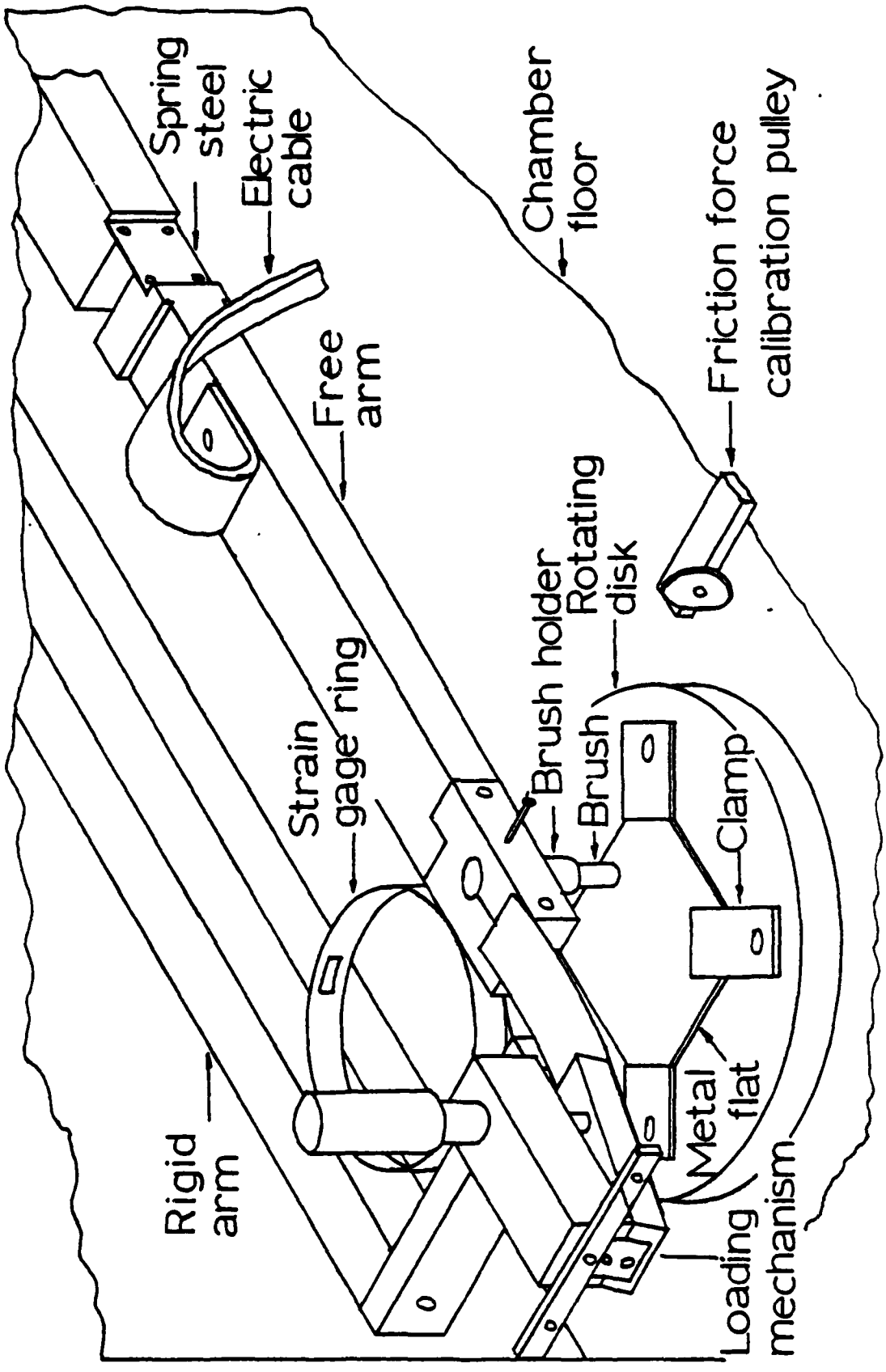

FIGURE 3.1: A SCHEMATIC ILLUSTRATION OF THE BRUSH-ON-FLAT WEAR TESTER

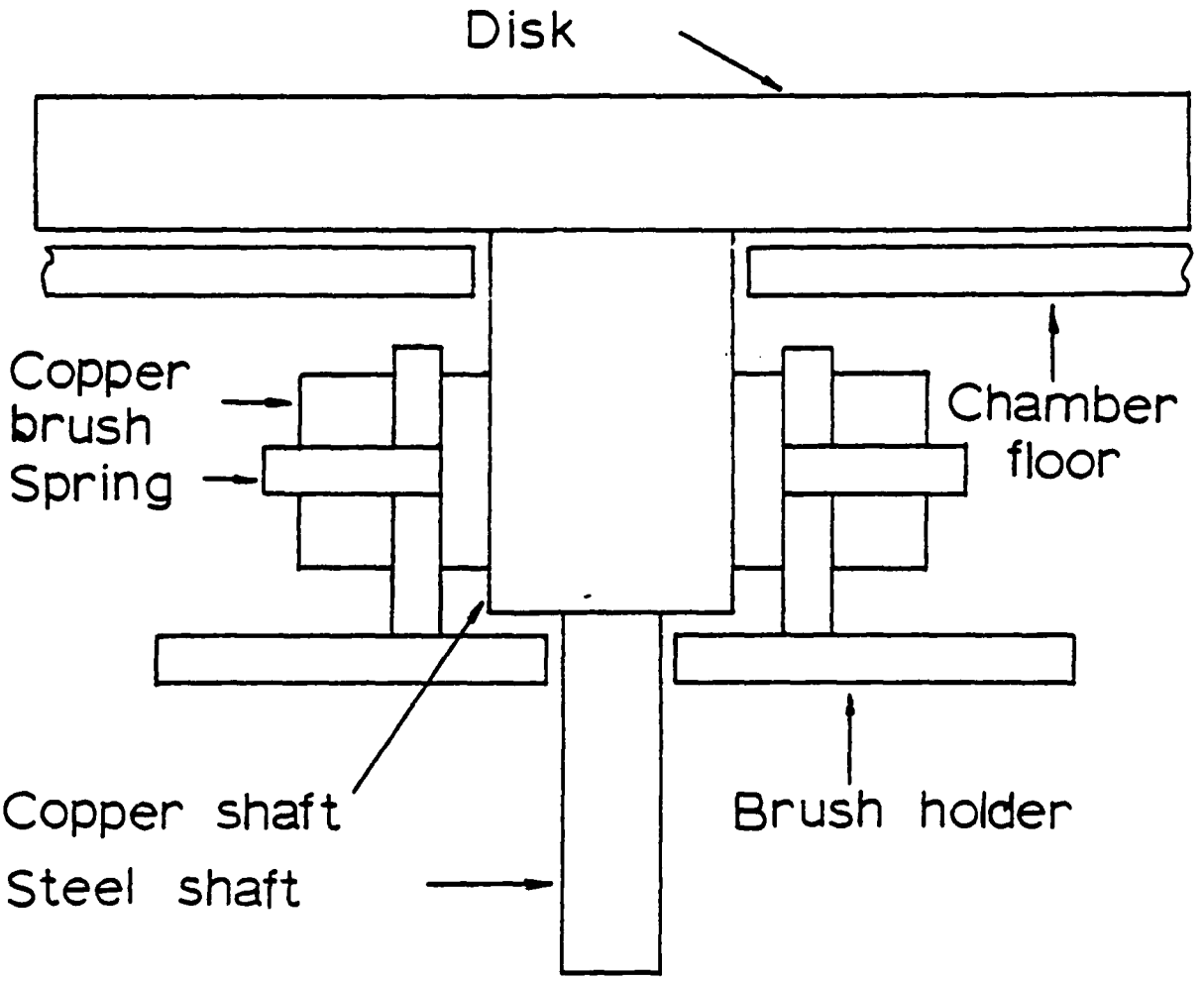

FIGURE 3.2: A SCHEMATIC ILLUSTRATION OF THE DISK AND THE POWER BRUSHES

less than 5%. The fourth copper brush, insulated from the other three, is used to measure the voltage drop across the sliding interface. The other contact for the voltage drop measurement originates in the brush holder as shown in Figure 3.3. The brush holder is designed to be light and easily removable for weight measurements.

The whole set up is then enclosed in a plexiglass environmental chamber to provide for different atmospheric conditions without sacrificing the visibility of the apparatus. The humidified carbon dioxide environment is provided by passing CO_2 gas from a cylinder through a bubbler system into the test chamber. The bubbler consists of three closed beakers containing water. The first beaker is heated almost to the boiling point of water, and the other two are at room temperature.

After passing through the bubbler the CO_2 gas is saturated with water. The gas is at room temperature, so that the concentration of water is 20 g per cubic meter of CO_2. The rate of the gas flow is approximately 10 cm^3/ sec.

The organic vapor atmosphere is obtained by passing compressed air through a beaker with 1-Bromo-Pentane Liquid. The air flow is 10 cm^3/sec. The concentration of the organic vapor is approximately 1 g/m^3 of air.

The tests performed in an ambient environment were conducted in winter dry air. From the average humidity measurements in Boston winter air and the average temperatures, the relative humidity was estimated to be 15% or 3 g of water per cubic meter of air.

3.2 PROCEDURE

The tests performed during this research are summarized in Figure 3.4.

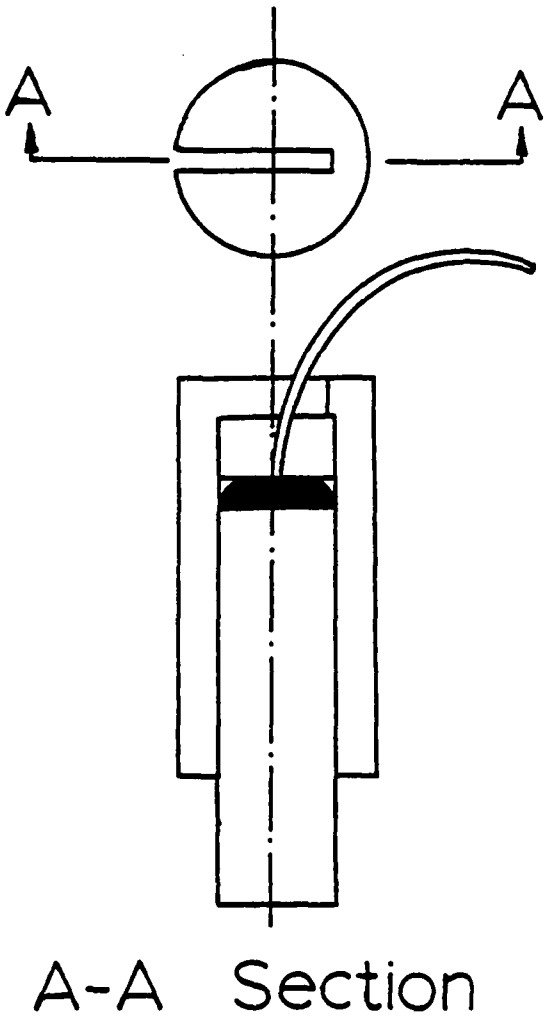

FIGURE 3.3: A SCHEMATIC ILLUSTRATION OF THE BRUSH HOLDER

FLAT METALS	BRUSH	SLIDING SPEED	ATMOSPHERE	CURRENT
			wet CO_2	50 A
		4 m/sec		
	Graphite		air	50 A
		8 m/sec	air	50 A
			air	50 A
Co, Ni, Cu and noble metals (except Os)			1-Br-Pentane	50 A
		4 m/sec		
				0 A
	Silver Graphite		wet CO_2	
				50 A
		8 m/sec	air	50 A
		4 m/sec	wet CO_2	0, 25, 50 75 A
Ir	Silver Graphite			
		8 m/sec	air	0, 25, 50, 75 A

FIGURE 3.4: A SUMMARY OF THE TEST CONDITIONS

The voltage drop across the contact was displayed on an oscilloscope screen. The voltage drop was either measured directly from the screen, or a photograph of the display was taken. Five measurements were usually obtained during each run. The average voltage drop for each run was divided by the current to obtain the contact resistance.

The friction force measurements were recorded five times, during a typical test. After each measurement the normal load on the brush was removed to zero the reading, thus eliminating the problems due to a drifting zero point and temperature effects. At the end of each run the strain gage ring was calibrated by a 200 g load.

The material removal was determined by weighting the brush and the slip ring material before and after each test. A balance with a resolution of 0.01 mg was used. From the weight loss, the wear coefficient was computed, for each surface, by the use of the Archard's wear equation:

$$V = \frac{kLx}{3p}$$

where

V is the volume of wear from the surface

k is the Archard wear coefficient for this surface

p is the penetration hardness of this surface

L is the normal load

x is the total distance of sliding

In most of the sliding tests, the brush lost a fair amount of weight (e.g. 10 mg) and the slip ring gained a moderate amount of weight (e.g. 2 mg). In these cases material from the brush could be seen adhering to the

slip ring surface after the tests. In analyzing such data, it was assumed the weight worn from the brush was the difference between its weight loss and the weight gain of the metal surface (8 mg for the numbers given above), while the weight loss, and thus the wear coefficient, for the slip ring was set at zero.

The tests were performed at sliding speeds of 4 m/sec and 8 m/sec. For the lower speed tests the normal load was set at 300 g, and for the higher speed tests the normal load was set at 500 g, giving values for the nominal pressure on the 6.3 mm diameter pin of 9.6 N/cm^2 (13.4 psi), and 16 N/cm^2 (22.4 psi) respectively. The total current through the interface was 50 A, giving a value for the current density of 160 A/cm^2 (1020 A/in^2). The speeds and the current densities are perhaps two orders of magnitude greater than used in early tests, although they are rather low (perhaps by a factor of 3) for the projected high current density high speed applications.

The duration of a typical test was 24 hours. In the case of some of the low wear combinations of materials the duration of these tests was extended to three days or more. In the case of high wear combinations of materials the duration of the tests was shortened to a few hours.

Before each test the slip ring was polished on a flat glass surface using a double zero emery paper to assure a flat and clean sliding surface. The brush holder was adjusted in the free arm of the tester to lay flat against the metal disk.

The friction and the contact voltage measurements were obtained during the second half of each run to allow sufficient time for the brush run in

and to allow for the steady-state conditions to persist.

3.3 MATERIALS

The graphite and the silver graphite brushes were supplied by Westinghouse Corporation. The silver graphite brushes (75 w/o Ag, 50 w/o C) were produced by sintering. The Vickers penetration hardness of the graphite material was measured to be 15 kg/mm^2 (150 N/mm^2) and its density was measured to be 1.57 gm/cm^3, (98 lb/ft^3). The hardness and the density of the silver graphite material were measured to be 15 kg/mm^2, (150 N/mm^2), and 4.9 g/cm^3 (305 lb/in^2) respectively. Both types of brushes were turned to a 6.3 mm (1/4 in.) diameter.

Some of the relevant physical properties of the slip ring metals are presented in Table 3.1. The metal surface conditions are presented in Table 3.2. All, except for the electroplated layers, are believed to have an impurity content of less than 0.2%. Osmium was unavailable in an extended surface form for these tests.

All of the metals tested were in the form of a 5 cm by 5 cm (2 in. by 2 in.) disk which was clamped to the rotating disk by means of four copper clamps.

TABLE 3.1: THE PHYSICAL PROPERTIES OF THE METALS STUDIED

ELEMENT	MELTING[42] POINT (°C)	SOLID[42] DENSITY (g/cm^3)	THERMAL[43] CONDUCTIVITY ($Cal/cm^2/cm/°C/s$)	AT ROOM TEMPERATURE ELECTRICAL[43] RESISTIVITY ($\mu\Omega.cm$)	CRYSTAL[42] STRUCTURE OF SOLID
Ag	960	10.5	1.0	1.6	FCC
Au	1063	19.3	0.71	2.3	FCC
Co	1495	8.9	0.17	6.24	HCP
Cu	1083	8.96	0.94	1.67	FCC
Ir	2454	22.5	0.14	5.3	FCC
Ni	1455	8.9	0.22	6.84	FCC
Pd	1554	12.0	0.17	10.8	FCC
Pt	1773	21.5	0.17	10.6	FCC
Re	3170	20	0.17	19	HCP
Rh	1966	12.4	0.21	4.5	FCC
Ru	2500	12.2		7.6 (0°C)	HCP

TABLE 3.2: THE FORM AND THE VICKERS PENETRATION HARDNESS OF THE SLIP RING METALS

MATERIAL	FORM	HARDNESS (kg/mm^3)
Silver	rolled flat	60
Gold	rolled flat	77
Copper	rolled flat	96
Cobalt	rolled flat	206
Iridium	rolled flat	606
Nickel	rolled flat	165
Palladium	rolled flat	116
Platinum	rolled flat	107
Rhenium	rolled flat	610
Rhodium	electroplated layer	540
Ruthenium	powder-metal compact	370

IV. EXPERIMENTAL RESULTS

This chapter will present the results of the tests and a discussion of the accuracy of the results.

4.1 ORGANIZATION OF THE RESULTS

The data obtained from running pin-on-disk tests are presented in Tables 4.1 to 4.10.

All of the results shown in Tables 4.1 to 4.5 were obtained using the silver graphite brushes. Table 4.1 shows the results of tests carried out in a wet CO_2 atmosphere, at a speed of 4m/sec, while a 50 A DC current flowed through the interface (with the brush positive and the metal flat negative). Table 4.2 presents results of tests performed in air, at a speed of 4m/sec, under a current of 50 A. The results in Table 4.3 were obtained from tests performed in a 1-Bromo-Pentane atmosphere, at a speed of 4m/sec, and a current level of 50 A. The data in Table 4.4 are for tests carried out at no current, in a wet CO_2 atmosphere, at a speed of 4m/sec. Table 4.5 presents data from tests run at 8m/sec, in ambient air, and at a current level of 50 A.

Tables 4.6 to 4.8 present data obtained from tests carried out using pure graphite brushes. Table 4.6 presents the results for tests performed in a wet CO_2 atmosphere, at a speed of 4m/sec, and a current of 50 A. Tables 4.7 and 4.8 show the data of tests obtained in air, with a current of 50 A, and speeds of 4m/sec and 8m/sec respectively.

Table 4.9 shows the results of tests obtained by using a silver graphite brush sliding on an iridium flat in a wet CO_2 atmosphere, at 4m/sec, and

TABLE 4.1

Brush: Silver Graphite (75% w/o Ag)
Load: 300 g
Speed: 4 m/sec
Current: 50 A
Atmosphere: wet CO_2
Average test time: 24 hrs.

FLAT MATERIAL	K_{brush}	K_{flat}	f	$\Delta R(m\Omega)$
Ag	8.6×10^{-7}	1.0×10^{-7}	0.24	4.3
Au	8.4	0(2.8)*	0.29	4.3
Co	8.5	0(1.8)	0.21	6.0
Cu	24	22	0.25	5.7
Ir	8.2	0(2.0)	0.20	6.2
Ni	61	230	0.21	7.3
Pd	7.9	0(2.0)	0.25	3.3
Pt	11	0(0)	0.25	3.7
Re	19	0(0.5)	0.19	5.9
Rh	9.5	0(2.0)	0.20	5.0
Ru	10	0(3.7)	0.20	4.9

* When $K_{flat} = 0$, the number in brackets represents the weight gain of the flat in mg.

TABLE 4.2

Brush: Silver Graphite (75% w/o Ag)
Load: 300 g
Speed: 4 m/sec
Current: 50 A
Atmosphere: air
Average test time: 24 hrs.

FLAT MATERIAL	K_{brush}	K_{flat}	f	$\Delta R(m\Omega)$
Ag	3.8×10^{-7}	0(2.3)*	0.30	6.3
Au	10	1.5×10^{-7}	0.29	5.5
Co	9.9	0(2.3)	0.34	6.5
Cu	13	2.8	0.26	7.3
Ir	5.9	0(2.4)	0.31	5.2
Ni	22	0(1.0)	0.20	5.8
Pd	7.0	0(2.7)	0.32	4.8
Pt	9.0	0(0.4)	0.27	5.1
Re	38	0(0.4)	0.18	8.0
Rh	3.3	0(3.0)	0.28	4.5
Ru	9.5	0(0.2)	0.26	5.5

* When $K_{flat} = 0$, the number in brackets represents the weight gain of the flat in mg.

TABLE 4.3

Brush: Silver Graphite (75% w/o Ag)
Load: 300 g
Speed: 4 m/sec
Current: 50 A
Atmosphere: air with 1-Br-Pentane
Average test time: 24 hrs.

FLAT MATERIAL	K_{brush}	K_{flat}	f	$\Delta R(m\Omega)$
Ag	26×10^{-7}	40×10^{-7}	0.17	12
Au	63	65	0.17	11
Co	15	0(1.4)*	0.18	12
Cu	23	13	0.11	11
Ir	2.2	0(2.1)	0.18	12
Ni	8.4	0(4.6)	0.19	11
Pd	12	0(0)	0.14	14
Pt	9.9	8.8	0.17	9.0
Re	18	0(5.8)	0.19	16
Rh	22	0(4.8)	0.15	12
Ru	16	0(5.8)	0.13	15

* When $K_{flat} = 0$, the number in brackets represents the weight gain of the flat in mg.

TABLE 4.4

Brush: Silver Graphite (75% w/o Ag)
Load: 300 g
Speed: 4 m/sec
Current: 0 A
Atmosphere: wet CO_2
Average test time: 24 hrs.

FLAT MATERIAL	K_{brush}	K_{flat}	f
Ag	0.77×10^{-7}	0(0.3)*	0.29
Au	3.7	0(0.6)	0.24
Co	3.7	2.9×10^{-7}	0.18
Cu	3.5	2.2	0.31
Ir	1.8	0(1.0)	0.24
Ni	5.6	14	0.22
Pd	5.9	0(2.1)	0.30
Pt	2.4	0(1.2)	0.26
Re	24	4.2	0.24
Rh	0.046	0(0.8)	0.30
Ru	1.3	0(0.3)	0.24

* When $K_{flat} = 0$, the number in brackets represents the weight gain of the flat in mg.

TABLE 4.5

Brush: Silver Graphite (75% w/o Ag)
Load: 500 g
Speed: 8 m/sec
Current: 50 A
Atmosphere: air
Average test time: 24 hrs.

FLAT MATERIAL	K_{brush}	K_{flat}	$\Delta R(m\Omega)$
Ag	41×10^{-7}	6.9×10^{-7}	5.6
Au	83	190	3.8
Co	12	0(1.4)*	5.2
Cu	17	20	5.5
Ir	16	0(0.4)	5.9
Ni	61	38	8.4
Pd	13	0(1.0)	3.6
Pt	11	0.93	7.5
Re	35	3.5	4.6
Rh	14	0(2.2)	3.7
Ru	15	0(1.9)	4.6

* When $K_{flat} = 0$, the weight in brackets represents the weight gain of the flat in mg.

TABLE 4.6

Brush: Pure Graphite
Load: 300 g
Speed: 4 m/sec
Current: 50 A
Atmosphere: wet CO_2
Average test time: 24 hrs.

FLAT MATERIAL	K_{brush}	K_{flat}	f	$\Delta R(M\Omega)$
Ag	27×10^{-7}	0.05×10^{-7}	0.22	31
Au	4.1	0(0.2)*	0.37	35
Co	50	61	0.15	27
Cu	24	4.4	0.16	26
Ir	200	80	0.29	17
Ni	69	4.8	0.19	39
Pd	13	0.44	0.19	29
Pt	22	1.0	0.18	22
Re	250	85	0.24	26
Rh	44	24	0.15	26
Ru	75	18	0.20	26

* When $K_{flat} = 0$, the number in brackets represents the weight gain of the flat in mg.

TABLE 4.7

Brush: Pure Graphite
Load: 300 g
Speed: 4 m/sec
Current: 50 A
Atmosphere: air
Average test time: 24 hrs.

FLAT MATERIAL	K_{brush}	K_{flat}	f	$\Delta R(M\Omega)$
Ag	51×10^{-7}	2.8×10^{-7}	0.21	60
Au	12	0.49	0.47	33
Co	45	28	0.17	27
Cu	11	6.2	0.30	19
Ir	17	2.0	0.21	16
Ni	83	7.9	0.13	33
Pd	20	1.3	0.13	24
Pt	36	1.9	0.15	16
Re	220	78	0.21	16
Rh	27	20	0.18	14
Ru	47	7.3	0.19	28

TABLE 4.8

Brush: Pure Graphite
Load: 500 g
Speed: 8 m/sec
Current: 50 A
Atmosphere: air
Average test time: 24 hrs.

FLAT MATERIAL	K_{brush}	K_{flat}	ΔR
Ag	37×10^{-7}	1.3×10^{-7}	21
Au	17	0.74	11
Co	23	3.1	33
Cu	8.8	0.40	22
Ir	200	80	17
Ni	44	2.1	19
Pd	14	1.5	15
Pt	1500	74	12
Re	100	52	25
Rh	18	0.0	20
Ru	57	6.7	14

TABLE 4.9

Brush: Silver Graphite (75% w/o Ag)
Flat: Iridium
Load: 300 g
Speed: 4 m/sec
Atmosphere: wet CO_2
Average test time: 24 hrs.

CURRENT(A)	K brush	FLAT WEIGHT GAIN (mg)	f	ΔR(mΩ)
0	7.1×10^{-7}	1.2	0.26	--
25	18	1.2	0.25	6.2
50	8.2	2.0	0.20	6.2
75	2000	- 1.4	0.15	6.8

TABLE 4.10

Brush:	Silver Graphite (75% w/o Ag)
Flat:	Iridium
Load:	500 g
Speed:	8 m/sec
Atmosphere:	air
Average test time:	24 hrs.

CURRENT(A)	K brush	FLAT WEIGHT GAIN (mg)	ΔR(mΩ)
0	4.6×10^{-7}	1.4	--
25	7.7	0.7	5.0
50	16	0.4	5.9
75	1300	0.7	4.3

with different current levels. Table 4.10 shows data for a set of tests similar to those in Table 4.10, except they were run in air at 8m/sec.

The tables list the wear coefficients for the brush, the wear coefficients for the flat (in the cases in which the flat gained weight, the weight gained is shown in brackets in mg), the average friction coefficient for the test (for the tests performed at 8m/sec, the friction data is not presented since the apparatus did not contain a friction force measuring transducer), and the average electrical contact resistance for the test (for the tests in which current was passed).

4.2 ACCURACY OF THE RESULTS

In order to determine the accuracy of the results six tests were performed under identical conditions. The results of the tests are presented in Table 4.11. A silver graphite brush was riding on an iridium flat in a wet CO_2 atmosphere, at 4m/sec, with a current of 50 A. It is apparent that the wear coefficient for the brush has the largest standard deviation of 32% of the mean value. The difference between the highest and the lowest brush wear coefficient is about a factor of three, which is a quite common deviation for wear coefficients in wear tests. The next largest standard deviation is for the weight gain of the flat metal which is 28% of the mean value. The standard deviation for the friction coefficient is 20% of the mean value. The standard deviation is the smallest for the electrical contact resistance values being 13% of the mean value. If the value of 4.4 mΩ is eliminated from the calculation than the standard deviation becomes 1.6% of the mean value. Thus it can be assumed that the wear

TABLE 4.11

Brush: Silver Graphite (75% w/o Ag)
Flat: Iridium
Load: 300 g
Speed: 4 m/sec
Current: 50 A
Atmosphere: wet CO_2
Average test time: 24 hrs.

TEST #	K	FLAT WEIGHT GAIN (mg)	f	$\Delta R(m\Omega)$
1	5.2×10^{-7}	3.0	0.19	6.6
2	8.2	1.9	0.16	4.4
3	12	2.0	0.14	6.6
4	11	2.2	0.22	6.5
5	6.5	2.3	0.24	6.4
6	5.5	1.0	0.25	6.7
mean	8.1	2.1	0.20	6.2
standard deviation	2.6	0.59	0.04	0.8

coefficient and weight gain values are accurate to within 30%, the friction coefficient values are accurate to about 20%, while the contact resistance values are accurate to 10%.

The main reasons for the errors are due to the fact that the wear tests are very sensitive to changing sliding conditions. The variations can be due to the differences in local strength of material, the variations in the composition of the atmosphere, particularly the presence of small amounts of alient materials, and the load changes due to waviness of the sliding surfaces. There is very little error introduced due to accuracy of the weight readings since the balance used had a resolution of 0.01 mg, while the measured differences in weights were typically 10 mg. A possible source of error is the fact that the flat metal was wiped with a clean tissue paper before weighting, thus possibly removing some of the adhering graphite film. The friction force and the contact resistance were measured during the second half of the tests, so that steady state conditions existed. From Table 4.11 it can be seen that for the tests with more wear, the friction tends to be smaller. This is a general result which will be discussed more in the next chapter.

V. DISCUSSION OF THE RESULTS

The results of the tests suggest that the performance of the slip ring system depends not only on the brush selection, but also on the selection of the commutator metal. Wear, friction and electrical contact resistance vary for different slip ring combinations and also under different sliding conditions. The results of the tests have a moderate amount of statistical scatter, but some general trends and conclusions can be made regarding the brush performance. The following sections will present the discussions on the parameters studied in this experiment.

5.1 PARAMETERS INFLUENCING THE WEAR OF SLIP RINGS

The wear of the brushes is influenced most by the slip ring combinations and to some degree by the various sliding conditions as can be seen from Tables 4.1 to 4.10. In order to see how the wear coefficients for silver graphite brush tests vary with compatibility Table 5.1 is constructed. The table shows the average measured parameters for all silver graphite brush tests and the compatibilities of the slip ring (flat) metals against graphite and against silver. The metals are presented in the order of decreasing wear coefficients. K_{ave} is the geometric average of $(K_{brush} + K_{flat}) / 2$ for all tests. The values from Table 5.1 are averaged as functions of compatibilities against graphite in Table 5.2, and against silver in Table 5.3. The tables show that for the slip ring systems in which the flat metal is compatible against both graphite and silver the wear coefficients are higher than for those slip ring systems in which the flat metal is less compatible or incompatible against graphite and silver.

TABLE 5.1: THE AVERAGE VALUES FOR SILVER GRAPHITE BRUSHES BASED ON TABLES 4.1 TO 4.5

FLAT MATERIAL	K_{ave} [i]	f_{ave} [ii]	ΔR_{ave} [iii] ($m\Omega$)	COMPATIBILITY VS. GRAPHITE	SILVER
Ni	20×10^{-7}	0.21	7.9		
Au	15	0.25	5.6		
Re	13	0.20	7.7		
Cu	11	0.23	7.1		
Co	5.0	0.23	5.9		
Ag	4.9	0.25	6.5		
Pd	4.4	0.25	6.2		
Pt	4.4	0.24	6.0		
Ru	3.9	0.21	6.6		
Ir	2.5	0.23	6.9		
Rh	1.7	0.23	6.6		

i K_{ave} is the geometric average of $(K_{brush} + K_{flat}) / 2$

ii f_{ave} is the arithmetic average

iii ΔR_{ave} is the geometric average

TABLE 5.2: THE AVERAGE VALUES FOR SILVER GRAPHITE BRUSHES AS FUNCTIONS OF COMPATIBILITY AGAINST GRAPHITE

FLAT MATERIAL	K_{ave} [i]	f_{ave} [ii]	ΔR_{ave} [iii] (mΩ)	COMPATIBILITY
Co, Ni, Pt, Re	8.7×10^{-7}	0.22	6.8	
Au, Ir, Pd, Rh Ru	4.1	0.23	6.2	
Ag, Cu	7.3	0.24	6.8	

i Geometric average

ii Arithmetic average

iii Geometric average

TABLE 5.3: THE AVERAGE VALUES FOR SILVER GRAPHITE BRUSHES AS FUNCTIONS OF COMPATIBILITY AGAINST SILVER

FLAT MATERIAL	K_{ave} [i]	f_{ave} [ii]	ΔR_{ave} [iii] (mΩ)	COMPATIBILITY
Ag, Au, Cu, Pt	7.7×10^{-7}	0.24	6.3	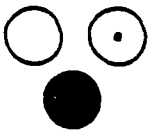
Re, Rh, Ru Co, Ir, Ni, Pd	5.1	0.22	6.6	

i Geometric average

ii Arithmetic average

iii Geometric average

However the dependence does not appear to be very strong as shown by Figures 5.1 and 5.2, which present the correlations between the average wear coefficients and the compatibilities of the flat metals against graphite and against silver respectively. The correlation coefficient for the two plots is around 0.25.

The fact that both graphite and silver in silver graphite brushes influence the compatibility requirements suggests a rating system based on both materials. Such a rating is established by assigning points to the compatibility elements in Figure 1.2. An identical pair of materials (represented by an open circle) is assigned a value of 0 points. A compatible pair (a circle with a dot) is assigned 1 point. A partially compatible pair (a quarter blackened circle) is assigned 2 points. A partially incompatible pair (a half blackened circle) is assigned 3 points, and finally an incompatible pair (a black circle) is assigned a value of 4 points. The total rating is calculated from the following formula:

$$I.R. = P_g \phi_g + P_s \phi_s$$

where I.R. is the incompatibility rating, P_g is the points assigned for compatibility of the flat metal against graphite, ϕ_g is the volume fraction of graphite in the brush, for a 75% w/o Ag brush $\phi_g = 0.65$, P_s is the points assigned for compatibility of the flat metal against silver, and ϕ_s is the volume fraction of silver, $\phi_v = 0.35$ for the above mentioned brush.

Figure 5.3 presents the correlation between the average wear coefficient and the incompatibility ratings for silver graphite brush tests. The figure shows a strong tendency for the slip rings with a high incompatibility

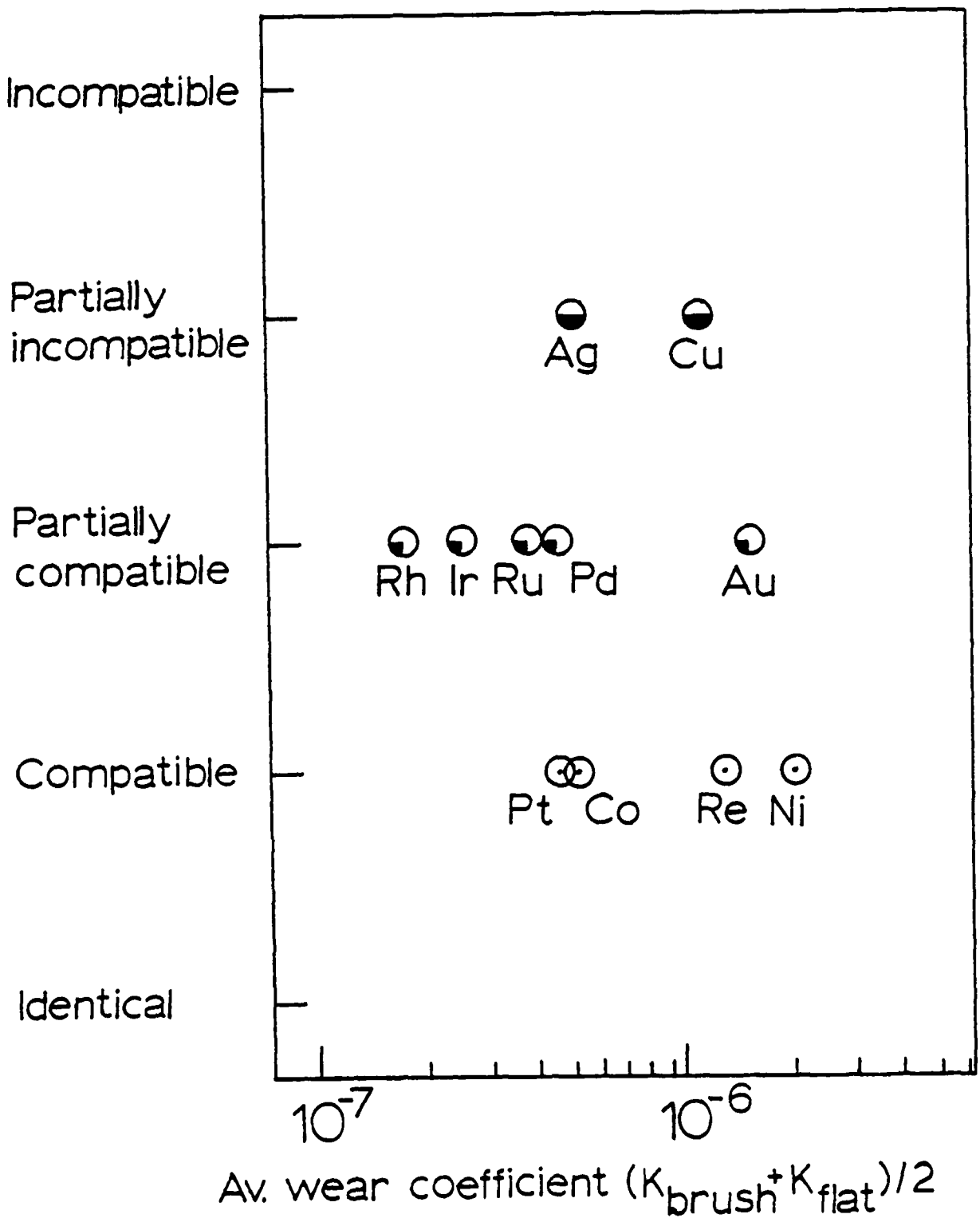

FIGURE 5.1: A PLOT OF THE AVERAGE WEAR COEFFICIENTS VERSUS THE COMPATIBILITY OF THE FLAT MATERIALS AGAINST GRAPHITE FOR SILVER GRAPHITE BRUSH TESTS

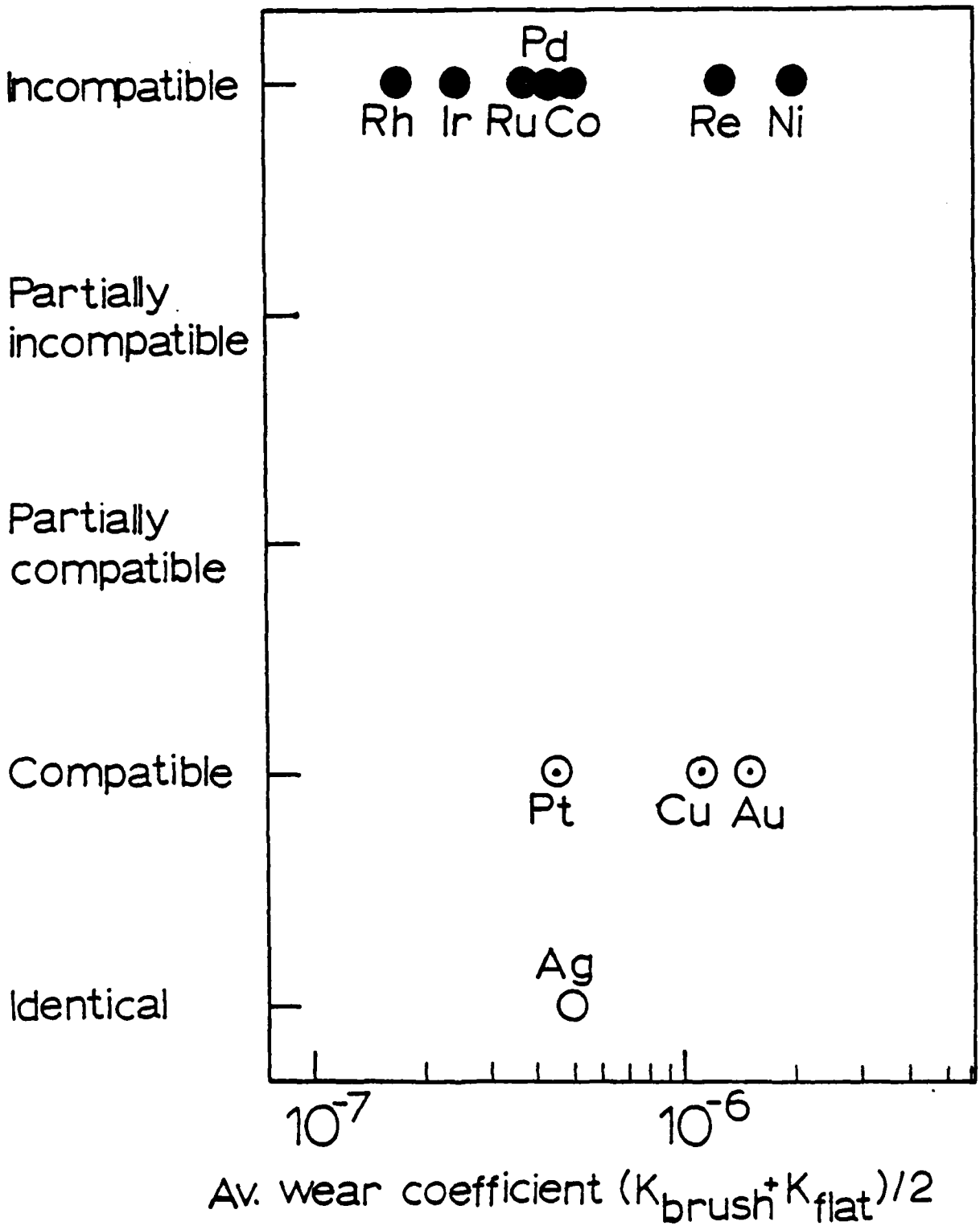

FIGURE 5.2: A PLOT OF THE AVERAGE WEAR COEFFICIENTS VERSUS THE COMPATIBILITY OF THE FLAT MATERIALS AGAINST SILVER FOR SILVER GRAPHITE BRUSH TESTS

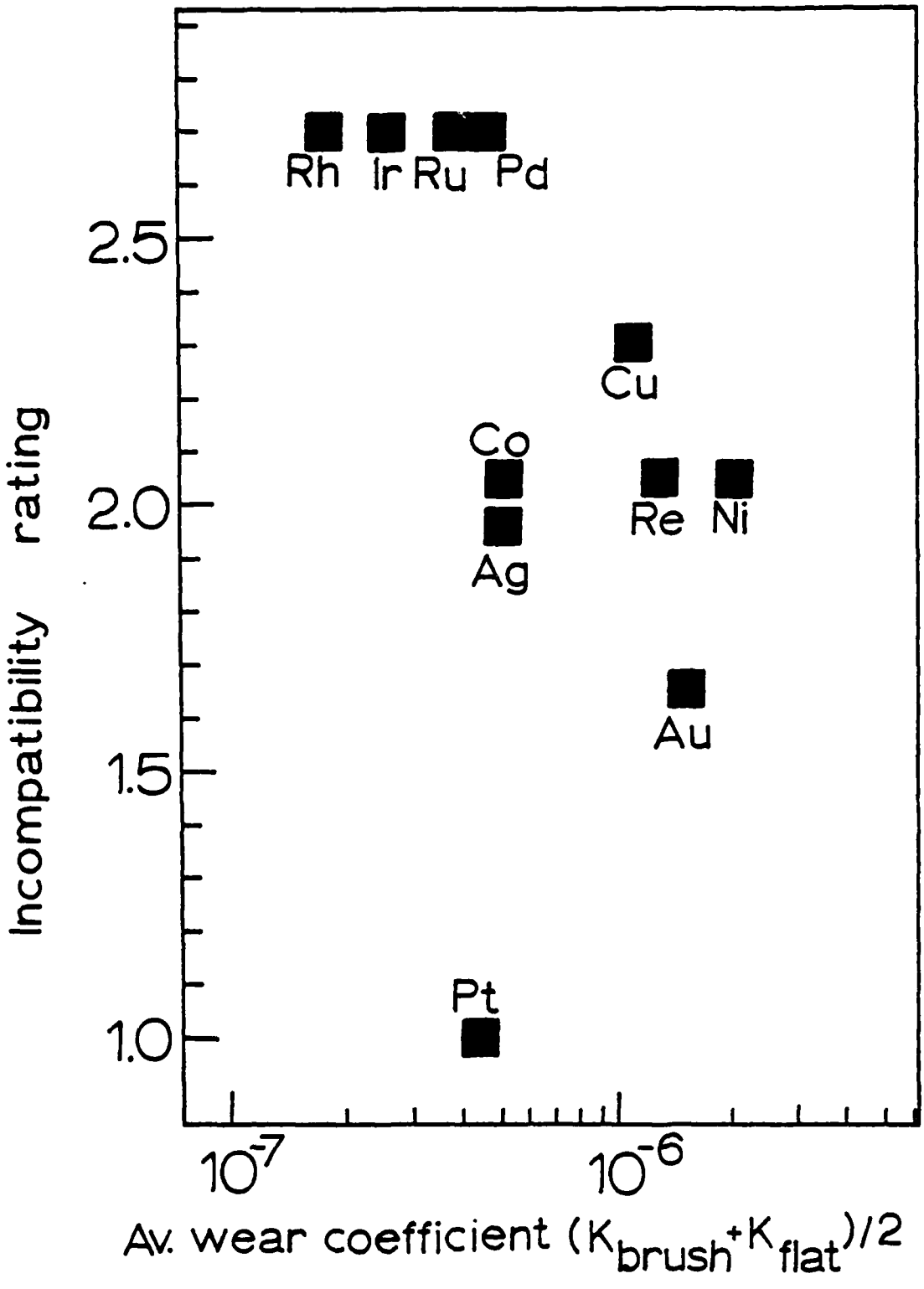

FIGURE 5.3: A PLOT OF THE AVERAGE WEAR COEFFICIENTS VERSUS THE INCOMPATIBILITY RATING OF THE FLAT MATERIALS AGAINST THE BRUSH FOR SILVER GRAPHITE BRUSH TESTS

rating (a high degree of incompatibility) to have lower wear coefficients. The correlation for the figure is 0.55. The figure suggests that the wear can be decreased by a factor of 5 or more by choosing a slip ring metal with a high incompatibility rating against the brush, as cumpared to a low rating system.

Figure 5.4 shows a plot of the brush wear coefficients versus the weight gains of the flats. The plot has a rather small correlation of 0.23 which means that when the brush wear is high there is a tendency for the brush material to be transferred to the commutator surface. However the flat metals which readily oxidize (i.e. Cu, Ni) usually show a weight loss and thus a wear coefficient value in silver graphite brush tests, as can be seen from Tables 4.1 to 4.5.

The oxide forming metals have high wear coefficients, thus showing that the oxide layer when disturbed can result in abrasive action thus producing more wear.

The hexagonal close packed metals cover the whole range in terms of wear. Ruthenium has one of the lowest wear coefficients of all slip ring metals in silver graphite brush tests, while rhenium has the third largest wear coefficient, and cobalt having an intermediate wear coefficient. The crystalline structure appears to be overshadowed by the compatibility requirements and the fact that a surface layer of transferred brush material is present at the sliding interface.

Table 5.4 presents the average values for the pure graphite brush tests and the compatibilities of the flat metals against graphite. The average values of these results appear as functions of compatibilities of the flat

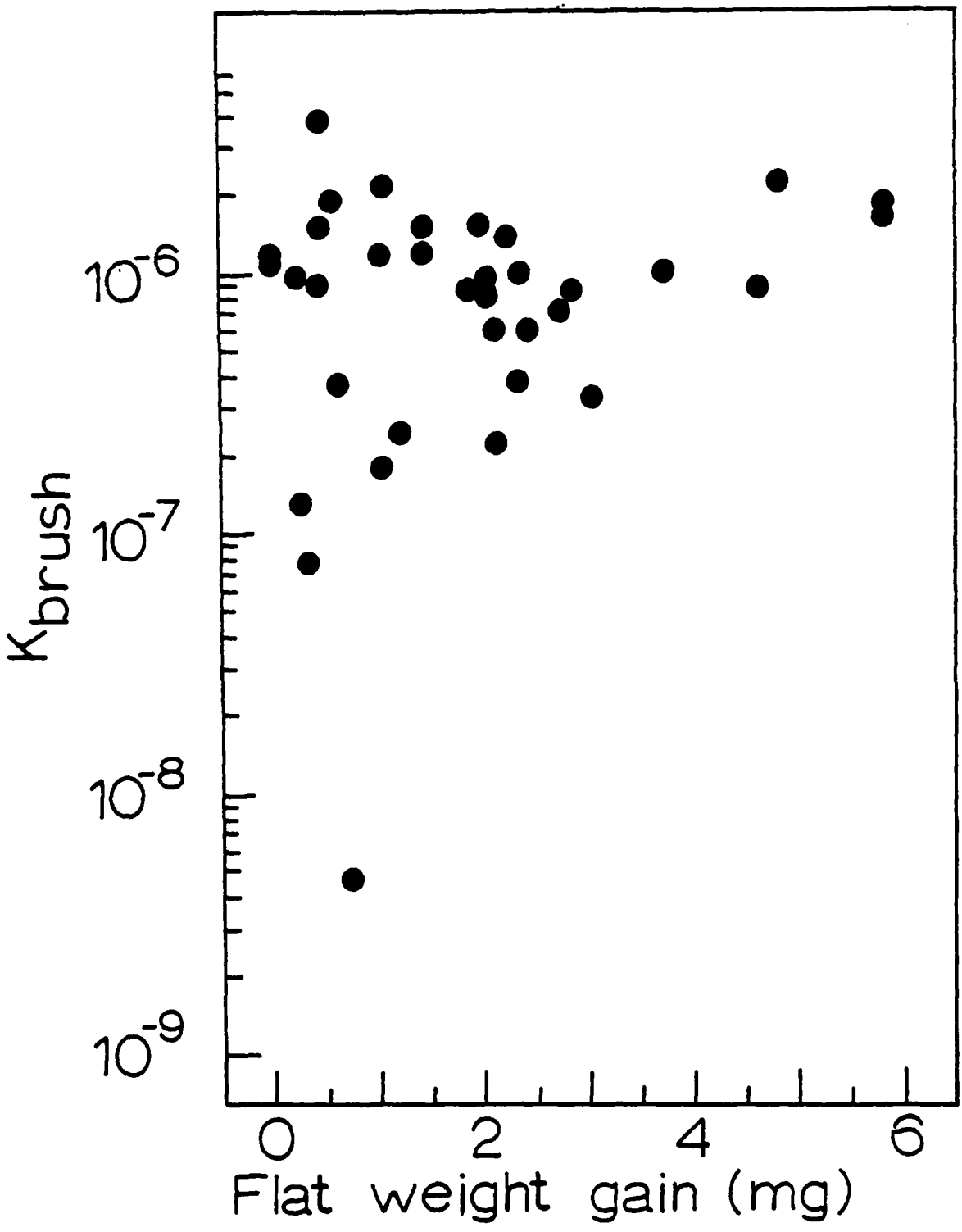

FIGURE 5.4: A PLOT OF THE BRUSH WEAR COEFFICIENTS VERSUS THE WEIGHT GAIN OF THE FLATS FOR SILVER GRAPHITE BRUSH TESTS

TABLE 5.4: THE AVERAGE VALUES FOR PURE GRAPHITE BRUSHES BASED ON TABLES 4.6 TO 4.8

FLAT MATERIAL	K_{ave} [i]	f_{ave} [ii]	ΔR_{ave} [iii] ($m\Omega$)	COMPATIBILITY
Re	120×10^{-7}	0.23	22	
Ir	57	0.25	17	
Pt	42	0.17	16	
Ni	34	0.16	29	
Ru	34	0.20	22	
Co	30	0.16	29	
Ag	19	0.22	34	
Rh	19	0.17	19	
Pd	8.3	0.16	22	
Cu	8.2	0.23	22	
Au	4.9	0.42	23	

i K_{ave} is the geometric average of $(K_{brush} + K_{flat}) / 2$

ii f_{ave} is the arithmetic average

iii ΔR_{ave} is the geometric average

metals against graphite in Table 5.5. The incompatible combinations show significantly smaller wear coefficients than the compatible combinations. Figure 5.5 shows the correlation between wear and compatibility, with the correlation being 0.61. As with the silver graphite brushes, the wear of the pure graphite slip rings strongly depends on the compatibility of the flat metal against the brush. However the flat metals usually show a weight loss and thus produce wear coefficients, as can be seen from Tables 4.6 to 4.8. A plot of the brush wear coefficients versus the flat wear coefficients for a test performed in wet CO_2, at a load of 300 g, a speed of 4 m/sec, and a current of 50 A is shown in Figure 5.6, where the correlation is 0.81. The combination of materials with higher brush wear produce more wear of the flat in pure graphite brush tests.

The oxide forming slip ring metals tend to have moderate wear, and the HCP metals again cover a wide range in terms of wear showing the dominance of compatibility requirements.

Table 5.6 is constructed to show the effects of the sliding conditions on the wear, friction and contact resistance of the slip rings. The table shows the average values for all sets of tests performed. There is no significant change in the wear of the slip rings in the tests performed in a wet CO_2 atmosphere with the tests for pure graphite brushes showing slightly less wear in CO_2, and the tests for silver graphite brushes showing more wear in CO_2. The reason for the small difference is probably that the air atmosphere contained enough moisture to assure adequate graphite lubrication. The tests performed with 1-Bromo-Pentane vapors gave wear close in value to those in wet CO_2 and a little higher than those in air, again suggesting

TABLE 5.5: THE AVERAGE VALUES FOR PURE GRAPHITE BRUSHES AS FUNCTIONS OF COMPATIBILITY AGAINST GRAPHITE

FLAT MATERIAL	k_{ave} [i]	f_{ave} [ii]	ΔR_{ave} [iii] ($m\Omega$)	COMPATIBILITY
Co, Ni, Pt, Re	48×10^{-7}	0.18	23	
Au, Ir, Pd, Rh Ru	17	0.24	20	
Ag, Cu	12	0.23	27	

i Geometric average

ii Arithmetic average

iii Geometric average

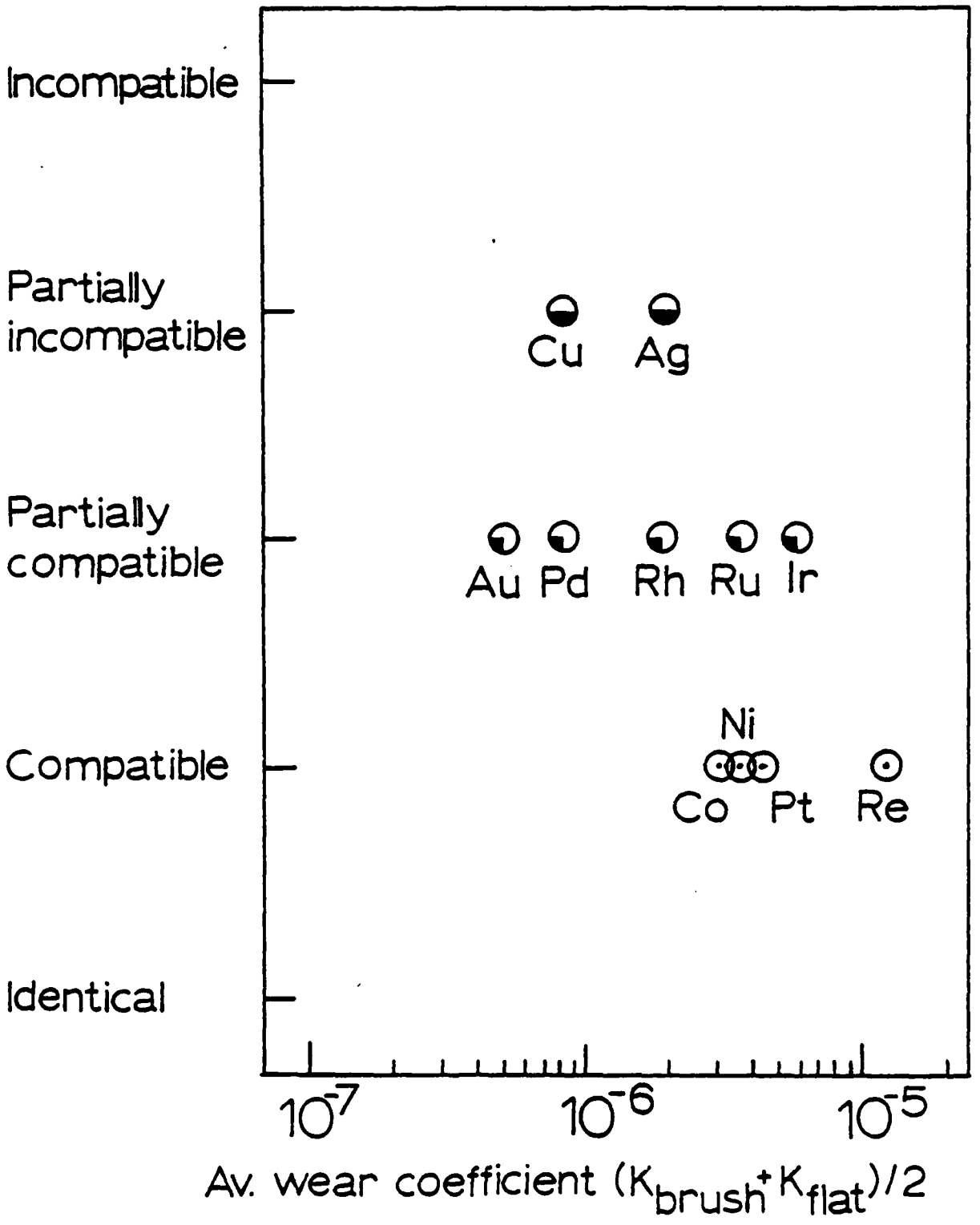

FIGURE 5.5: \ PLOT OF THE AVERAGE WEAR COEFFICIENTS VERSUS THE COMPATIBILITY OF THE FLAT MATERIALS AGAINST GRAPHITE FOR PURE GRAPHITE BRUSH TESTS

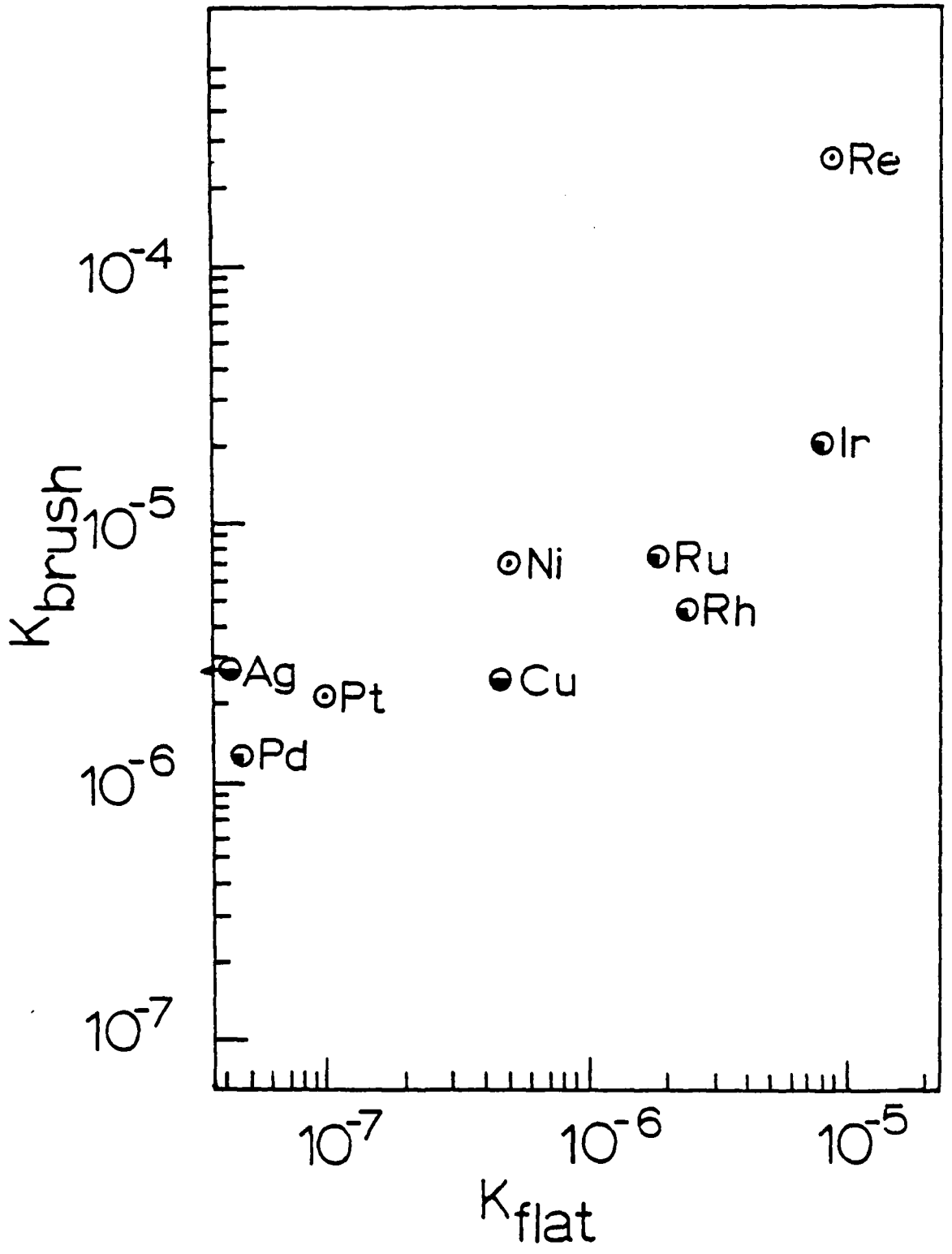

FIGURE 5.6: A PLOT OF THE BRUSH WEAR COEFFICIENTS VERSUS THE FLAT WEAR COEFFICIENTS FOR PURE GRAPHITE BRUSH TESTS IN WET CO_2 ATMOSPHERE, AT A SPEED OF 4 M/SEC, A LOAD OF 300 g, AND A CURRENT OF 50 A

TABLE 5.6: AVERAGE VALUES FOR ALL TESTS

BRUSH	SPEED (m/sec)	LOAD (g)	CURRENT (A)	ATMOSPHERE	K_{ave} [i]	f_{ave} [ii]	ΔR_{ave} [iii] (mΩ)
Silver Graphite	4	300	0	wet CO_2	1.5×10^{-7}	0.26	--
Silver Graphite	4	300	50	wet CO_2	7.7	0.23	5.0
Silver Graphite	4	300	50	air	4.9	0.27	5.8
Silver Graphite	4	300	50	1-Br-Pentane	9.5	0.16	12
Silver Graphite	8	500	50	air	14	--	5.1
Graphite	4	300	50	wet CO_2	25	0.21	27
Graphite	4	300	50	air	22	0.21	24
Graphite	8	500	50	air	19	--	19

i K_{ave} is the geometric average of $(K_{brush} + k_{flat}) / 2$

ii f_{ave} is the arithmetic average

iii ΔR_{ave} is the geometric average

that the ambient winter air contained more than the critical amount of moisture.

The speed of sliding does not significantly influence the wear as shown by the tests performed at two speeds. However at even higher speeds it is possible that the increased heat input due to friction force will raise the temperature of the interface, thus causing more wear. In this experiment the difference in speeds is not large enough to produce significant temperature changes. However, if the temperature does rise significantly then the metals with high melting points are expected to perform better in terms of wear, than the metals with low melting points. For the tests performed at the two speeds the correlations between the wear coefficient and the melting point did not differ significantly.

An important parameter during sliding is the current level that passes through the brush-commutator interface. The set of tests performed with silver graphite brushes at a current of 50 A per brush shows five times higher wear than the set of tests performed at no current. The effect of current can be seen more clearly in Figure 5.7. The figure shows a plot of the brush wear coefficients versus the current level for two experiments in which a silver graphite brush was sliding on an iridium flat. There is a slight increase in wear as the current is increased from 0 A to 50 A. At a current of 75 A the wear is two orders of magnitude higher than at 50 A. The increased current density increases the heat input into the brush-commutator interface, thus raising the temperature of the interface. The high temperature may have two effects on wear. The local strength of the brush material is reduced, thus producing a higher probability of generating

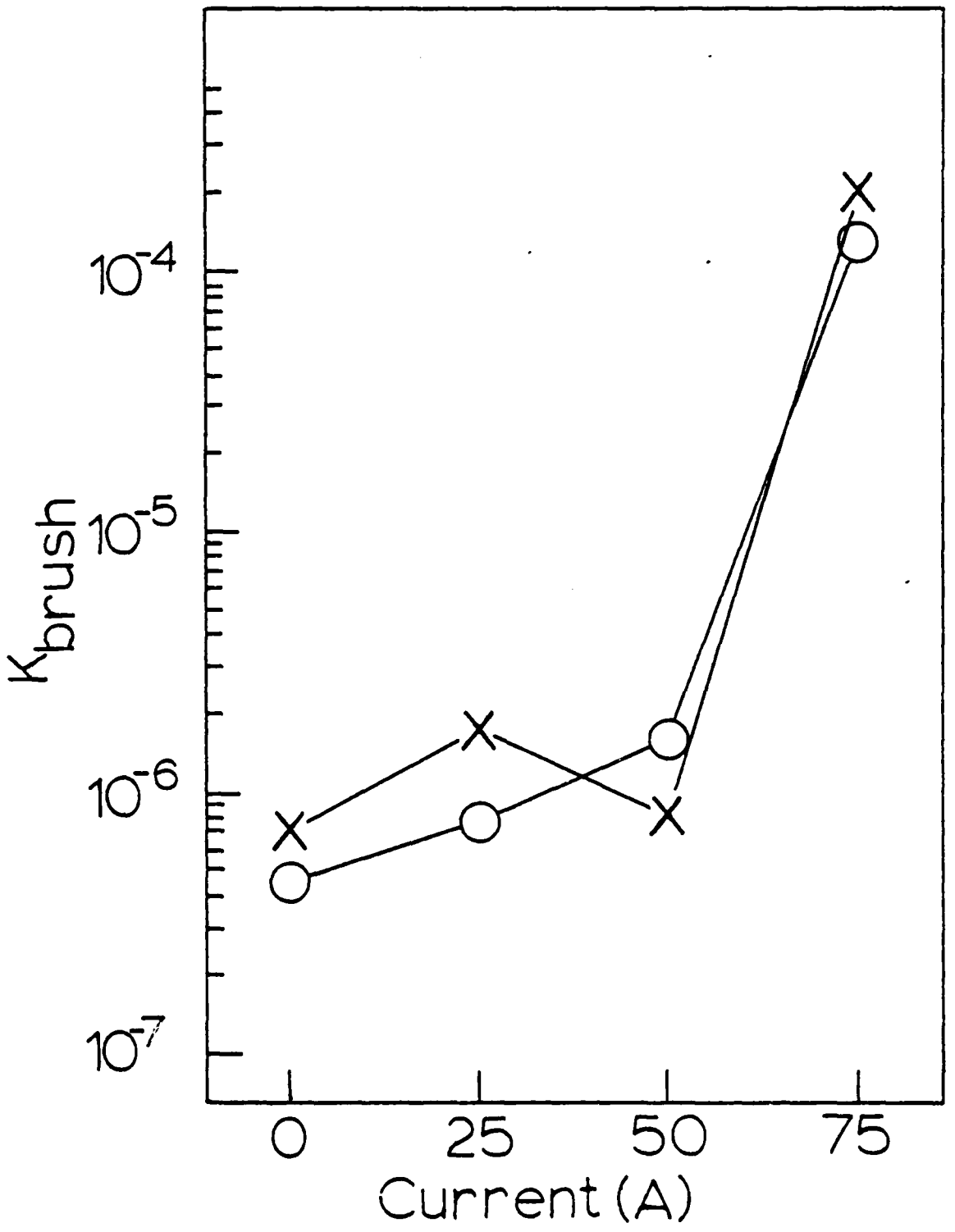

FIGURE 5.7: A PLOT OF THE BRUSH WEAR COEFFICIENTS VERSUS CURRENT LEVEL FOR A SILVER GRAPHITE BRUSH SLIDING ON AN IRIDIUM FLAT. X IS FOR TESTS RUN IN WET CO_2, AT A SPEED OF 4 M/SEC, A LOAD OF 300 g. O IS FOR TESTS RUN IN AIR, AT A SPEED OF 8 M/SEC, A LOAD OF 500 g

wear particles (higher K values). The second effect is the formation of a local region of low humidity. The reduced humidity reduces the ability of graphite to perform as a solid lubricant in which case the wear is higher.

Generally the slip ring systems containing noble metals produce less wear than the slip ring systems which contain oxide forming metals regardless of compatibility ratings. For the silver graphite brush tests all of the noble metals tested have smaller wear coefficients than nickel and six noble metals slip rings have lower wear than copper or cobalt. For the pure graphite brush tests only a gold slip ring has less wear than copper, and palladium has a similar wear coefficient to copper. Five noble metals have less wear than nickel.

Table 5.7 presents the comparison between the wear of silver graphite brushes and pure graphite brushes for the sets of tests performed under similar sliding conditions. The silver graphite brushes have an average wear coefficient three times lower than the average wear coefficient for the graphite brushes.

5.2 PARAMETERS INFLUENCING THE FRICTION OF SLIP RINGS

Two significantly different parameters influencing the friction are present during the sliding of the electrical brush on the commutator surface. The first parameter is the compatibility requirement, which states that a combination of incompatible materials will produce a smaller friction coefficient than a combination of compatible materials. The other parameter is a lubricating graphite layer. In order to obtain low friction a complete lubricating graphite layer is required to be present on the commutator surface, and this tends to produce high brush wear rates. As was shown in

TABLE 5.7: AVERAGE VALUES FOR SILVER GRAPHITE AND PURE GRAPHITE BRUSHES FOR TESTS PERFORMED UNDER SIMILAR CONDITIONS

BRUSH	K_{ave} [i]	f_{ave} [ii]	ΔR_{ave} [iii] ($m\Omega$)
Silver Graphite	8.2×10^{-7}	0.25	5.3
Graphite	22×10^{-7}	0.21	23

i Geometric Average

ii Arithmetic Average

iii Geometric Average

the previous section the compatible pairs of materials produce higher wear, and thus according to the second parameter, will produce lower friction. Figure 5.8 shows the plot of the incompatibility ratings of the combinations versus the friction coefficients for the silver graphite brush tests. There is a small correlation of 0.30 showing that the second parameter is stronger and compatible pairs produce slightly less friction. Another proof of the dominance of the second mechanism is shown in Figure 5.9, where the average wear coefficients are plotted against the friction coefficients for the silver graphite brush tests. The friction does indeed decrease with increasing wear, showing a correlation of -0.50. Figure 5.10 shows wear versus friction for a set of tests performed with silver graphite brushes, in wet CO_2, at a load of 300 g, a speed of 4 m/sec, and a current of 50 A. Here again there is a negative correlation between wear and friction. Table 5.5 and Figure 5.11 show that for pure graphite brushes the incompatible combinations of the materials produce higher friction values. The wear versus friction plot in Figure 5.12 results in a negative correlation of -0.35.

The low correlation values suggest that other parameters influence the friction behavior of the slip rings. The results in Table 5.6 show that for silver graphite brushes the presence of 1-Bromo-Pentane vapors significantly reduce the friction coefficient. The organic vapors produce a surface layer at the sliding interface after being absorbed by graphite. This surface layer aids in lubrication of the system, thus lower friction coefficients are obtained.

From Table 5.7 it can be seen that the pure graphite brushes show

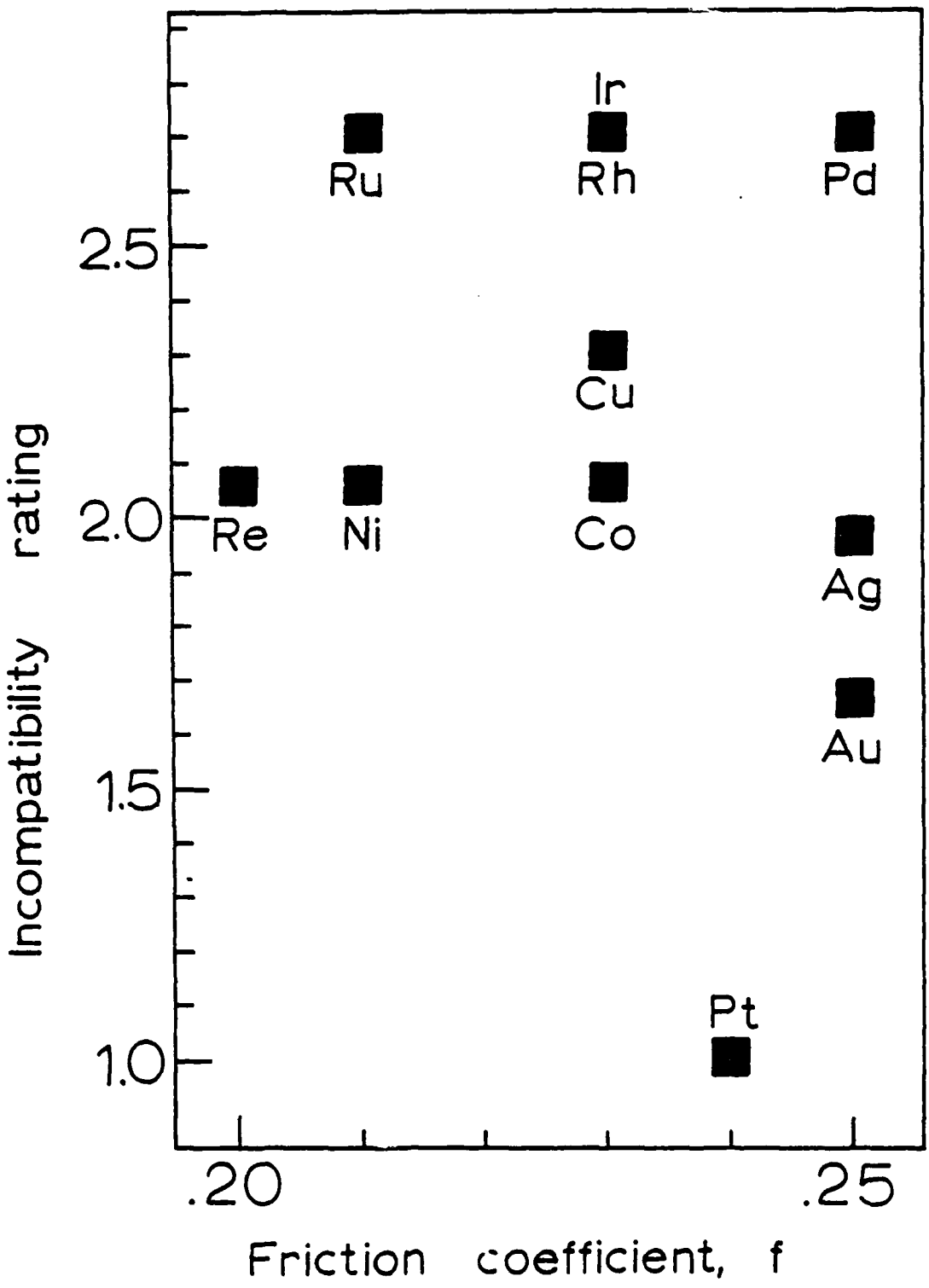

FIGURE 5.8: A PLOT OF THE AVERAGE FRICTION.COEFFICIENTS VERSUS THE THE INCOMPATIBILITY RATING OF THE FLAT MATERIALS AGAINST THE BRUSH FOR SILVER GRAPHITE BRUSH TESTS

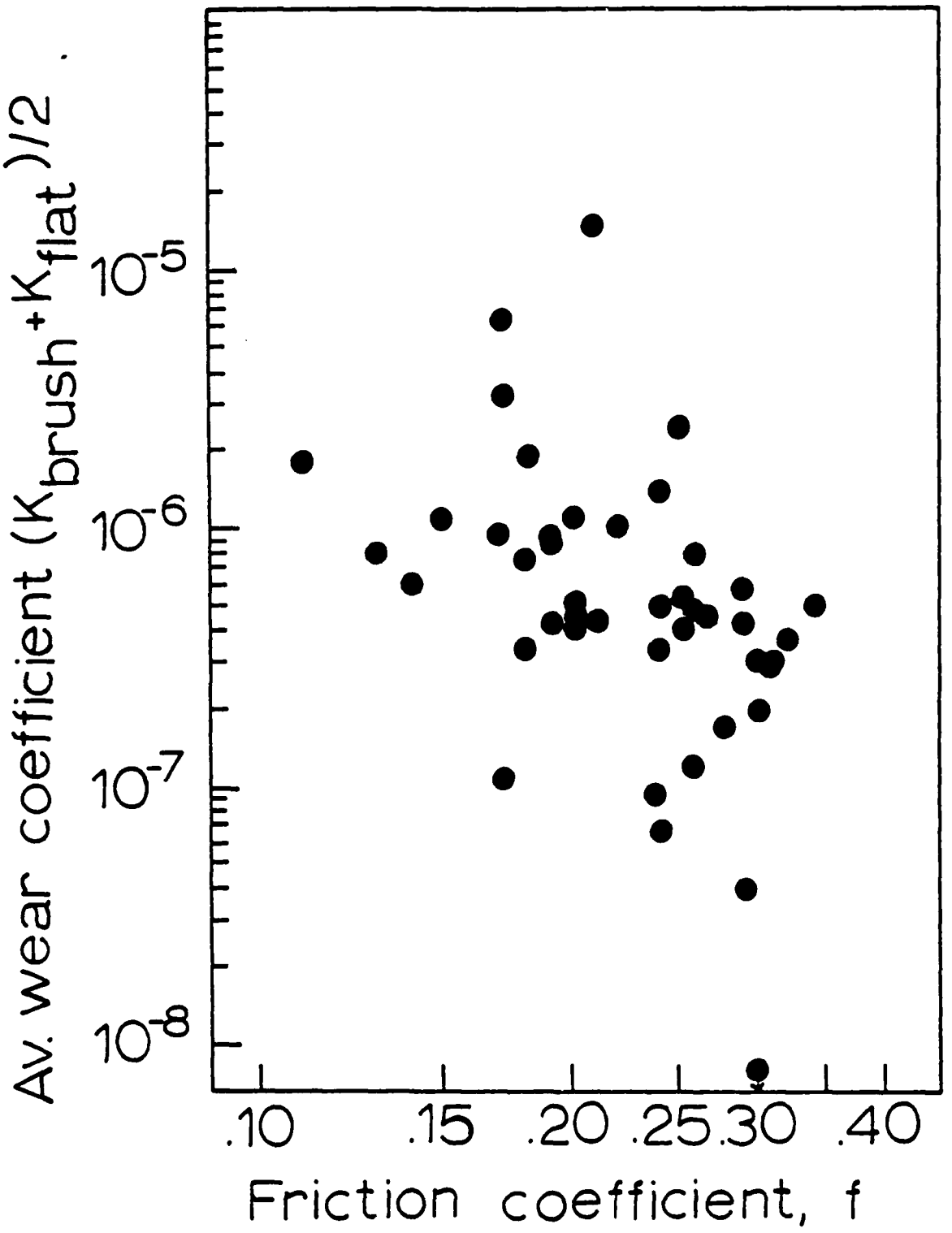

FIGURE 5.9: A PLOT OF THE AVERAGE WEAR COEFFICIENTS VERSUS THE FRICTION COEFFICIENTS FOR SILVER GRAPHITE BRUSH TESTS (EXCEPT THE 8 M/SEC SET OF TESTS)

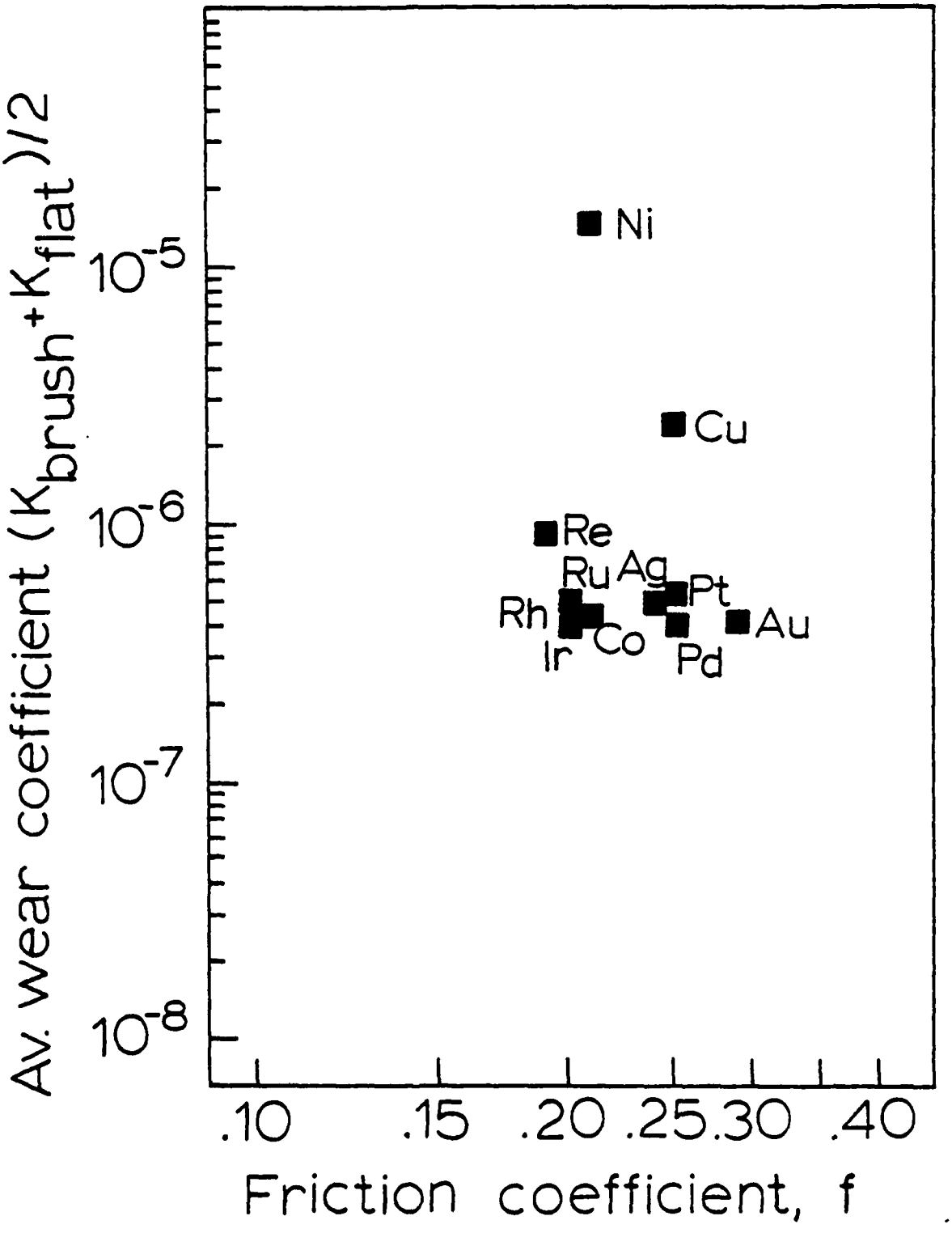

FIGURE 5.10: A PLOT OF THE AVERAGE WEAR COEFFICIENTS VERSUS THE FRICTION COEFFICIENTS FOR A SET OF SILVER GRAPHITE BRUSH TESTS PERFORMED IN WET CO_2, AT A LOAD OF 300 g, A SPEED OF 4 M/SEC, A CURRENT OF 50 A

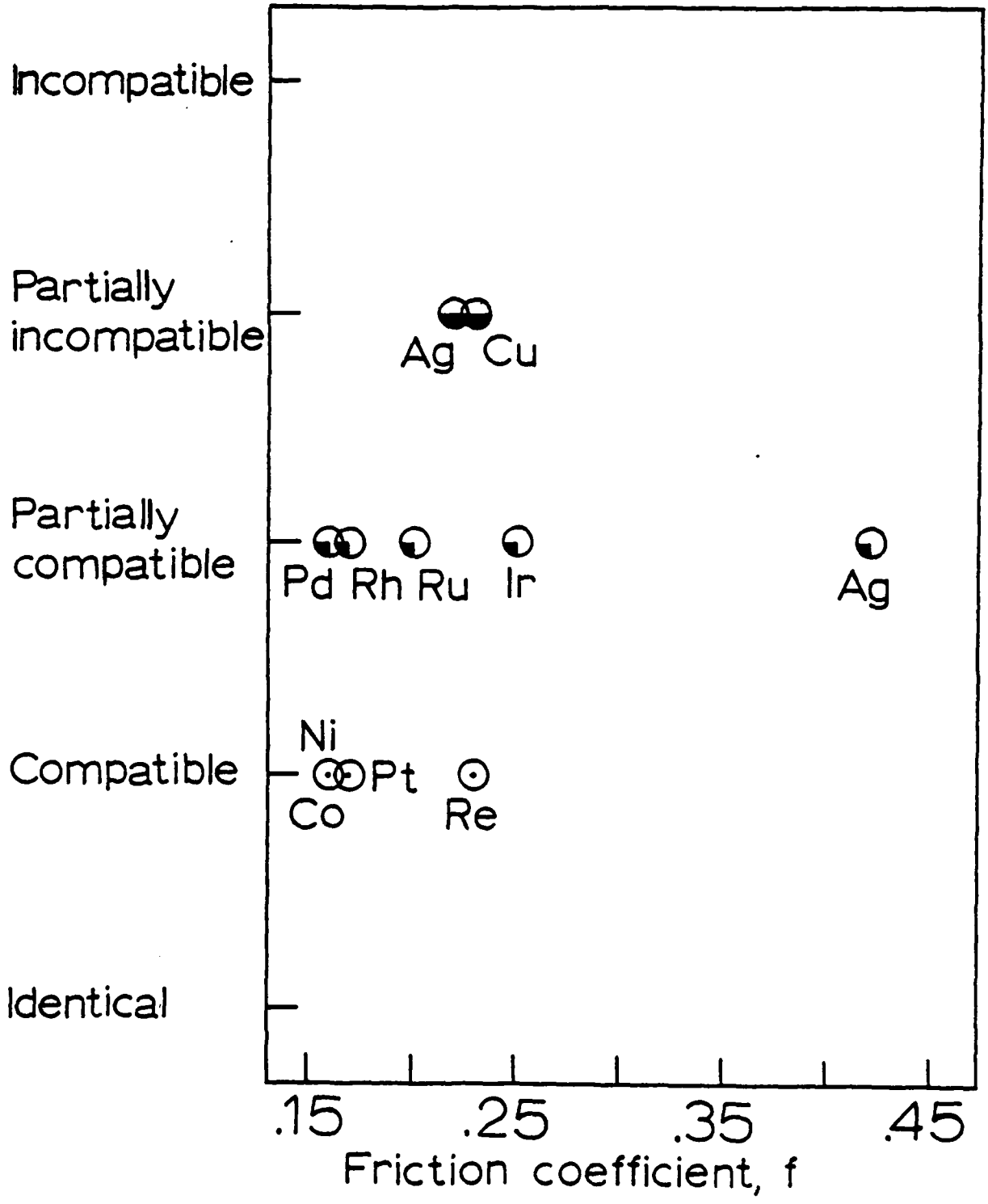

FIGURE 5.11: A PLOT OF THE AVERAGE FRICTION COEFFICIENTS VERSUS THE COMPATIBILITY OF THE FLAT MATERIALS AGAINST GRAPHITE FOR PURE GRAPHITE BRUSH TESTS

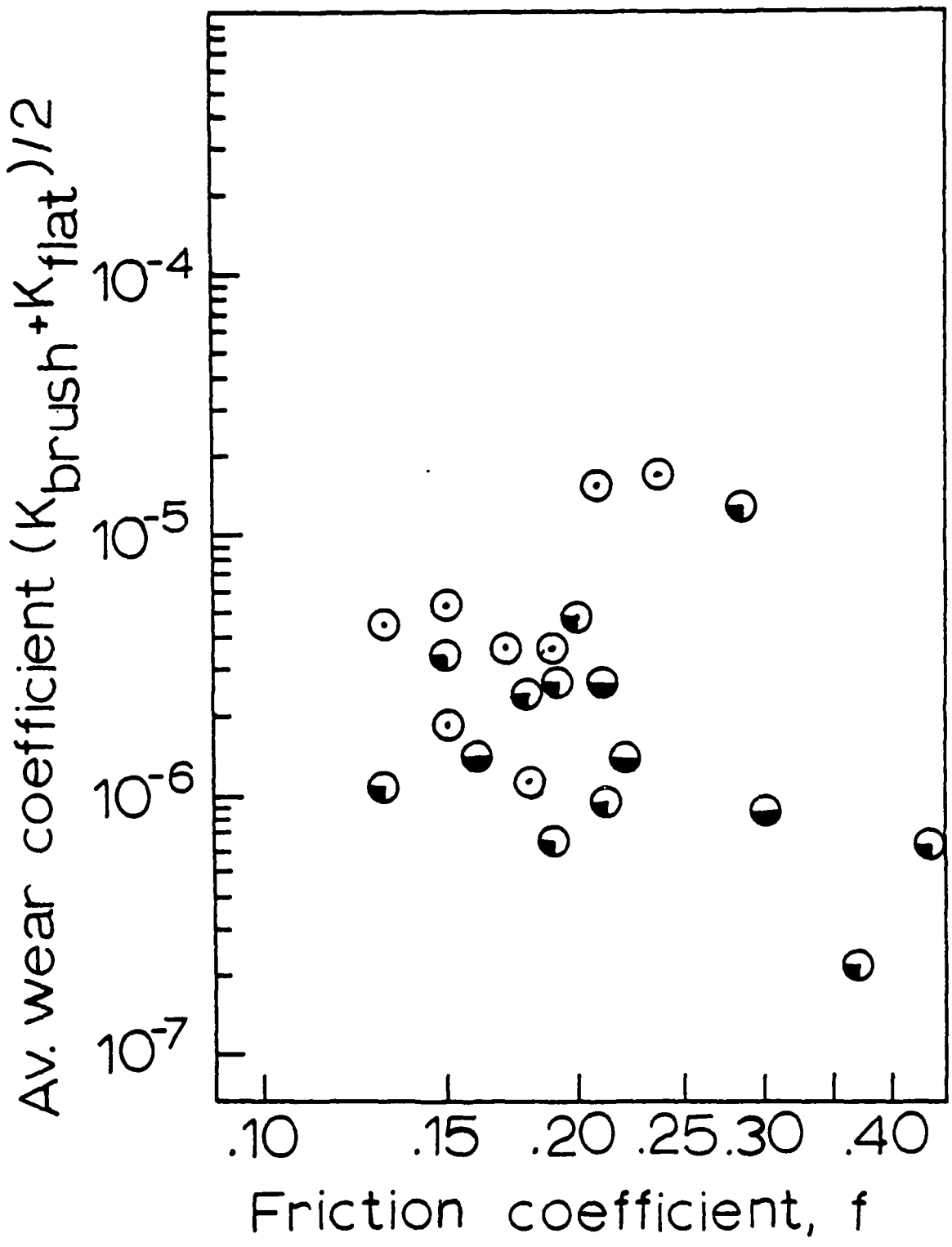

FIGURE 5.12: A PLOT OF THE AVERAGE WEAR COEFFICIENTS VERSUS THE FRICTION COEFFICIENTS FOR PURE GRAPHITE BRUSH TESTS (EXCEPT THE 8 M/SEC SET OF TESTS)

smaller friciton coefficients than the silver brushes. The pure graphite brushes are capable of providing a better graphite layer, which aids in reduction of friction.

Another observation from Table 5.6 is that the tests performed at no current result in higher friction coefficients than those run with a current of 50 A. Figure 5.13 shows a plot of friction coefficients versus current level for the silver graphite on iridium experiment discussed before. The friction drops linearly from 25 A to 75 A. The drop in friction can be attributed to the decrease of the local shear strength of the brush material as a result of higher temperatures at high currents.

5.3 PARAMETERS INFLUENCING THE ELECTRICAL CONTACT RESISTANCE OF SLIP RINGS

Figure 5.14 shows the correlation between the incompatibility ratings of the flat metals against the brush and the average contact resistances for the silver graphite brush tests. The correlation of 0.37 suggests that the compatible combinations tend to have smaller contact resistance values than the incompatible combinations, which can be expected due to higher mutual attraction between the brush and the commutator. However the correlation is not strong because of many other parameters influencing the contact resistance. For instance 5.15 shows that the contact resistance for silver brushes increases with wear with a correlation of 0.35. Also the oxide forming metals produce higher contact resistances, as shown in Table 5.1. The contact resistances for the tests performed in the organic vapor environment result in higher resistances due to the complications from the surface layers.

Figures 5.16 to 5.17 show plots of the average contact resistances for

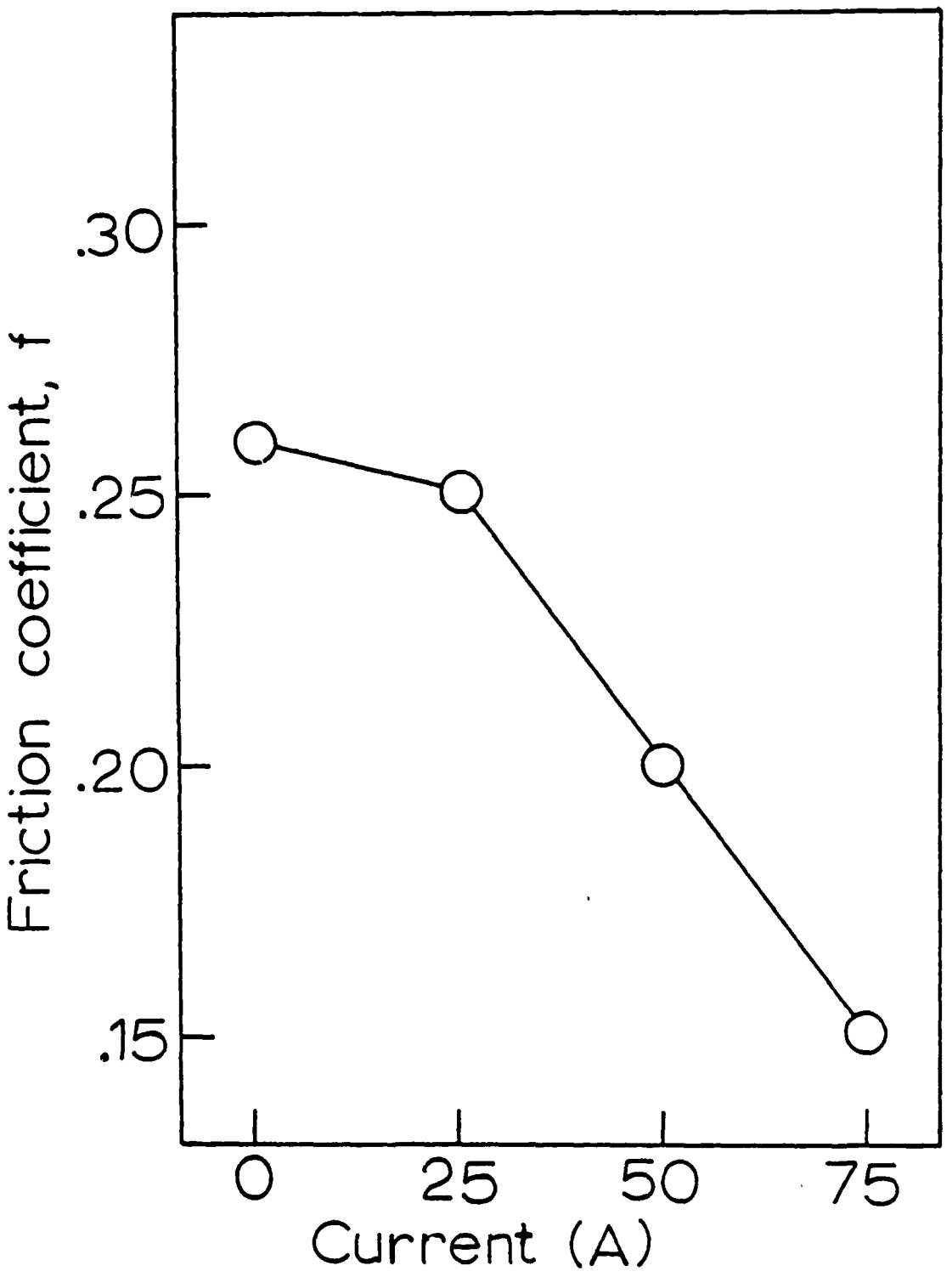

FIGURE 5.13: A PLOT OF THE BRUSH FRICTION COEFFICIENTS VERSUS CURRENT LEVEL FOR A SILVER GRAPHITE BRUSH SLIDING ON AN IRIDIUM FLAT TEST PERFORMED IN WET CO_2, AT A LOAD OF 300 g, A SPEED OF 4 M/SEC

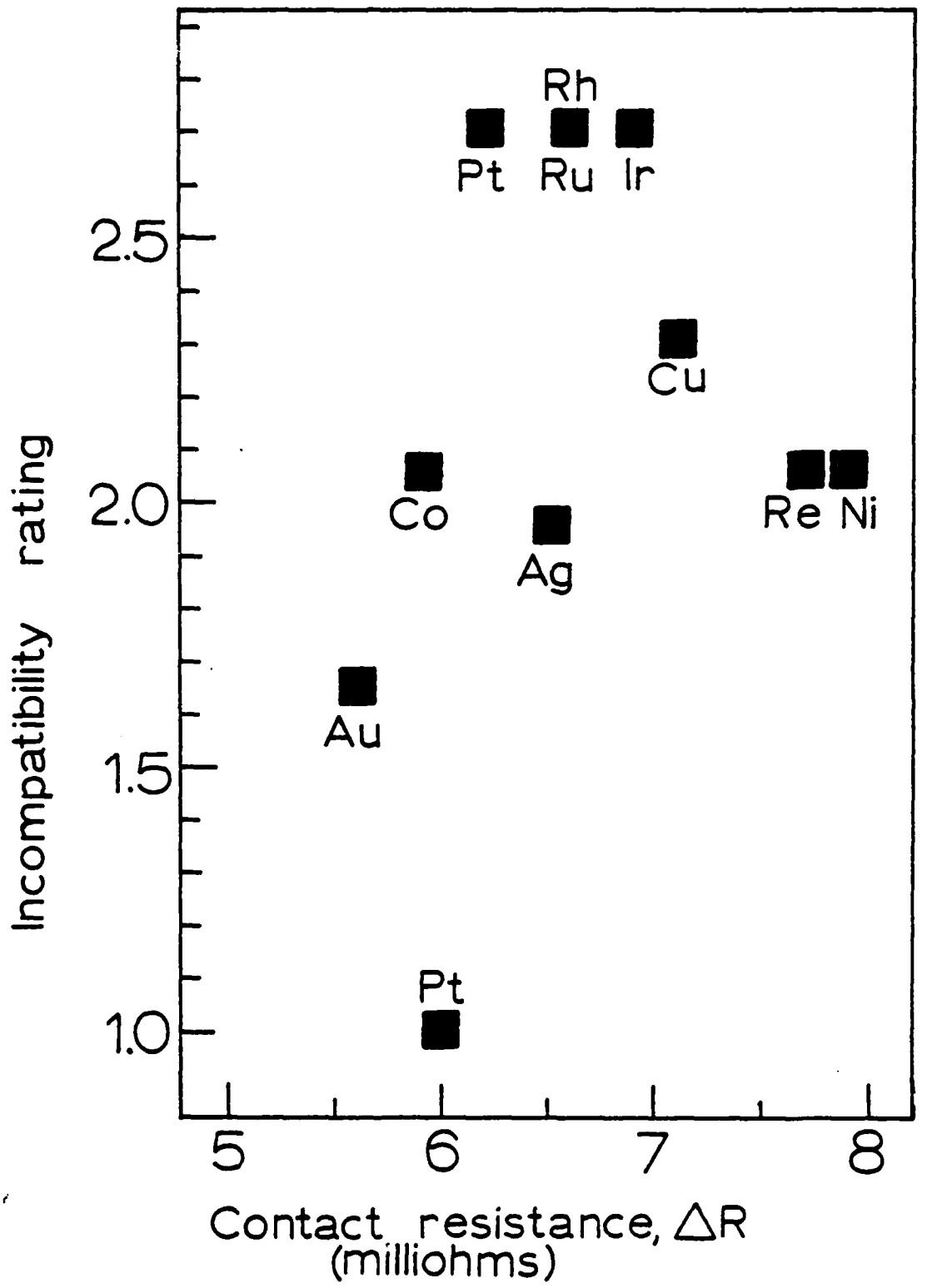

FIGURE 5.14: A PLOT OF THE AVERAGE CONTACT RESISTANCES VERSUS THE INCOMPATIBILITY RATING OF THE FLAT MATERIALS AGAINST THE BRUSH FOR SILVER GRAPHITE BRUSH TESTS (EXCEPT THE SET OF TESTS AT NO CURRENT)

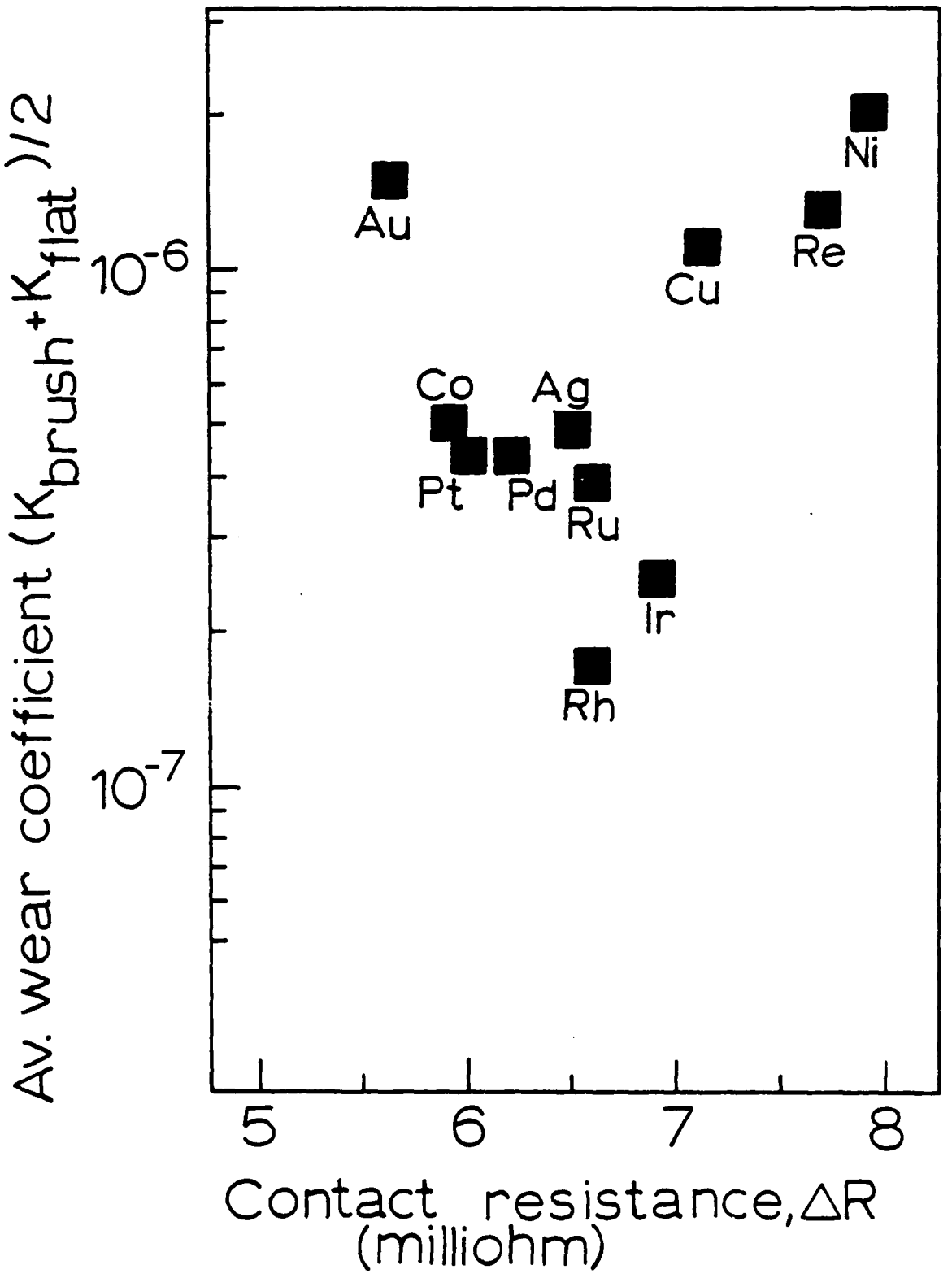

FIGURE 5.15: A PLOT OF THE AVERAGE WEAR COEFFICIENTS VERSUS THE AVERAGE CONTACT RESISTANCES FOR SILVER GRAPHITE BRUSH TESTS (EXCEPT THE SET OF TESTS AT NO CURRENT)

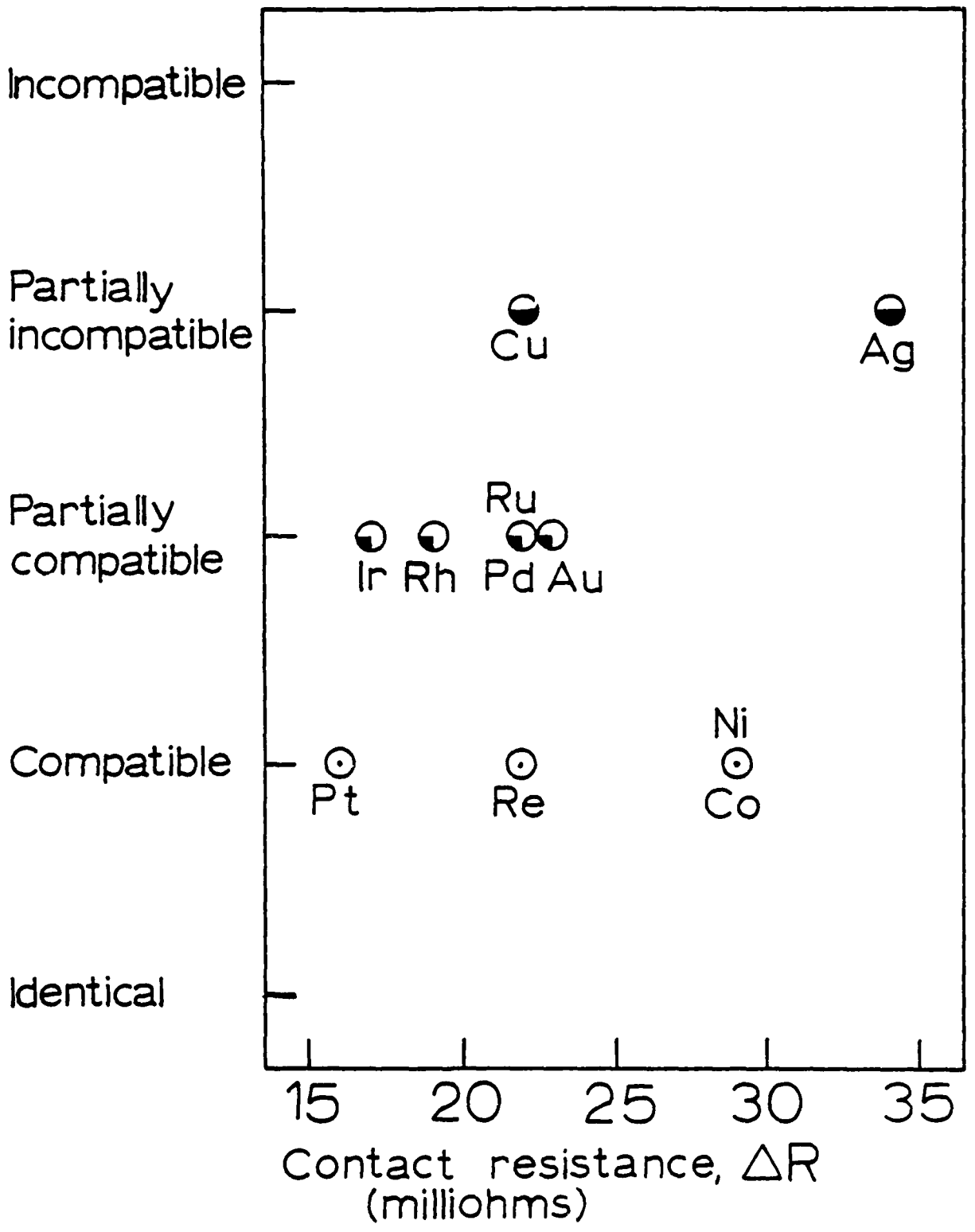

FIGURE 5.16: A PLOT OF THE AVERAGE CONTACT RESISTANCES VERSUS THE COMPATIBILITY OF THE FLAT MATERIALS AGAINST GRAPHITE FOR PURE GRAPHITE BRUSH TESTS

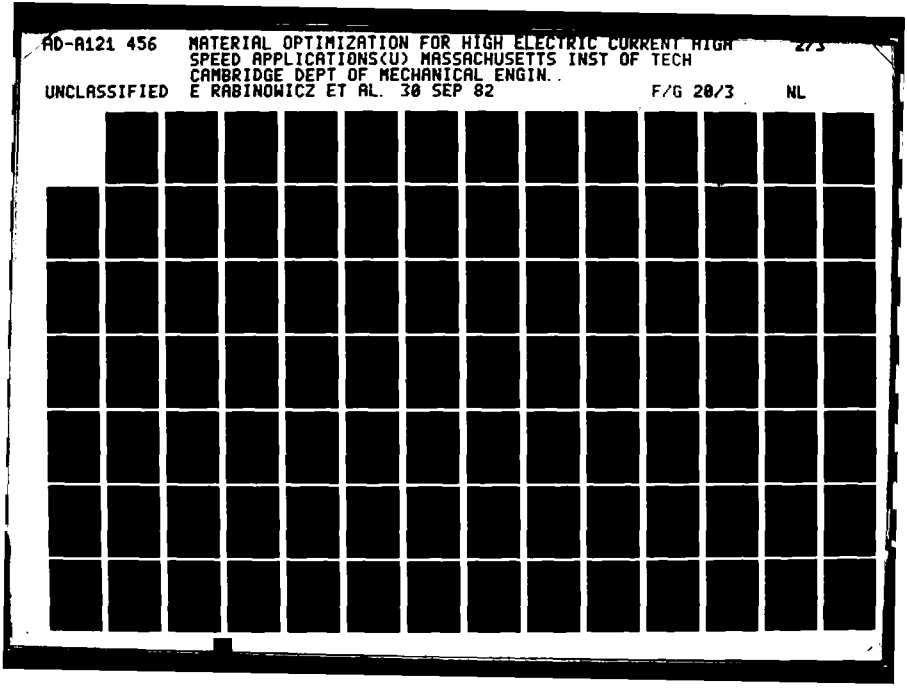
AD-A121 456 MATERIAL OPTIMIZATION FOR HIGH ELECTRIC CURRENT HIGH
SPEED APPLICATIONS(U) MASSACHUSETTS INST OF TECH
CAMBRIDGE DEPT OF MECHANICAL ENGIN..
UNCLASSIFIED E RABINOWICZ ET AL. 30 SEP 82 F/G 20/3 NL

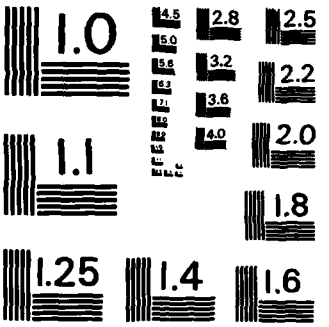

MICROCOPY RESOLUTION TEST CHART
NATIONAL BUREAU OF STANDARDS-1963-A

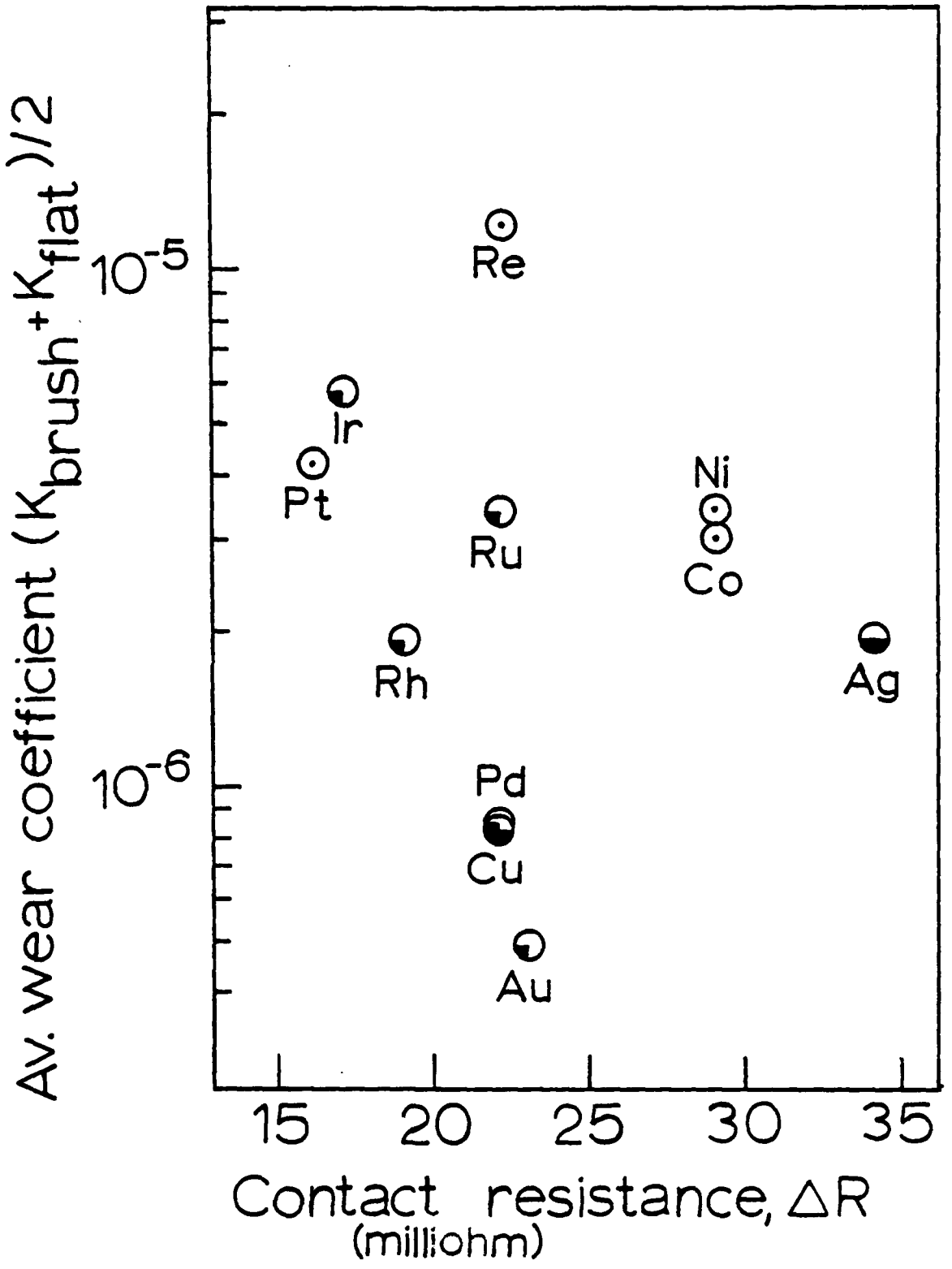

FIGURE 5.17: A PLOT OF THE AVERAGE WEAR COEFFICIENTS VERSUS THE AVERAGE CONTACT RESISTANCES FOR PURE GRAPHITE BRUSH TESTS

pure graphite brushes versus the compatibilities of the slip ring combinations and the wear coefficients respectively. The spread of values for the resistances is larger than for the silver graphite brushes. The spread of values is too large for any general conclusions.

Table 5.7 shows that the contact resistances for the silver graphite brushes are over four times smaller than those for pure graphite brushes. This result is due to the fact that silver has better electrical properties than graphite (i.e. lower resistivity).

VI. CONCLUSION

As the result of tests performed using pure graphite and silver graphite brushes the following conclusions have been reached.

1. The compatibility between the flat metal and the brush significantly influence the behavior of slip ring systems. When the brush material is incompatible against the slip ring metal the wear is lower. In silver graphite systems both graphite and silver have to be included in the compatibility requirements.

2. The friction of slip ring systems is inversely proportional to the wear of the system.

3. Ambient air contains adequate amounts of moisture to provide graphite lubrication and thus low wear rates.

4. Increased current level increases the temperature of sliding, which in turn increases the wear rate but decreases the friction.

5. Increasing the speed by two does not significantly change the performance of the slip ring systems.

6. Silver graphite brush slip ring systems show four times less wear and five times less contact resistance than [illegible]aphite brush systems.

7. The noble metals usually perform better than the oxide forming metals, especially with silver graphite brushes, where silver, palladium, platinum, ruthenium, iridium and rhodium slip rings have wear coefficients two to six times smaller than copper.

VII. RECOMMENDATIONS

A possible direction for future research would be studying the performance of the slip rings as a function of temperature. There are a few ways to observe the temperature dependence. One approach would be to perform the tests on noble metals at much higher speeds than were encountered in this experiment. However, special care should be given to the equipment design for the high speed conditions, since the mechanics of the sliding can significantly influence the brush performance. Another possible approach is the use of higher current densities. It was shown in this report, that iridium slip rings reach a critical current level above which the wear rate is very high. By varying the current levels it would be possible to find the critical value for all of the noble metals. Finally the tests can be run at high ambient temperatures, thus making it easier to estimate the temperature of sliding.

It is possible that the adverse effect due to temperatures approaching the melting point of slip ring metals will be more pronounced with the low melting copper than with other noble metals, which have higher melting points. It would be desirable to measure the interface temperature or to find a reliable model for calculating the temperature. Some of the elements of the model can include the number of the contact asperities, the size of the conducting junctions and their relative positioning.

If the major effect of the current is to raise the temperature of the contact, than cooling of the commutator and/or the brush should allow higher currents to be passed through the interface without increasing the wear.

Finally, the effect of the atmospheric conditions on the performance of the slip rings should be studied in more detail. Tests would have to be performed under different humidities and in different gases. Some impurities can be introduced into the test chamber to see their effect on commutation.

REFERENCES

1. Casstevens, J.M., Rylander, H.G., Eliezer, Z., "Influence of High Velocities and High Current Densities on the Friction and Wear Behavior of Copper-Graphite Brushes," Wear, Vol. 48, 1978, pp 121-130.

2. Lewis, D.L., "Practical Homopolar Machines, Use of Liquid-Metal Slip Rings," Journal of Science and Technology, Vol. 38, No. 2, 1971, pp 46-54.

3. Brennan, M., Eliezer, Z., Weldon, W.F., Rylander, H.G., Woodson, H.H., "The Testing of Sliding Electrical Contacts for Homopolar Generators," Proceedings of the Holm Conference on Electric Contact Phenomena, 1978, Chicago, pp 577-582.

4. McNab, I.R., "Pulsed High Power Brush Research," Proceedings of the Holm Conference on Electric Contact Phenomena, 1977, Chicago, pp 105-114.

5. Johnson, J.L., Moberly, L.E., "High Current Brushes I-Effect of Brush and Ring Materials," Proceedings of the Holm Conference on Electric Contact Phenomena, 1977, Chicago, pp 99-104.

6. Ohmae, N., Rabinowicz, E., "The Wear of the Noble Metals," ASLE Transactions, Vol. 23, No.1, 1978, pp 86-92.

7. Rabinowicz, E., "The Dependence of the Adhesive Wear Coefficient on the Surface Energy of Adhesion," Wear of Materials, 1977, ASME, New York, pp 36-40.

8. Hanson, M., Anderko, K., "Constitution of Binary Alloys," McGraw Hill, New York, 1958.

9. Elliot, R.P., "Constitution of Binary Alloys," First Supplement, McGraw Hill, New York, 1965.

10. Shunk, F.A., "Constitution of Binary Alloys," Second Supplement, McGraw Hill, New York, 1969.

11. Moffatt, W.G., "Binary Phase Diagrams Handbook," General Electric Co., Schenectady, New York, 1976.

12. Savage, R.H., "Graphite Lubrication," Journal of Applied Physics, Vol. 19, No. 1, 1948, pp 1-10.

13. Pardee, R.P., "Moisture Dependence of Silver-Graphite Brushes in Air, Nitrogen, Helium and Carbon Dioxide," IEEE Transactions, Vol. PAS-86, No. 5, 1967, pp 616-625.

14. Lee, P.K., Johnson, J.L., "High Current Brushes II-Effects of Gases and

Hydrocarbon Vapors," Proceedings of the Holm Conference on Electric Contact Phenomena, 1977, Chicago, pp 115-122.

15. Johnson, J.L., Moberly, L.E., "Brush Life and Commutation in Atmospheres of Air, SF_6, and SO_2," Electrical Contacts - 1967, Chicago, pp 109-116.

16. Shobert, E.I. II, "Carbon Brushes," Chemical Publishing Company, Inc., New York, 1965, pp 1-73.

17. Schreurs, J., Johnson, J.L., McNab, I.R., "High Current Brushes, Part VI: Evaluation of Slip Ring Surface Films," Proceedings of the Holm Conference on Electric Contacts, Chicago, 1979, pp 145-151.

18. Holm, R., "Electric Contacts," Springer-Verlag Inc., New York, 1967, pp 199-273.

19. Lancaster, J.K., "The Influence of the Conditions of Sliding on the Wear of Electrographic Brushes," British Journal of Applied Physics, Vol. 13, 1962, pp 468-477.

20. Rabinowicz, E., "Friction and Wear of Materials," John Wiley and Sons, New York, 1965, Ch. 6.

21. Archard, J.F., "Contact and Rubbing of Flat Surfaces," Journal of Applied Physics, Vol. 24, No. 8, 1953, pp 981-988.

22. Rabinowicz, E., "Influence of Surface Energy on Friction and Wear Phenomena," Journal of Applied Physics, Vol. 32, No. 8, 1961, pp 1440-1444.

23. Bowden, F.P., Tabor, D., "Friction and Lubrication of Solids," Clarendon Press, Oxford, Vol. 1, 1950.

24. Clark, W.T., Connolly, A., Hirst, W., "The Friction and Wear of Electrographite," British Journal of Applied Physics, Vol. 14, 1963, pp 20-27.

25. Savage, R.H., Schaefer, D.L., "Vapor Lubrication of Graphite Sliding Contacts," Journal of Applied Physics, Vol. 27, No. 2, 1956, pp 136-138.

26. Millet, J., "Behavior of Carbon Brushes in Dry and Wet Atmosphere," Proceedings of the 4th Conference on Carbon, Buffalo, New York, 1960, pp 727-728.

27. Marshall, R.A., "The Mechanism of Current Transfer in High Current Sliding Contacts," Wear, Vol. 37, No. 2, 1976, pp 233-240.

28. Greenwood, J.A., "Constriction Resistance and the Real Area of Contact," British Journal of Applied Physics, Vol. 17, 1966, pp 1621-1632.

29. Rabinowicz, E., Chan, P., "Wear of Silver Graphite Brushes Against

Various Ring Materials at High Current Densities," Proceedings of the Holm Conference on Electric Contact Phenomena, 1978, Chicago, pp 513-520.

30. McNab, I.R., Johnson, J.L., "High Current Brushes III-Performance Evaluation for Sintered Silver Graphite Grades," Proceedings of the Holm Conference on Electrical Contact Phenomena, 1978, Chicago, pp 493-499.

31. Marshall, R.A., Slepian, R.M., "Pulsed High Power Brush Research III. Experiments at 15.5 MA/m^2 and 277 m/sec," Proceedings of the Holm Conference on Electrical Contact Phenomena, 1978, Chicago, pp 513-520.

32. Brennan, M., Tolk, K.M., Weldon, W.F., Rylander, H.G., Woodson, H.M., "Test Data on Electrical Contacts at High Surface Velocities and High Current Densities for Homopolar Generators," 7th Symposium on Engineering Problems of Fusion Research, Knoxville, Tennessee, 1977, pp 522-526.

33. Dillich, S., Kuhlmann-Wilsdorf, D., "Effect of Surface Films on the Performance of Silver Graphite (75 w/o Ag, 25 w/oC) Electric Brushes," Holm Conference on Electrical Contacts, 1979, Chicago, pp 185-190.

34. Betz, D., "Relationship Between Contact Resistance and Wear in Sliding Contacts," Proceedings of the Holm Conference on Electric Contact Phenomena, 1973, Chicago, pp 164-169.

35. Johnson, J.L., Taylor, O.S., "High Current Brushes, Part IV: Machine Environment Tests," Holm Conference on Electrical Contacts, Chicago, 1979, pp 129-135.

36. Marshall, R.A., Reichner, P., Slepian, R.M., "Current Collection Systems for Pulse Power Homopolar Machines," 7th Symposium on Engineering Problems of Fusion Research, Knoxville, Tennessee, 1977, pp 434-438.

37. Dobson, J.V., "The Effect of Humidity on Brush Operation," Electric Journal, Vol. 32, 1935, pp 527-528.

38. Johnson, J.L., McKinney, J.L., "Electrical-Power Brushes for Dry Inert-Gas Atmospheres," Proceedings of the Holm Seminar on Electric Contact Phenomena, Chicago, 1970, pp 155-162.

39. Moberly, L.E., Johnson, J.L., "Wear and Friction of Carbon Brushes as a Function of Air Humidity," Proceedings of the 4th Conference on Carbon, Buffalo, New York, 1960, pp 711-718.

40. Taylor, O.S., Reichner, P., "Mechanical Load Aspects of High Current Brush System Design," Proceedings of the Holm Conference on Electrical Contact Phenomena, 1978, Chicago, pp 507-512.

41. Cook, N.H., Rabinowicz, E., "Physical Measurement and Analysis," Addison-Wesley Publishing Company, Inc. Reading, Massachusetts, 1963, pp 160-164.

42. Van Vlack, L.H., "Elements of Material Science," Addison-Wesley Publishing Company, Inc., Reading, Mass., 1960, pp 462-466.

43. Lyman, T., et al., "Metals Handbook, Vol. 1, Properties and Selection of Materials," 8th ed., American Society for Metals, 1961, pp 48-49.

APPENDIX: ESTIMATION OF THE TEMPERATURE RISE DURING SLIDING

In order to calculate the temperature rise at the point of contact the contributions of heat input due to frictional heating and due to electrical losses have to be considered separately. According to Rabinowicz[20] the following formula can be used to calculate the temperature rise due to frictional heating:

$$\Theta_m = \frac{fLv^{1/2}}{3.6J(\rho c\, r^3 k)^{1/2}} \qquad (1)$$

where Θ_m is the mean temperature rise at the point of contact, f is the coefficient of friction, L is the normal load, v is the sliding speed, J is mechanical equivalent of heat. Assuming a pin-on-disk geometry, ρc is the volume specific heat for the disk, k is the thermal conductivity of the disk, and r is the radius of the true contact area. Formula 1 can be applied for conditions of high speed sliding.

The temperature rise due to electrical losses can be estimated by modifying equation 1. By rewriting the numerator of the equation as:

$$\frac{fLv}{v^{1/2}}$$

It can be seen that fLv is the frictional power input. For the electrical losses equation the electrical power loss is substituted for the frictional power loss in equation 1 to obtain:

$$\Theta^*_m = \frac{I^2 R}{v^{1/2} 3.6J(\rho c\, r^{3*} k)^{1/2}} \qquad (2)$$

where the star superscript denotes electrical contact conditions, I is the current passing through the contact, and R is the contact resistance. According to Holm the conduction area is only 1% to 10% of the actual mechanical area of contact. It is assumed that the conducting area is 5% of the contact area then:

$$r^* = .2r \tag{3}$$

To estimate r, surface profiles of various slip ring metals tested were obtained. The profiles show from two to fifteen high peaks where contact could take place. An example of one of the profiles is shown in Figure A-1. Ten contacts was assumed to be the average number of contacts. Next it is assumed that the contact points are plastically deformed, and the load carried by the contacts is expressed by:

$$L = 10\pi r^2 p \tag{4}$$

where p is the penetration hardness of the softer material (the brush), then:

$$r = \left(\frac{L}{10\pi p}\right)^{1/2} \tag{5}$$

For a typical test of a silver graphite brush sliding on a gold flat the following parameters apply:

$p = 15\ kg/mm^2$

$L = 300\ g$

$f = 0.29$

$v = 4\ m/sec$

$I = 50\ A$

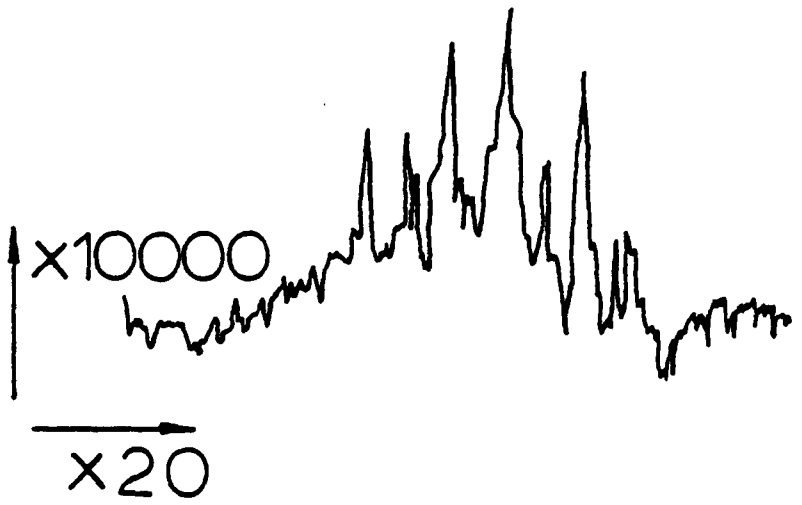

FIGURE A-1: A PROFILE OF A GOLD SLIP RING SURFACE AFTER A TYPICAL TEST. THE BRUSH MATERIAL WAS SILVER GRAPHITE. AT LEAST FIVE HIGH PEAKS CAN BE SEEN WHERE CONTACT COULD TAKE PLACE.

$R = 5.5\ m\Omega$

$\rho c = 202$ in lb/in^3 ^oF

$k = 37.1$ in lb/sec in^2 ^oF/in

For a single contact point from equations 5 and 3

$r = 2.5 \times 10^{-2}$ mm

$R^* = 5 \times 10^{-3}$ mm

The load and the current and the contact resistance for a single contact are:

$$L_i = \frac{L}{10} = 30\ g$$

$$I_i = \frac{I}{10} = 5A$$

$$R_i = 10R = 55\ m\Omega$$

From the expression 1 then:

$$\Theta_m = 15^oC$$

From the expression 2:

$$\Theta^*_m = 625^oC$$

The total temperature rise is about 640^{o}C. The most important conclusion from the temperature results is that the temperature rise due to electrical losses is significantly larger than the temperature rise due to frictional heating. Also the frictional power loss varies with the first power of speed, while the electrical power loss varies with the square of current. This fact explains why the performance of the slip rings did not change significantly when the speed was doubled, but the performance did change for the iridium slip ring when the current was changed from 50 A to 75 A. At

75 A the temperature rise was approaching the melting temperature of the brush, decreasing its strength and thus increasing wear.

It should be noted that many assumptions have been made during the temperature rise calculations, and the values would change when more information about the size and number of contacts is available.

Appendix B

Wear, 78 (1982) 29 - 37

THE TEMPERATURE RISE AT SLIDING ELECTRICAL CONTACTS*

ERNEST RABINOWICZ

Department of Mechanical Engineering, Massachusetts Institute of Technology, Cambridge, MA 02139 (U.S.A.)

(Received November 5, 1981)

Summary

The equations for the temperature rise due to ohmic heating at stationary electric contacts and to frictional heating at sliding electric contacts are combined to give closed-form equations for the temperature rise of sliding electric contacts. The relationship applicable at high sliding speeds indicates that in many cases increasing the sliding speed can reduce the interfacial temperature. An experimental program has been carried out to test the applicability of the equation, using wear tests carried out on graphite–Cu sliding systems in a high temperature friction apparatus to determine the relationship between wear coefficient and surface temperature. Tests using a graphite brush sliding against a copper disk at speeds of around 10 m s^{-1} show that the wear increases with current density, and application of the temperature equation confirms that the wear coefficient is determined by the interfacial temperature, whether that temperature is produced by bulk heating in a furnace, by interfacial heating as a result of sliding or as a result of ohmic heating of the interface.

1. Introduction

In sliding electric contacts carrying very high currents, one of the obvious limitations to the transmittal of even higher currents results from interfacial heating. If the temperature at the interface becomes too great, the materials may soften or even melt, or else excessive oxidation may occur. Associated with effects such as these there is likely to be excessive wear.

In spite of the obvious importance of interfacial heating in the operation of sliding electric contacts, it does not seem that equations for the interfacial temperature of sliding current-carrying contacts are in regular use, nor

*Paper presented at the Advanced Current Collection Conference, Chicago, IL, U.S.A., September 23 - 25, 1981.

Elsevier Sequoia/Printed in The Netherlands

are the way that variables such as velocity or load affect the temperature well known. It is the purpose of this paper to derive such expressions, to illustrate their application to a simple graphite–Cu sliding system and then to test the correctness of the expression experimentally.

2. Theoretical background

The theoretical analysis of the temperature rise at contacting surfaces is generally based on the work of Blok [1] and Jaeger [2], and the relationships obtained by these workers have been discussed and applied to the problem of the temperature rise caused by friction by Archard [3] and Rabinowicz [4]. The temperature rise of electric contacts, especially the static case, has been discussed by Holm [5 - 7], and Shobert [8] has considered also the case of sliding contacts.

Taking first the situation where slow speed sliding occurs and heating is caused by friction, it turns out that if there is a circular region of contact between the sliding surfaces (Fig. 1), the average temperature rise θ is given by the relationship

$$\theta = \frac{fLv}{4Jr(k_1 + k_2)} \tag{1}$$

where J is the mechanical equivalent of heat (a conversion factor from thermal to mechanical units of heat), r is the radius of the junction, f is the friction coefficient, L is the normal load at the junction, k_1 is the thermal conductivity of body 1, k_2 is the thermal conductivity of body 2 and v is the velocity.

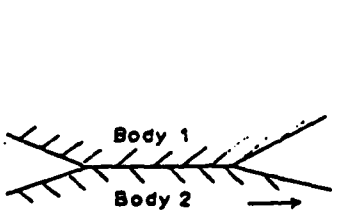

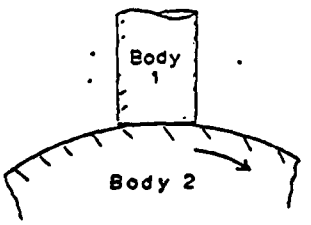

Fig. 1. Schematic illustration of a junction or contact between two solid bodies.

Fig. 2. The system analyzed at high sliding speeds considers a small body 1 always in contact with a large body 2. Points in body 2 only make contact periodically.

This relationship (ref. 9, eqn. (4.14)) assumes that heat originates at the interface and is then conducted into the two adjacent bodies. The reason why the temperature rise is proportional to the velocity is because the rate of heat generation per unit of time is itself proportional to the velocity.

When the sliding speed becomes large this relationship is no longer applicable. Let us consider the simplest case when body 1 is a small specimen while body 2 has an extended surface. In that case the small specimen will be continually in contact and will slide always over fresh areas of the large specimen (Fig. 2). For that case the temperature rise is given by

$$\theta = \frac{fLv^{1/2}}{3.6J(\rho_2 c_2 r^3 k_2)^{1/2}} \tag{2}$$

where f, L, v, r, J and k_2 have the same definitions as above and $\rho_2 c_2$ is the volume specific heat of the extended surface.

This relationship (ref. 9, eqn. (4.16)) differs from the previous one in two ways. First, it is unsymmetrical as regards the top and bottom surfaces because the top surface, being small and continually in contact, soon becomes hot, while the bottom surface, being always fresh, is much cooler, so essentially all the heat travels into it and thus only its thermal properties are significant.

Secondly, it will be noted that velocity to the power one-half comes into eqn. (2). This comes about because as we raise the speed we increase the rate of heating, but we also increase the amount of cool bottom material into which this heat can be dissipated. Thus, it is logical to expect that the temperature rise increases with v but less rapidly than to the first power.

In general, eqn. (1) is applicable when a certain dimensionless parameter $vr\rho_2 c_2/k_2$ is less than 2, while eqn. (2) is applicable when the parameter is greater than 2 [3].

So far we have considered only the frictional heating. As regards electrical heating, Holm (ref. 6, eqn. (11)) states that for a stationary junction the temperature rise (using our terminology) is given by

$$\theta = \frac{i^2 R}{4Jr(k_1 + k_2)} \tag{3}$$

where i is the current carried by the junction and R is the electric resistance of the junction.

This is very similar to the low speed friction temperature rise expression (eqn. (1)) except that i^2R, the electrical heat input per unit of time, has replaced fLv, the mechanical heat input per unit of time. Holm (ref. 7, Section 43) argues that the expression for θ in eqn. (3) should be reduced by a factor of about 2, because the heat input is throughout the constriction (*i.e.* to some extent away from the interface rather than being localized at the interface). However, there are in practice a large number of uncertainties involved. All sorts of corrections might be applied, and it seems best to keep eqn. (3) as simple as possible.

If we add the mechanical and electrical temperature rise terms we have for the overall temperature increase in the slow speed regime

32

$$\theta = \frac{fLv + i^2R}{4Jr(k_1 + k_2)} \tag{4}$$

It is this expression which (although never stated in closed form) is implicitly assumed by Holm and by Shobert.

If we are in the high speed regime then by adding the electrical heating term to eqn. (2) we obtain

$$\theta = \frac{fLv + i^2R}{3.6J(r^3k_2\rho_2c_2v)^{1/2}} = \frac{1}{3.6J(r^3k_2\rho_2c_2)^{1/2}}\left(fLv^{1/2} + \frac{i^2R}{v^{1/2}}\right) \tag{5}$$

In this case the influence of velocity on the temperature is difficult to estimate, since a higher velocity will increase the temperature caused by friction (the first term in parentheses in eqn. (5)) while it will reduce the electrical heating effect (the second term in parentheses in eqn. (5)). Since most tribologists find it hard to believe that raising the sliding speed can lower the interfacial temperature, it seemed appropriate to test eqn. (5) experimentally.

There are some difficulties in measuring the temperature of sliding electric contacts over and above the problems of measuring the interfacial temperature of sliding bodies in general. In particular, the use of the interface as the hot junction of a thermocouple system, often used successfully in friction studies [10], is of course impossible. It was decided to use the fact that in many sliding systems the wear rate increases rapidly when the interfacial temperature reaches a critical point known as the transition temperature, and that this can be used as a measure of the temperature.

3. Experimental testing

3.1. In high temperature friction apparatus

Tests were carried out in the friction apparatus shown in Fig. 3. Three pieces of one material are pressed against a disk of the other material which rotates via the motor and transmission system. The sliding surfaces are inside a metallurgical-type furnace which can be heated up to 1000 °C. The three pieces are loaded by a dead weight and prevented from rotation by a strain ring outside the furnace. The apparatus has been described more completely elsewhere [11].

For these tests, rods of electrographite of 9 mm diameter were slid against a copper disk. The speed of sliding was kept low (0.41 m s^{-1}) so as to keep the temperature rise due to sliding small. The normal load was 1/kgf per rod and the duration of the tests was 0.5 h. Most of the testing was in air, in the spring (*i.e.* at a reasonably high humidity level). Tests in a wet CO_2 environment gave rather similar wear results. The wear was measured for various ambient temperatures and the plot of wear coefficient as a function

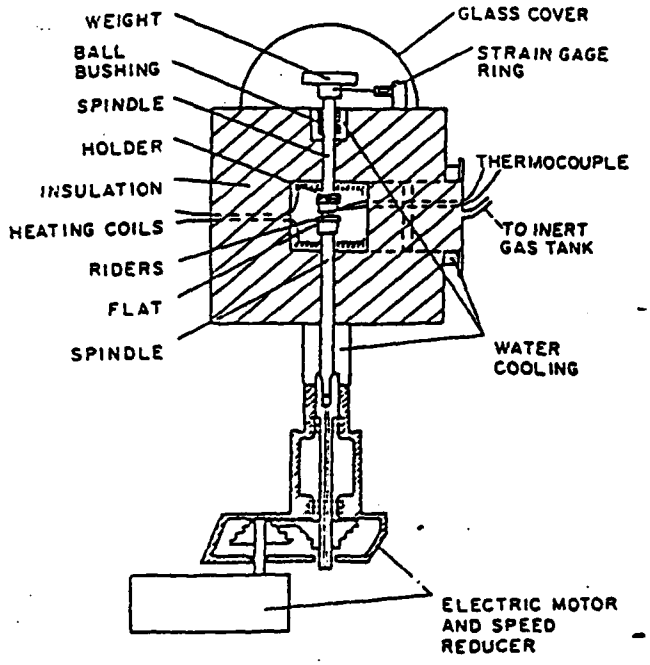

Fig. 3. Schematic illustration of high temperature friction apparatus using the geometry of three pins of graphite sliding against a copper flat.

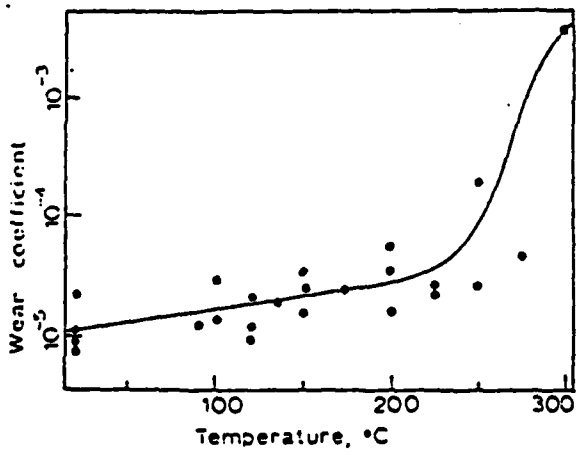

Fig. 4. Plot of the dimensionless wear coefficient for graphite–Cu (the volume of wear multiplied by the hardness and divided by the normal load and the distance of sliding) as a function of the surface temperature in low speed sliding tests carried out using the apparatus shown in Fig. 3. There is a drastic increase in wear as the temperature approaches 300 °C.

of temperature is shown in Fig. 4. The wear coefficient increases drastically when the temperature reaches 300 °C and in general increases monotonically with temperature. Further details of the testing are available [12].

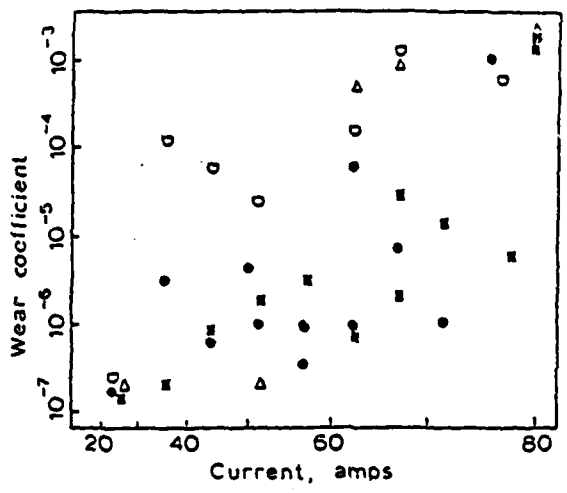

Fig. 5. Plot of wear coefficient as a function of the electric current (on a scale linear in i^2) for various sliding speeds: ○, 1.5 m s^{-1}; △, 5 m s^{-1}; ●, 9 m s^{-1}; ■, 13 m s^{-1}. The low speeds tend to give greater wear for the same current.

3.2. High current sliding tests

These tests were carried out in the high speed friction apparatus described earlier [10], using a pin of graphite on a cylindrical disk of copper. The graphite pin traces out a continuous track on the curved surface of the disk. A high current was passed through the interface, and the wear coefficient was measured after some length of sliding. Both the current and the speed of sliding were varied. The load was 0.7 kgf, the diameter of the electrographite pins was 6 mm, the diameter of the copper disk was 150 mm and the duration of the tests was generally 4 h. Testing was in the ambient air, in the summer (*i.e.* at a high humidity level).

The plot of wear coefficient as a function of current for various sliding speeds is shown in Fig. 5. In general, wear is higher when the current becomes greater, and for any level of current the wear becomes lower as the sliding speed increases.

The wear data were analyzed in terms of eqn. (5), assuming that at the interface there was at any time only one circular contact, whose radius was given by the plastic deformation equation:

$$p\pi r^2 = L \tag{6}$$

where p is the hardness of the softer surface, the graphite.

Figure 6 shows the plot of wear coefficient as a function of temperature computed by the use of eqn. (5). The parameters used in the equation are given in Table 1.

In general, the wear coefficient increases as a function of computed interfacial temperature, slowly at moderate temperatures, but sharply at around 300 °C. The line from Fig. 4 is drawn on Fig. 6 as a broken curve and

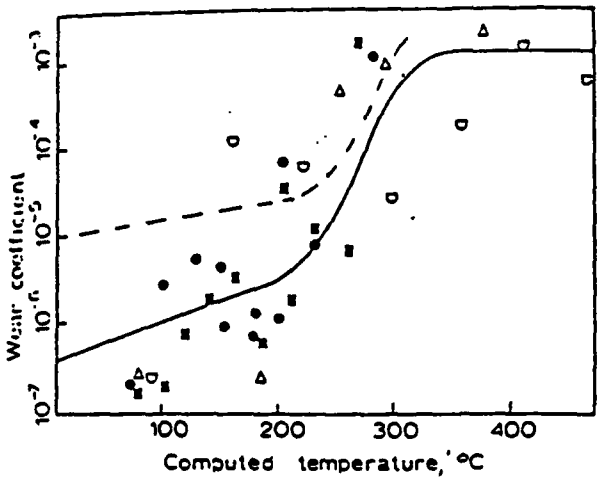

Fig. 6. Plot of wear coefficient as a function of interface temperature computed by the use of eqn. (5) for various sliding speeds: ○, 1.5 m s^{-1}; △, 5 m s^{-1}; ●, 9 m s^{-1}; ▫, 13 m s^{-1}. The scatter of wear rates is much lower than in Fig. 5, the low speed and high speed results are well intermingled, and there is a drastic rise in wear at computed temperatures of just under 300 °C.

TABLE 1

Units and values of the parameters used in eqn. (5)

Parameter	*Unit or value in the following systems*	
	Old engineering units	*Metric units*
f	0.25	0.25
L	1.54 lbf	0.60 kgf
J	1	4.2 W s cal^{-1}
ρc	254 lb in^{-2} $°F^{-1}$	8.2×10^5 cal m^{-3} $°C^{-1}$
k	51 lb s^{-1} $°F^{-1}$	91 cal m^{-1} s^{-1} $°C^{-1}$
r	4.8×10^{-3} in	1.2×10^{-4} m
R	—	21×10^{-3} Ω (W A^{-2})
v	in s^{-1}	m s^{-1}
i	—	A

gives a reasonable fit for the experimental data points at high temperatures, since the experimental data points indicate a drastic increase in wear coefficient in the vicinity of 300 °C. Thus, it seems that the temperatures computed by the use of eqn. (5) are realistic ones.

4. Discussion

The reason why wear coefficients from the high temperature tests shown in Fig. 4 do not fit the experimental data shown in Fig. 6 at low

temperatures is as follows. Stephenson [12] found that at moderate temperatures the wear rate was high for the first hour of testing and was then reduced by about an order of magnitude. His tests were all in the high wear regime, while the tests shown in Fig. 6, being at higher speeds for longer periods of time, were mainly in the low wear regime.

While Holm and Shobert have carried out analyses of the temperature rise of sliding electric contacts which are roughly equivalent to the use of eqn. (5), I have been unable to find any indication that the equation itself has been used, and the remarkable fact that increases in sliding speed can reduce the interfacial temperature of current-carrying contacts seems not to have been previously reported.

In our tests, eqn. (5) seems to give rather accurate values for the temperature rise because of a number of compensating factors. The first of these, mentioned above, is that all the electrical heat is assumed to be generated at the interface, whereas it is in fact generated within the constriction and some of it never reaches the interface. The second factor is that the disk is assumed to be at all times at room temperature, whereas it may become quite warm after extensive sliding. A third factor is that it is assumed that all the heat is carried away from the interface by conduction through the disk, whereas some travels through the pin and some is convected away. This is seen most clearly by noting that in initial tests the pin holder was made of copper, and in this case the pins were distinctly cooler because heat could be more easily dissipated through the holder.

For our top current of 80 A, calculations indicate that at a speed of 77 m s^{-1} the mechanical and electrical energy inputs are equal. Almost all our tests were done in a regime in which the electrical heating exceeded the mechanical, so that the surface temperature–velocity function was negative.

The assumption that the contact between pin and disk was made at only one junction proved surprisingly accurate, possibly because in many cases a thermal patch as postulated by Burton [13] was formed. It should be noted that our pins were of 6 mm diameter. Presumably when brushes of large area are used there are a sizable number of contacts, perhaps about 10 as assumed by Holm. This fragmentation of the contact area would reduce the temperature at the interface to below the value given by eqn. (5).

5. Conclusion

This study started in an attempt to explain an anomaly, namely that in studying the wear of current-carrying Ag–graphite contacts sliding against copper, experiments at Massachusetts Institute of Technology (MIT) [14] were producing more wear that was being experienced at Westinghouse [15], even though our sliding speeds were much lower (4 m s^{-1} at MIT as against 13 m s^{-1} at Westinghouse). It is now clear that the experimental results are perfectly logical in that the surface temperature, and hence the wear, is lower at 13 m s^{-1} than at 4 m s^{-1}.

Acknowledgments

I wish to thank the Office of Naval Research for sponsoring this work, Ms. Jennifer Shandling for carrying out much of the experimental testing, and John L. Johnson and Ian R. McNab of the Westinghouse Corporation for the supply of test specimens and helpful discussions.

References

1 H. Blok, Fundamental mechanical aspects in boundary lubrication, *SAE Trans.*, *46* (1940) 54 - 68.
2 J. C. Jaeger, Moving sources of heat and the temperature at sliding contacts, *J. R. Soc. N.S.W.*, *56* (1942) 203 - 224.
3 J. F. Archard, The temperature of rubbing surfaces, *Wear*, *2* (1959) 438 - 455.
4 E. Rabinowicz, Friction temperatures, *Prod. Eng. (NY)*, (March 30, 1964) 97 - 99.
5 R. Holm, Calculation of the temperature development in a contact heated in the contact surface, and application to the problem of the temperature rise in a sliding contact, *J. Appl. Phys.*, *19* (1948) 361 - 366.
6 R. Holm, Temperature development in a heated contact with application to sliding contacts, *J. Appl. Mech.*, *19* (1952) 369 - 374.
7 R. Holm, *Electric Contacts*, Springer, New York, 4th edn., 1967, Section 21.
8 E. I. Shobert, *Carbon Brushes*, Chemical Publishing Co., New York, 1965, Chap. 7.
9 E. Rabinowicz, *Friction and Wear of Materials*, Wiley, New York, 1965.
10 F. J. Garigan and E. Rabinowicz, Friction and wear at high sliding speeds, *ASLE Trans.*, *24* (1980) 451 - 459.
11 M. Imai and E. Rabinowicz, Lubrication by low-melting-point metals at elevated temperatures, *ASLE Trans.*, *6* (1963) 286 - 294.
12 D. Stephenson, Wear of high speed, high current density slip ring materials at elevated temperatures, *S.B. Thesis (Mech. Eng.)*, Massachusetts Institute of Technology, June 1981.
13 R. A. Burton, Thermal deformation in frictionally heated contact, *Wear*, *59* (1980) 1 - 20.
14 E. Rabinowicz and P. Chan, Wear of silver-graphite brushes against various ring materials at high current densities, in *Proc. Conf. on Electrical Contacts, 1979*, Illinois Institute of Technology, Chicago, IL, 1979, pp. 123 - 127.
15 I. R. McNab and J. L. Johnson, High current brushes — III — performance evaluation for sintered silver-graphite grades, in *Proc. Conf. on Electrical Contacts, 1978*, Illinois Institute of Technology, Chicago, IL, 1978, pp. 493 - 499.

Appendix
C-2

THE INTERFACIAL TEMPERATURE RISE OF SLIDING, ELECTRICAL CONTACTS

by

JEANNE M. TANNER

Submitted to the Department of Mechanical Engineering on April 26, 1982 in partial fulfillment of the requirements for the Degrees of Bachelor of Science in Mechanical Engineering and Master of Science

ABSTRACT

The interfacial temperature rise of dry sliding, electrical contacts was measured using the dynamic thermocouple technique. The response of a dynamic thermocouple cannot be recorded while an electric current flows across the sliding interface. A dynamic thermocouple composed of the contact materials, graphite on copper, monitored the temperature decay of the sliding, electrical contacts after the heat generating equipment was turned off. The temperature decay curves were extrapolated back to when both the frictional and electrical sources were supplying heat to the contacts.

Good agreement between experimental data and theory was achieved depending upon the number of contacts assumed per brush. Further research should be conducted with particular attention paid to the number of contacts formed at the interface.

Thesis Supervisor: Dr. Ernest Rabinowicz
Title: Professor of Mechanical Engineering

ACKNOWLEDGMENTS

I sincerely wish to thank Prof. Ernest Rabinowicz for his valuable guidance throughout the course of this study.

I also wish to thank Fred Anderson, Ralph Whittemore, Bob Kane, and Fred Cote for sharing their machining experience with me and special thanks to Mike Demery and John Ford for their help in solving equipment problems.

Finally, I wish to especially thank my fiance Richard Parnas for his many helpful comments during this study, and his unflagging support of my work.

TABLE OF CONTENTS

LIST OF TABLES

LIST OF FIGURES

NOMENCLATURE

a : reciprocal of time constant

b : half length of contact

c : specific heat

f : friction coefficient

I : current

J : mechanical equivalent of heat

k : pre-exponential factor

K_1 : thermal coefficient of graphite

K_2 : thermal coefficient of copper

L : Jaeger's dimensionless parameter

Q,q : heat generated/ unit time/ unit area

r : radius of a circular contact

R : constriction resistance

v : sliding speed

W : load

z : Holm's dimensionless parameter

θ : average temperature of contact surface

θ_0 : average temperature of contact surface at time equal to infinity

χ : $K/\rho c$

ρ : density

I. INTRODUCTION

The interactions between the surfaces of sliding, electrical contacts are important from both a practical as well as an academic point of view. In order to understand more about friction and wear, we must first understand the nature of the dynamic interface. One of the important basic processes occurring at the interface is the generation of heat and the corresponding temperature rise.

High speed sliding results in significant frictional heating which may lead to thermoelastic instability[1]. This mode of failure has been recognized in the sliding gas path seals of turbine engines, the high energy disk brakes of aircraft, and certain thrust bearing and face seal applications. Another example of failure due to frictionally heated contacts is encountered in gearing situations, where the high temperatures are due to the frictionally heated Hertzian contacts[1].

Recent interest in pulsed homopolar generators and smaller, more compact electric motors has directed research towards brush systems that can withstand high current densities and high sliding speeds. Homopolar generators that can operate at speeds from 200 to 300 m/s with current densities of 17MA m^{-2} for pulse durations of 30 to 65 ms are envisioned[2]. These advanced homopolar machines greatly depend upon the development of brushes able to operate under these conditions. Here temperature related phenomena, such as thermoelastic instability, will dominate the friction and current transfer processes.

Most of the research on the interfacial temperature rise of sliding contacts has dealt with frictionally generated heat only. Jaeger[3] derived the temperature rise as generated by a plane heat source over the area of contact, and particularized it to the case of frictionally generated heat. Later investigators used a variety of methods, such as embedded thermocouples, surface transformations, and dynamic thermocouples, to attempt to measure this temperature rise.

Holm[4] studied electric contacts, especially static, in great depth. He derived a relationship for the temperature rise of electrical contacts and then extended this relationship to the case of sliding contacts. Schobert[5] superimposed the results of these two calculations to arrive at the temperature rise of sliding, electrical contacts. Rabinowicz[6] has examined both sliding contacts and sliding, electrical contacts from a theoretical standpoint and has merged the formulations of Holm and Jaeger into a closed-form equation for the interfacial temperature rise of sliding, electrical contacts.

There is a decided lack of experimental data on the temperature rise of sliding, electrical contacts. This study was conducted to rectify this situation. The dynamic thermocouple technique was chosen as the simplest, most reliable, and economically feasible method for measuring the interfacial temperature. Briefly, the dynamic thermocouple metho n-sists of using two dissimilar metals for the sliding bodies, and measuring the thermoelectric voltages generated by the rise in contact temperature. This method poses a unique prob-

lem when the sliding contacts are also electrically heated. Rather than attempt to filter out the thermocouple's millivolt output from the voltage drop of the heat generating current, it was decided to measure the interfacial temperature decay immediately after all power was shut off. The decay curve was then extrapolated back to time zero, i.e. when the average temperature of the contact surface was at its maximum.

This chapter provides a general introduction to this paper. Chapter Two provides an historical and theoretical background for the research that was conducted. Chapter Three describes the experimental apparatus and procedure. Chapter Four details the extrapolation procedure used to obtain the maximum average surface temperatures and then lists these results. Chapter Five discusses the experimental results.

II. LITERATURE REVIEW

The theoretical basis for most of the work done on the interfacial temperature rise of sliding contacts was formulated by Blok[7] and Jaeger[3]. Jaeger derived the case of a semi-infinte slider, with a square contact, moving over the surface of another semi-infinite substance (Figure 1). Jaeger's basic assumptions were: i) a plane heat source, over the instantaneous contact area, liberated heat at a constant rate, and ii) there was no heat loss from the non-conducting surfaces. The equation for the heat flow over the contact surface of the sliding body was then derived by assuming a stationary heat source. Jaeger assumed a moving heat source in order to derive the equation for the heat flow into the stationary body.

Of the total heat generated, a fraction flows into the sliding body and the remaining fraction of heat flows into the stationary body. Jaeger determined the proportion of heat flow into each body by assuming that the average temperature over the area of contact was the same for each body.

At low speed, the heat source moving over the stationary body moves so slowly that the temperature distibution of a stationary heat source is established in the stationary body. The resulting equation for the average temperature over the area of contact is

$$.946\ q\ b\ /(K_1+K_2). \qquad (1\text{-II})$$

At high speeds, the temperature distribution of a stationary heat source is not established, and the average temperature over the area of contact is

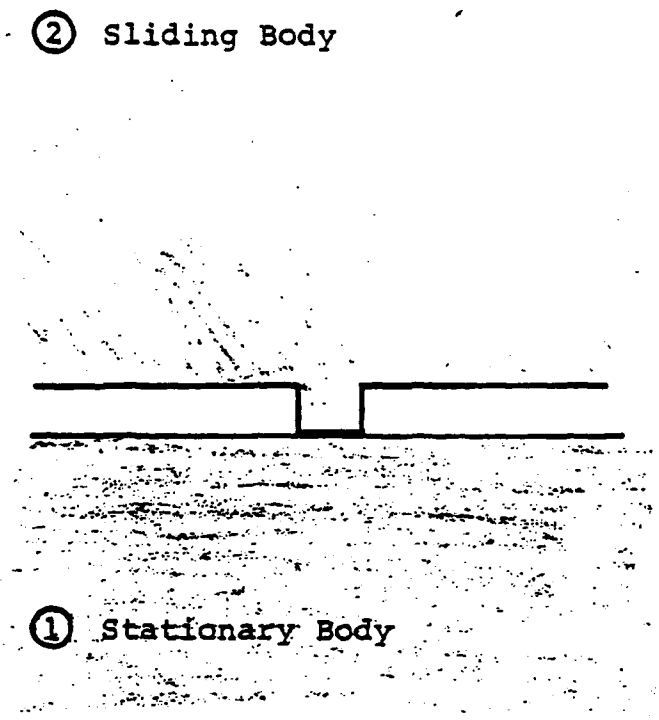

Figure 1. A semi-infinite slider(2) with square contact slides with velocity v on a semi-infinite stationary body(1).

$$1.064\ q\ b\sqrt{\chi_1}\ /\ (1.125\ K_1\sqrt{\chi_1}+K_2\sqrt{bv}). \qquad (2\text{-II})$$

The low speed regime occurs when the dimensionless parameter

$$L=vb/2\chi \qquad (3\text{-II})$$

is less than .1 according to Jaeger. The high speed regime occurs when L>5.

When .1<L<5, the equation of heat flow is solved numerically. The average temperature over the area of contact is then obtained from

$$.946\ q\ b\ \chi_1\ Y\ /(1.486\ b\ K_1\ v\ +\ K_2\ \chi_1\ Y) \qquad (4\text{-II})$$

where Y can be obtained graphically (Figure 2).

Later investigators have applied Jaeger's relationships to the case of frictionally generated heat. Archard[8] extended Jaeger's work one step further and arrived at a completely graphical solution for obtaining the flash temperatures for all values of the dimensionless parameter L (Figure 3).

Holm extensively studied the case of electrically heated contacts. Following a simpler mathematical approach than that taken by Jaeger, Holm[9-10] derived the equation for the temperature rise of a stationary contact heated in the contact surface

$$\frac{Q}{2\pi Kb}\left[\ 1\ -\ \frac{1}{\sqrt{\pi z}}\left(\ 1\ -\ \frac{1}{2z}\right)\ \right] \qquad (5\text{-II})$$

where

$$z\ =\ K\ t\ /\ c\ b^2 \qquad (6\text{-II})$$

is a dimensionless parameter of time. For sliding contacts Holm based the computations on the relationships for the

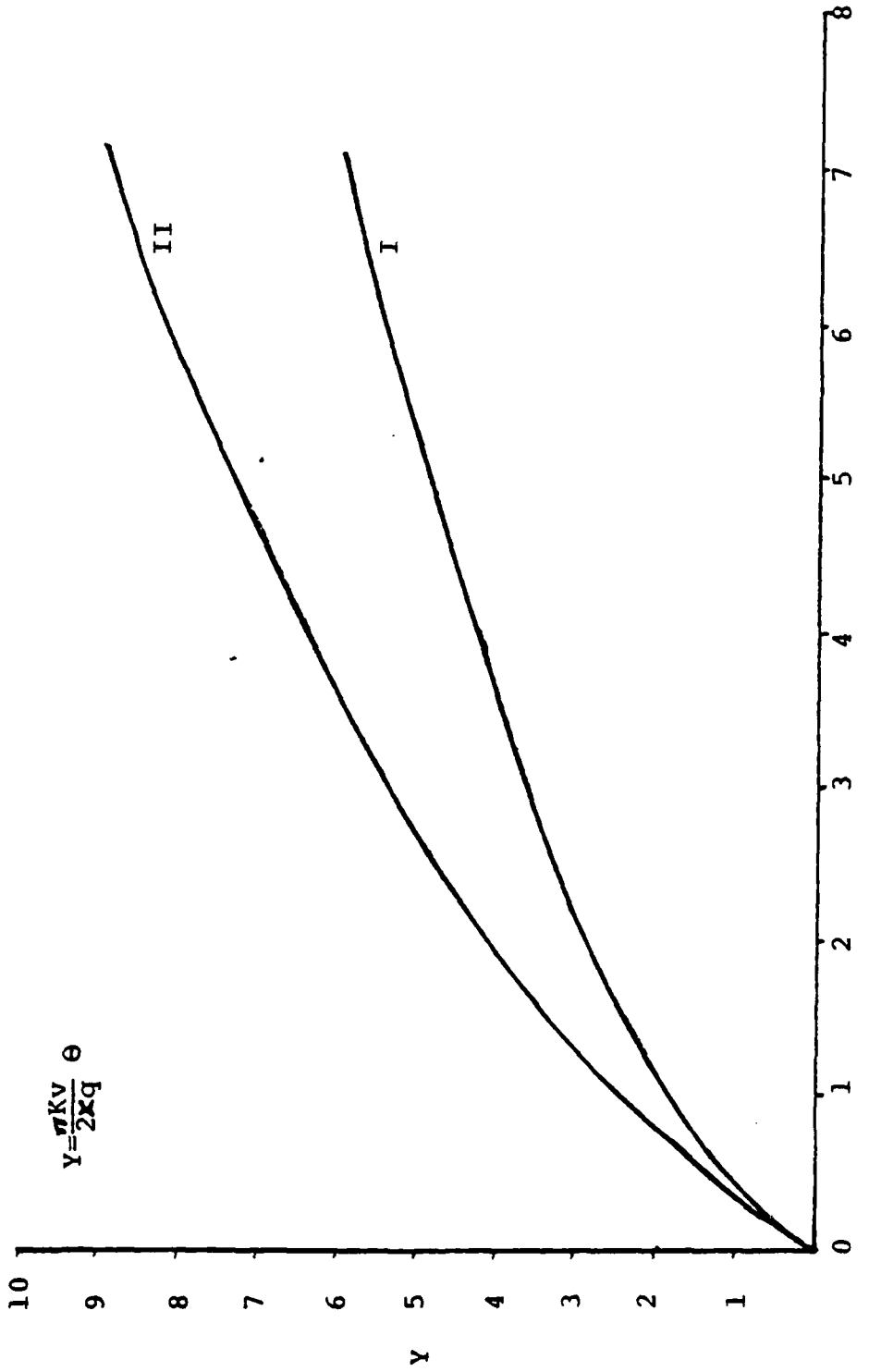

Figure 2. Average temperature for a square source (I), and maximum temperature for a square source (II). Based on Jaeger[1], Figure 7.

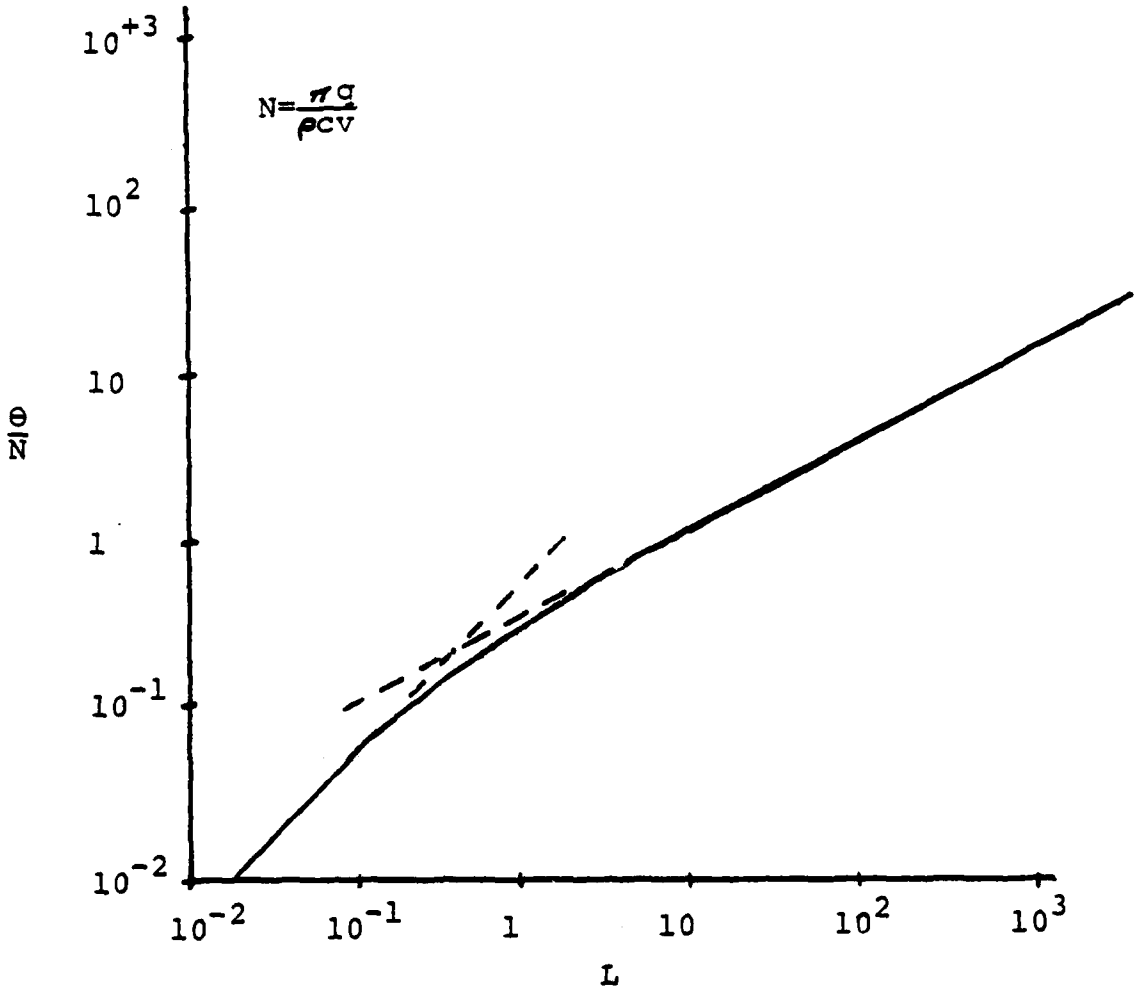

Figure 3. Average surface temperature of a moving heat source as a function of Jaeger's dimensionless parameter 'L'. From Archard[8], Figure 2.

stationary contact. But now the time which the stationary heat source is applied is of the same duration as the average time of sliding over the contact area.

Schobert[5] made the assumption that the temperature rise due to electrical heating could be added to the temperature rise due to frictional heating, although these temperature rise calculations are carried out separately and graphically. Schobert carried out Holm's relationships in considerable numerical detail for several applications.

Rabinowicz[6] extended the work of both Jaeger and Holm to arrive at a closed-form equation for the temperature rise of sliding, electrical contacts. Like Schobert, Rabinowicz assumed that the remperature rise due to both frictional and electrical heating could be simply added together. Following Jaeger's derivation, this is the same as assuming that the temperature rise due to electrical heating is generated at a plane heat source over the surface area of contact. Assuming a single, circular contact, Rabinowicz's relation for the low speed regime is

$$(f W v + I^2 R)/ 4 J r (K_1 + K_2). \qquad (7\text{-II})$$

For the high speed regime

$$(f W v + I^2 R)/ 3.6 J (r^3 K_2 \rho_2 c_2)^{1/2}. \qquad (8\text{-II})$$

Rabinowicz defines the low speed regime as $L<2$, and the high speed regime as $L>2$.

Experimental studies of the surface temperatures reached during sliding have been performed by several researchers.

One technique is the use of thermocouples embedded near the surfaces of the sliding bodies. This yields questionable results for two reasons: i) the embedded thermocouples interfere with the heat flow, and ii) the temperatures measured could be considerably below the temperatures reached at the surfaces. According to Jaeger, the penetration of the heat perpendicular to the plane of the source is extremely shallow.

Another technique is to examine the transformations that occur at the sliding surfaces and relate these transformations to the maximum temperatures reached. Archard[8] was able to determine the conditions under which the thermal breakdown of thermoplastics would occur and then relate this softening point to the theoretical maximum temperatures. Uetz and Sommer [11] examined the martensitic transformations in steels and compared the temperatures at which these transformations occur to experimentally and theoretically determined temperature rises. The temperature reached based upon the transformation was in good agreement with temperatures calculated using Archard's solution. At the same time, the transformation temperature was almost twice as high as the temperatures measured by the dynamic thermocouple technique.

The dynamic thermocouple, or the Herbert-Gottwein method, for measuring the temperature rises of frictionally heated surfaces has been used by several researchers. Furey[12] studied the temperature rise of sliding contacts using both the dynamic thermocouple technique and embedded thermocouples.

He concluded that the dynamic thermocouple measured the temperature of the peaks or asperities in contact, and therefore was a measure of the hottest temperature. The embedded thermocouples integrated the temperature over a larger area than just the asperities in contact and therefore recorded a lower temperature. Even so, Furey found that the temperatures measured by the dynamic thermocouple technique were quite a bit lower than those calculated from Jaeger's and Archard's relationships. Furey offered a few reasons why this might be so: i) the growth of the contact area due to the application of a tangential force, ii) if there is more than one contact point, the measured emf is an average value, iii) in most cases the sliding body makes multiple traverses over the same track, and iv) heat losses could occur due to convection, radiation, or melting of the substances. Holm and Schobert were able to arrive at reasonable values from theoretical calculations by assuming more than one contact. Dayson[13] assumed large scale adhesion and junction growth at the contacting asperities. He then reinterpeted Furey's data and achieved a much closer correlation between theory and experimental data.

Literature pertaining to the experimental measurement of the temperature rise of the contact surfaces of sliding, electrical contacts is extremely scarce. Dow, Stockwell and Kannel [14] investigated the thermomechanical effects in high-current-density electrical slip rings. They used an infrared temperature monitor to measure the temperature of a 1.3 mm spot near the rubbing edge of the brush. No attempt was made to

correlate this data to theory. Marshall[15] investigated the mechanism of current transfer in high current sliding contacts. Embedded thermocouples placed 2 mm beneath the surface were used to measure the temperatures reached during a high current pulse. Aside from the previous drawbacks mentioned, Marshall must have electrically isolated the embedded thermocouples and therefore further interfered with the flow of heat. It is assumed that Marshall was not attempting to measure the interfacial temperature rise, but rather the relative temperature distribution across the face of the brush.

A thermocouple generates a voltage, referred to as the Seebeck thermal emf, as a result of the temperature difference at its two junctions. This Seebeck emf is the algebraic sum of two other voltages: the Peltier emf and the Thompson emf. The Peltier effect relates the direction and magnitude of the flow of current across a junction of two dissimilar metals to the absorption or liberation of heat. The Thompson effect relates the direction and magnitude of the current flow to the direction and magnitude of the heat flow within each of the conductors[16].

The temperature-emf relationships of thermocouples can not be theoretically derived and therefore must be empirically determined. This relationship can be closely approximated by a parabolic curve[16].

Classical thermocouple theory states that the thermal emf developed in a thermocouple is independent of the temp-

erature gradient within the dissimilar conductors[16]. This is based upon the assumption that the conductors are ideally homogeneous. In actuality, a thermocouple integrates the temperature gradients between the junctions[17]. This implies that a change in the metallurgical state of the conductors during use could throw the calibration off[17].

III. EXPERIMENTAL APPARATUS AND PROCEDURE

Approximately ninety tests were conducted to measure the interfacial temperature rise of a dry sliding, electrical contact. A graphite pin slid over a copper disk. Tests were conducted at loads of 500, 750, and 1000 grams; at speeds of 0, 1, and 10 meters per second; and at currents of 0, 10, 30, 40, 45, 50, 55, 60, 65, and 70 amperes. Figure 4 shows the range of the experiments. The tests were carried out at room temperature, 20°C, during the winter months, i.e. relatively low humidity.

The experimental apparatus can be divided into two main parts: the mechanical pin-on-disk wear tester (Figure 5), and the dynamic thermocouple system (Figure 6). The pin-on-disk wear tester has been extensively used and described before[18]. Basically, it is an inverted, variable-speed Rockwell drill press. The copper disk is bolted to the rotating spindle. The graphite pin is spring loaded against the surface of the rotating copper disk. A simple pulley and weight system in conjunction with a micrometer allows the spring load on the graphite pin to be varied.

The interfacial temperature rise measurement system was based on the principle of the Herbert-Gottwein dynamic thermocouple. The pin and disk materials composed the thermocouple. In order to pass the heat generating current across the graphite-copper interface, i.e. the same contact that comprised the hot junction of the dynamic thermocouple, the thermocouple had to be part of the power supplying circuit. As can be seen from Figure 5, current from a Marin Company high-current, low-voltage

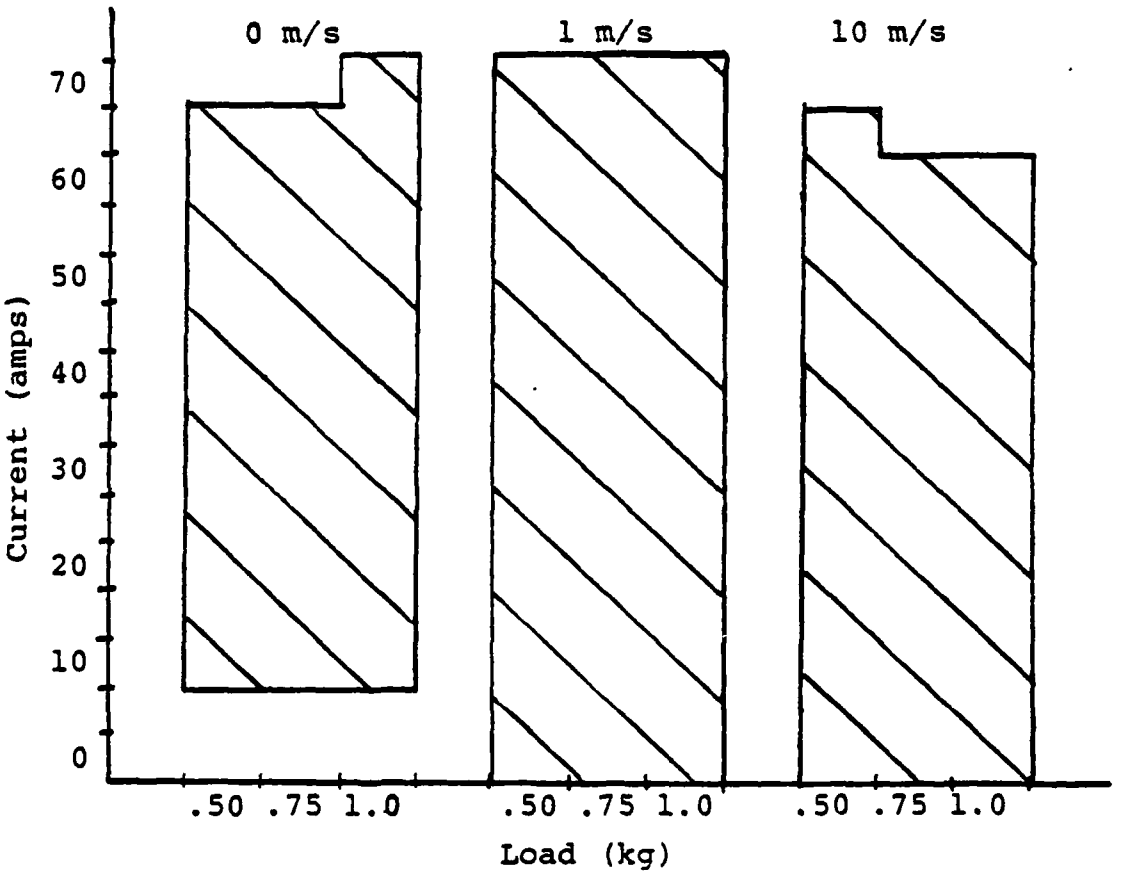

Figure 4. Range of experiments conducted during this study.

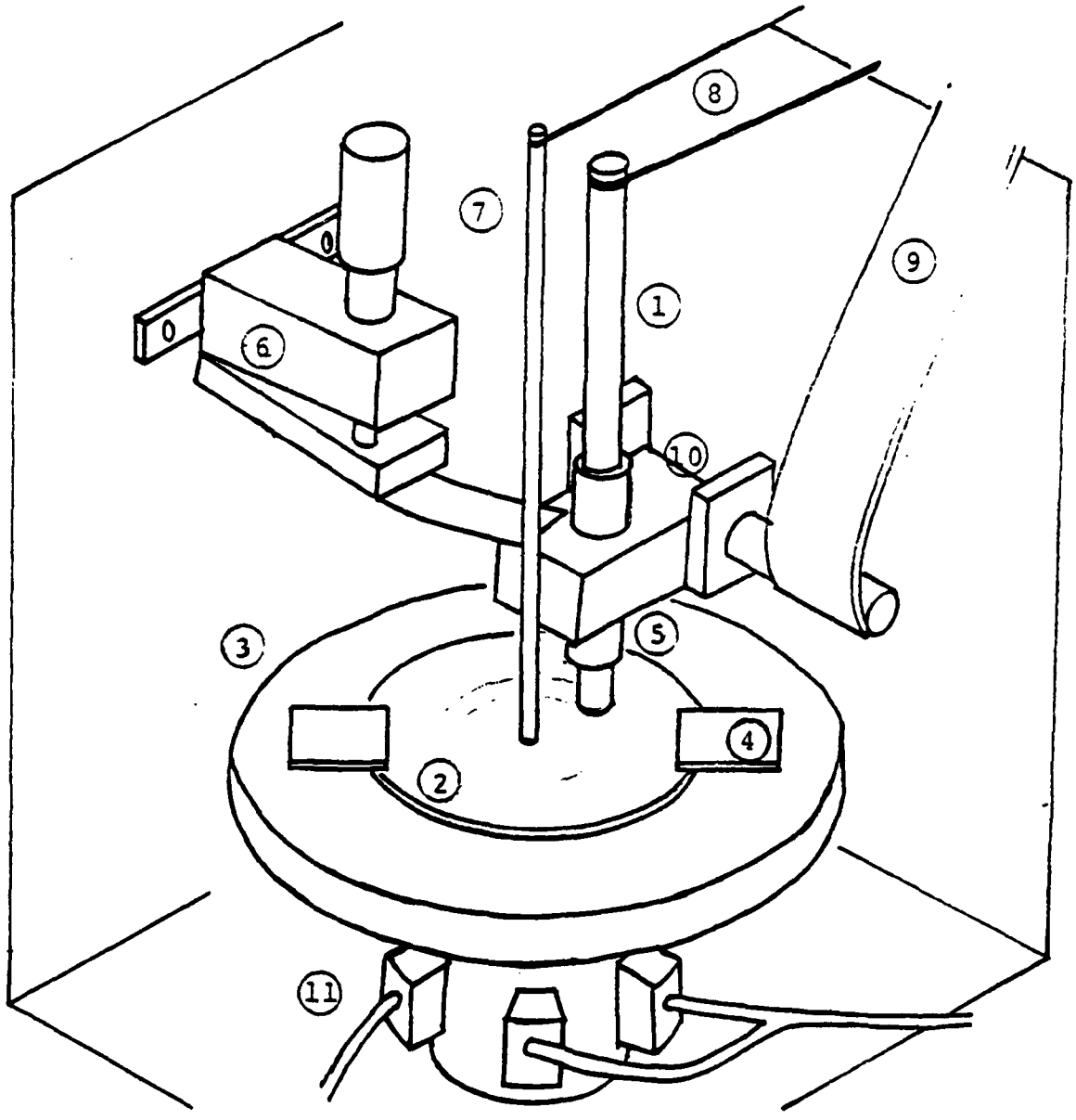

(1) Graphite pin
(2) Copper disk
(3) Rotating mount
(4) Clamps
(5) Brush holder
(6) Loading mechanism
(7) Copper rod
(8) Copper thermocouple wires
(9) Flexible cable
(10) Pivoting arm
(11) Copper brushes

Figure 5. Diagram of experimental apparatus.

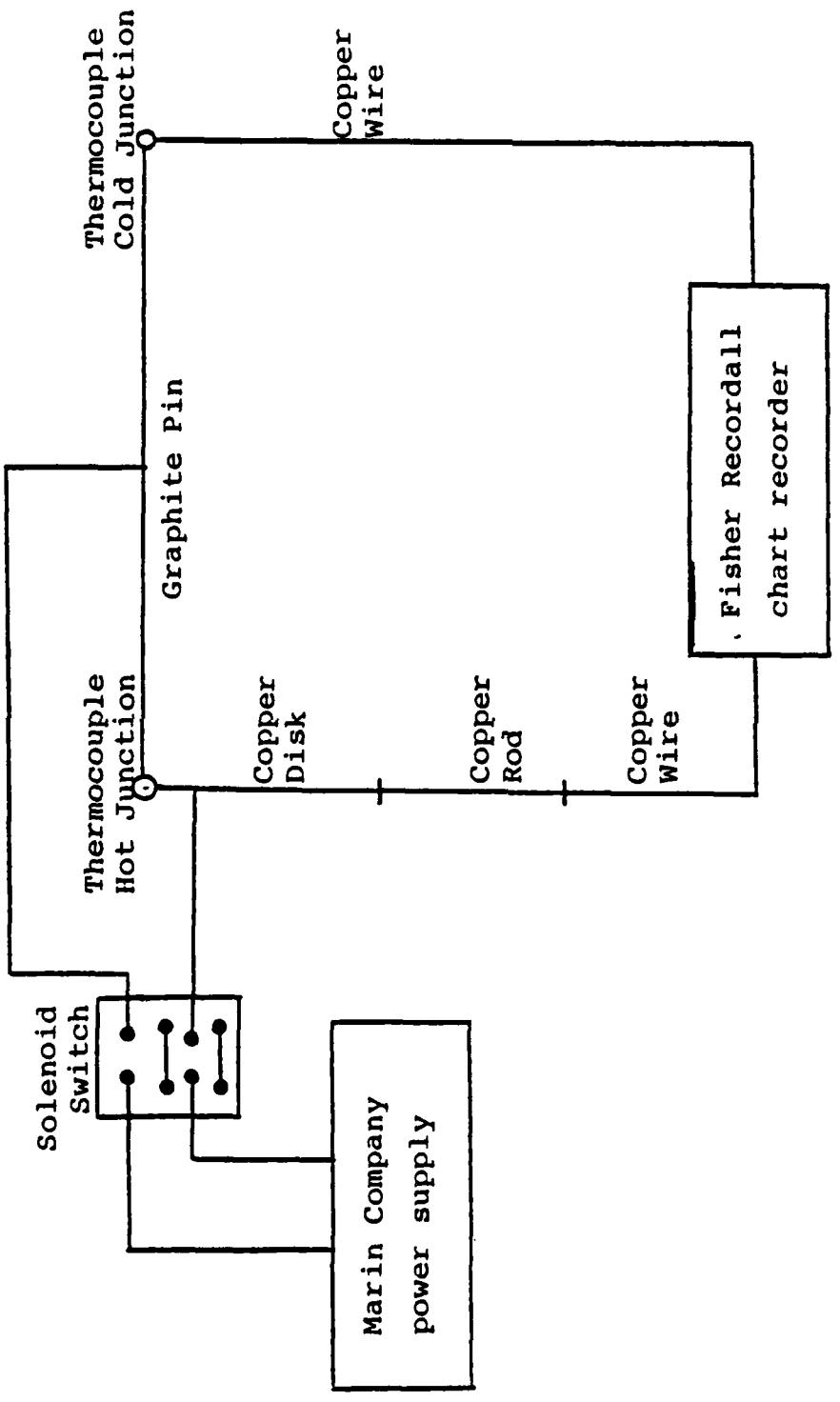

Figure 6. Diagram of electrical circuitry.

power supply flowed through a solenoid switch to a flexible cable. This cable was attached to the pivoting arm of the pin holder. The pin holder was aluminum and it held the graphite pin securely by means of a small steel set screw. The current flowed across the graphite-copper interface and was picked up by a set of three copper brushes that were spring loaded against the base of the rotating shaft. Finally, the current flowed through the other half of the solenoid switch and back to the power supply. When the dynamic thermocouple was to measure the interfacial temperature, the heat generating current circuit had to be opened.

The dynamic thermocouple circuit consisted of the graphite pin, the copper disk, a copper rod, and two copper wires. As can be seen from Figure 6, the graphite pin to copper disk junction composed the hot junction of the thermocouple. At the other end of the graphite pin was attached a copper wire, and this formed the cold junction of the thermocouple. A copper rod approximately 1/8 inch in diameter was placed at the center of the rotating copper disk. This picked up the thermocouple's signal and transmitted it back to the recorder. The recorder was a Fisher Recordall.

The copper-graphite thermocouple used in these tests was unique, and therefore had to be calibrated prior to testing. The thermo-electric characteristics were determined by heating the hot junction in a bath of mineral oil while the cold junction was maintained at room temperature. Using Gauss's Least Squares method, a quadratic was fit to these data (Figure 7). It was found that the temperature of the cold junction of the

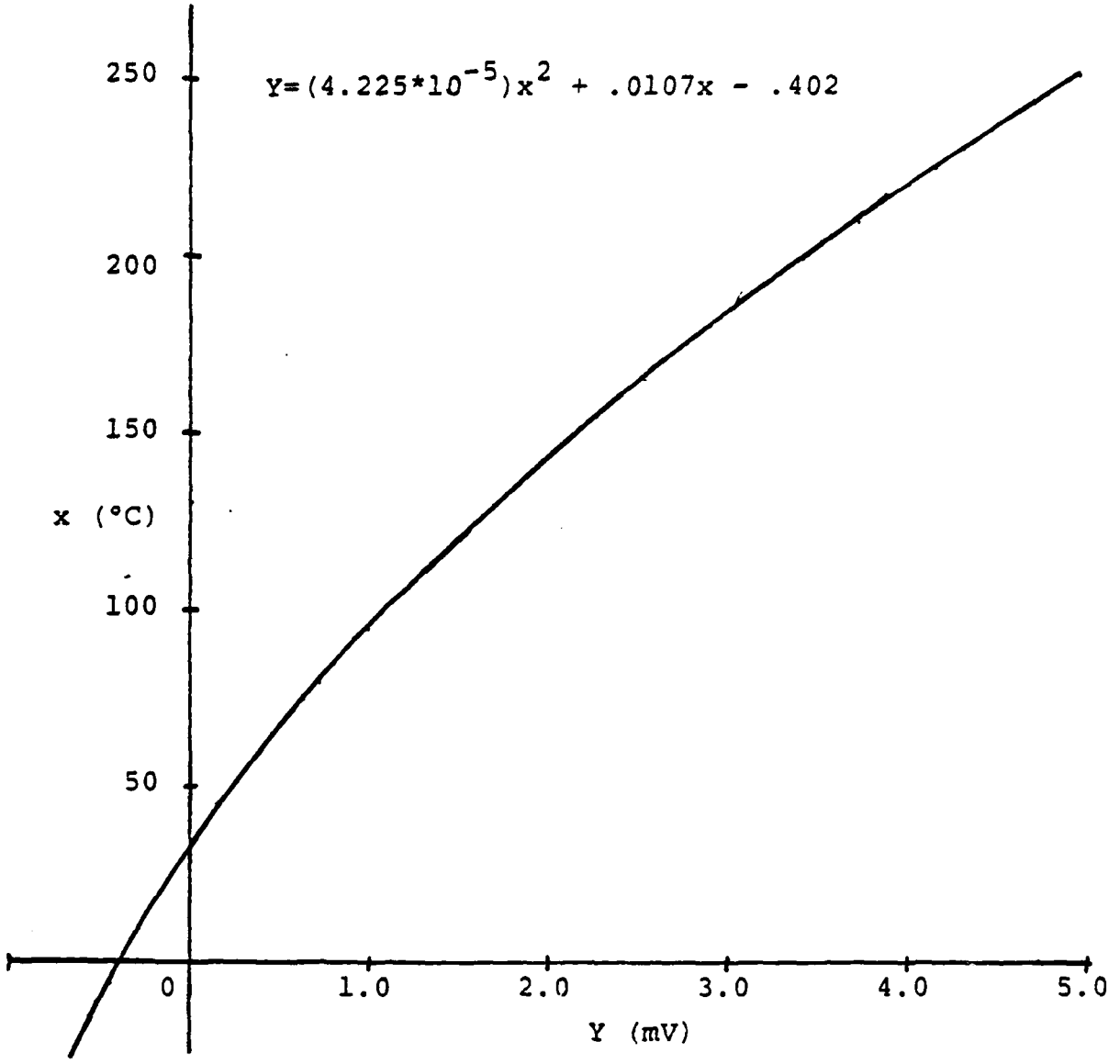

Figure 7. Temperature-emf characteristic curve of the copper-graphite dynamic thermocouple.

dynamic thermocouple rose significantly above the reference temperature of 20°C during some of the tests. An electrically isolated chromel-alumel thermocouple was taped to the cold junction in an effort to monitor the bulk temperature rise of this junction. The millivolt output of the copper-graphite dynamic thermocouple and of the chromel-alumel thermocouple were recorded simultaneously on the chart recorder while tests were run.

The tests can be divided into three different groups: i) those run with the copper disk spinning, but no current flowing, 2) those with current flowing and the disk stationary, and 3) those with both the disk spinning and current flowing. All the tests were conducted at steady state as determined by the temperature of the cold junction of the copper-graphite thermocouple.

During tests when there was no current flowing across the copper-graphite interface, the thermo-electric voltage from the dynamic thermocouple was monitored continuously. The Rockwell drill press was switched off, and the temperature decay curve was measured as the rotating copper disk slowed and then stopped. Obviously, these tests required no extrapolation.

Approximately 30 tests were conducted with current flowing and a stationary copper disk. During the period when the system was approaching steady state, the power supply with its floating ground was a part of the thermocouple's circuit. No data was collected while the power supply was part of the temperature measurement circuit. When steady state was reached

a solenoid switch was activated, completely cutting the power supply out of the circuit. The thermocouples signals were then recorded on the chart recorder as the interfacial temperature decayed. Due to a delay in the chart recorder, there was immediately introduced a lag time of approximately six-tenths of a second before the pen responded to the dynamic thermocouple's signal.

The majority of the tests were conducted with both the copper disk spinning and current flowing across the interface. These were conducted in much the same way as the tests conducted with the stationary copper disk. But now, when the solenoid was activated to cut off the power supply, the drill press was simultaneously switched off. The temperature decay curve, as indicated by the thermocouples' signals, was recorded as the rotating disk slowed and stopped.

The chart of the millivolt recorder was run at two different speeds during the course of collecting the experimental data; approximately half the tests were recorded at 25 cm/min, and the rest at 2.5 cm/min. Two different chart sensitivities were used depending upon the test: .001 or .01 volts full scale.

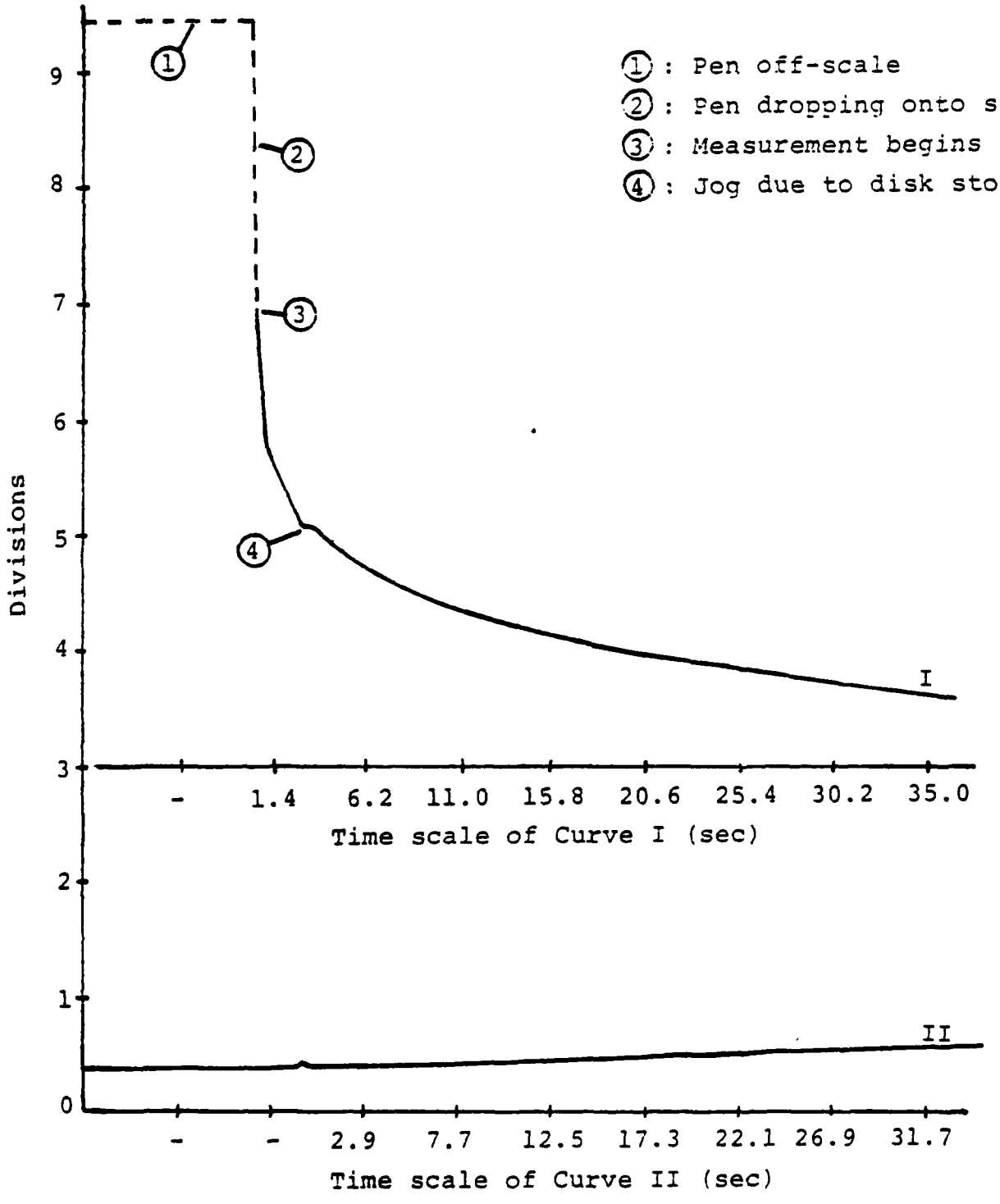

Figure 8. Example of thermocouples output at a sliding speed of 10 m/s, current of 50 amps, and load of .75 kg.
Curve I: copper-graphite thermocouple recorded at .1 mV/division
Curve II: chromel-alumel thermocouple recorded at 1.0 mV/division

IV. RESULTS

The output of the copper-graphite thermocouple and the chromel-alumel thermocouple were recorded simultaneously on the Fisher Recordall chart recorder. A sample of what this raw data looked like is shown in Figure 8. Millivolt readings from the copper-graphite thermocouple's curve and from the chromel-alumel thermocouple's curve were taken at specific time intervals. When the chart speed was 2.5 cm/s, the readings were taken at 1 second intervals for the first 4 seconds, and then at 4 second intervals for the remaining time. When the chart ran at 25 cm/s, the readings were taken at .4 second intervals for the first 4 seconds, and then again at 4 second intervals for the remaining time. The time from when the power was cut off to when the pen of the chart recorder responded to the thermocouple's signal was determined from each chart, and added to the time readings. Each temperature decay curve was monitored for approximately 40 seconds.

The characteristic temperature-emf curves of both the copper-graphite thermocouple and the chromel-alumel thermocouple were used to calculate the hot and cold junction temperatures from the millivolt readings. This was done on a VAX 11/780 computer. Curves of the decaying interfacial temperature were plotted using the VAX computer for each test (Figure 9). These temperature decay curves were plotted to check the consistency and reasonableness of the data. For the tests which were frictionally heated, the points at which the copper disk stopped spinning can be noted by the slight

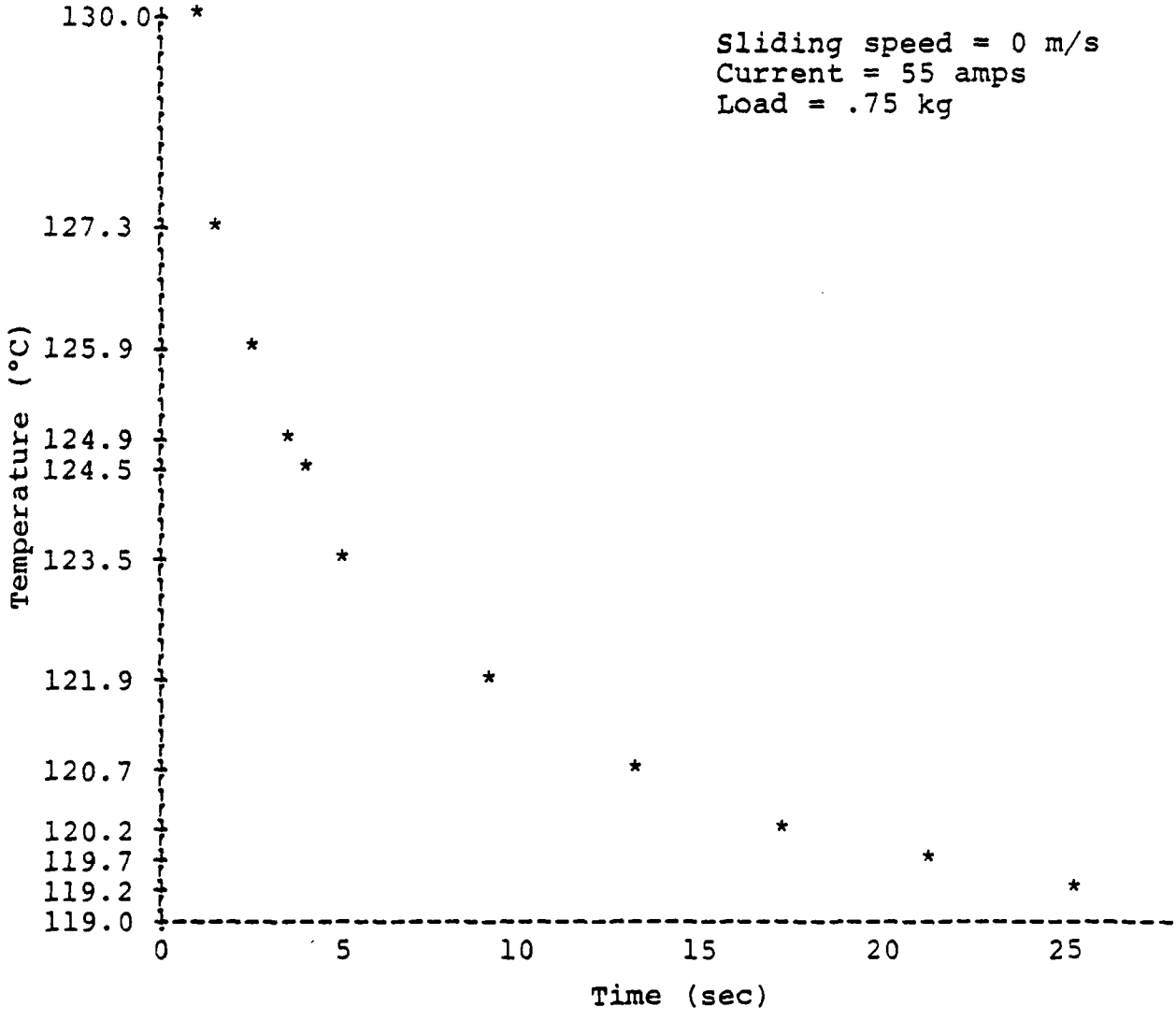

Figure 9(a). Example of a temperature decay curve as plotted by the VAX 11/780 -electrical contact.

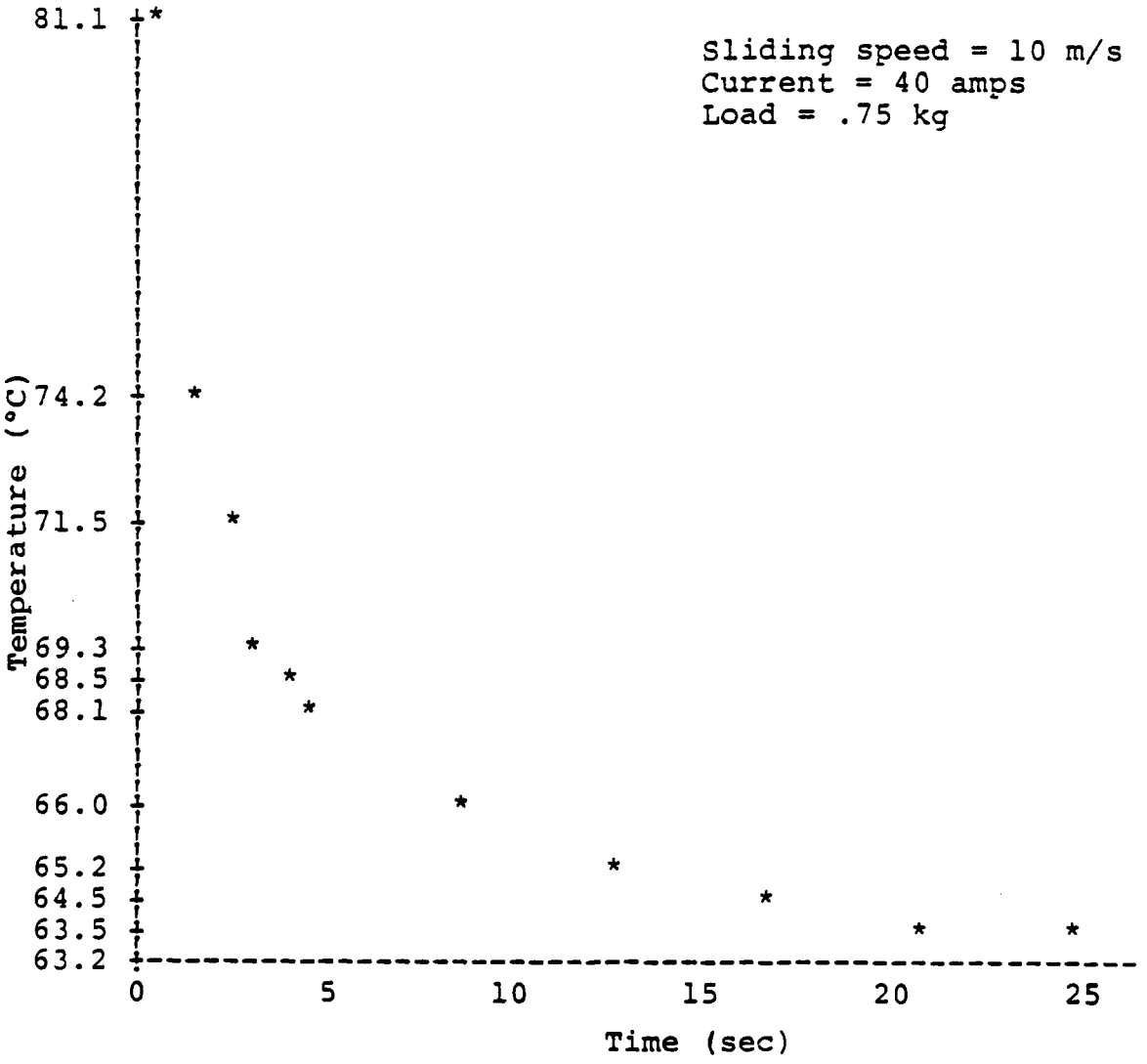

Figure 9(b). Example of a temperature decay curve as plotted by the VAX 11/780 - sliding, electrical contact.

jog in the temperature decay curve. At a spinning speed of 10 m/s the jog occurs about 3 seconds after the drill press was turned off. At a speed of 1 m/s the jog occurs at approximately 1-1/2 to 2 seconds. These jogs are due to the fact that when the disk stops spinning the contact is not cooled as quickly as when the spinning disk takes the heat away.

These temperature decay curves are interesting, but what we are looking for is the maximum average surface temperature of the contact. This maximum average surface temperature occurs when power is still being supplied to the contact, i.e. at time equal to zero on the temperature decay curves. A variety of extrapolation techniques were considered in order to determine this temperature at time zero. These included: i) fitting all of the data points to a single exponential, ii) assuming the decay curve is an infinte sum of exponentials, and fitting a single exponential to the first few points, and iii) again, assuming an infinite sum of exponentials, and using a modified exponential fitting technique in order to weight the fit towards the first two data points.

The first extrapolation procedure considered was to fit all of the data points from each test to a single exponential decay curve,

$$\theta - \theta_0 = k\, e^{-at} \quad . \qquad (1\text{-IV})$$

This procedure fit most of the points very well, but differed greatly from the data points that were closest to time zero

(Figure 10). The extrapolated temperature calculated from the single exponential was usually less than the temperature measured one or more seconds after the power had been shut off. Since this was the area of greatest concern, this procedure was deemed inadequate. This curve fitting procedure emphasized that the temperature decay curve of the contact was governed by more than one time constant.

From a theoretical standpoint the temperature decay curve will most likely be an infinite sum of exponentials,

$$\theta = \theta_0 + \sum_{n=1}^{\infty} (k_n \, e^{-a_n t}) \qquad (2\text{-IV})$$

Fitting the data to an infinte sum of exponentials is not possible. Fitting the data to a sum of only two exponentials would be a difficult and time consuming iterative process, and not necessarily accurate. Upon examining a curve composed of the sum of exponentials, it is found that different areas of the curve are governed more strongly by different exponentials. At large values of time, the exponentials with small time constants will have approached zero more rapidly than those with large time constants. Therefore at large values of time, the exponentials with large time constants will dominate the behavior of the curve. Conversely, the same line of reasoning holds for very small values of time. Those exponentials with the smallest time constants will dominate the shape of the curve close to zero. Based upon this information and the characteristics of the temperature decay curves, it was assumed that for the time span of interest only a single empirically determined exponential would be of importance.

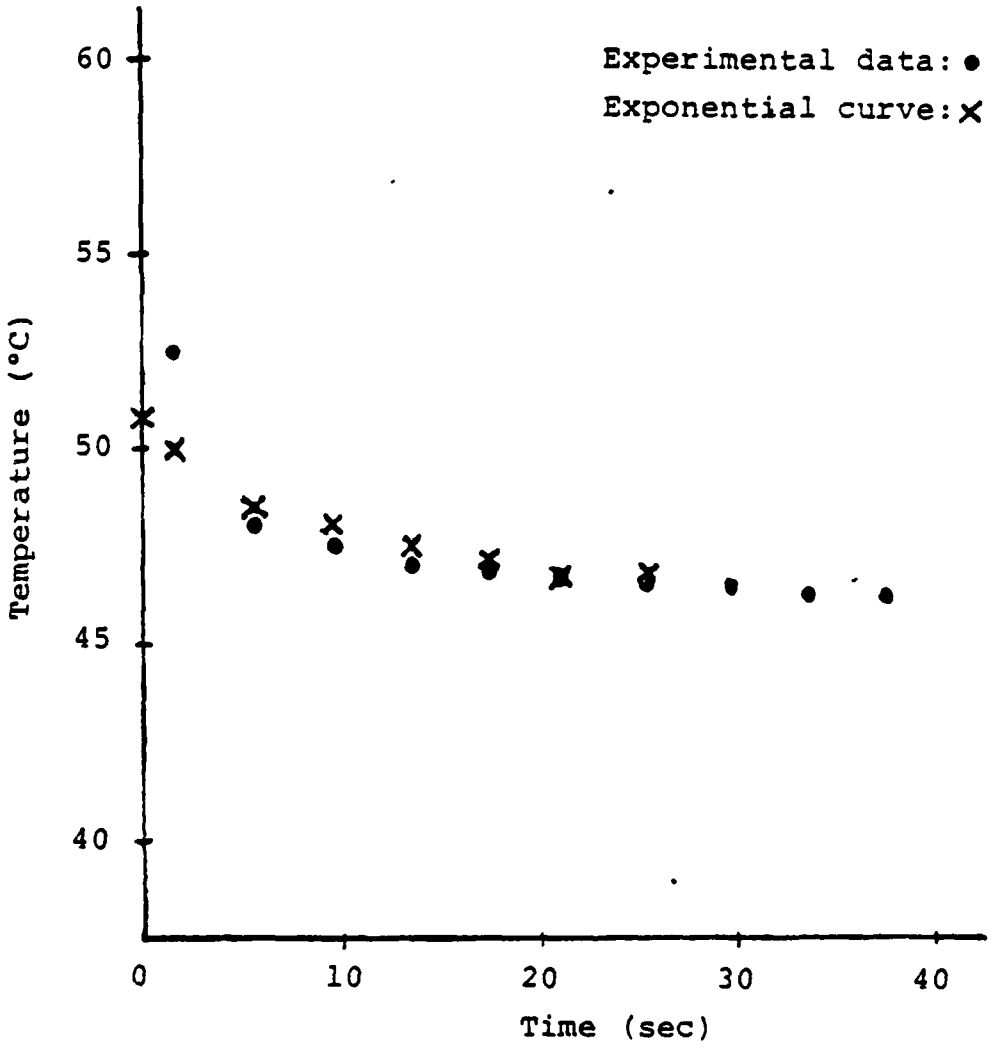

Figure 10. Example of fitting all of the data points to a single exponential.

The problem that now remains is to find the values that define that exponential.

Working with only the first three data points from each test, a single exponential curve was fit and then extrapolated back to time zero. When fitting this exponential to the data it was assumed that there were three unknowns: a, k, and Θ_0. The procedure followed is explained in detail by Rabinowicz[19]. This extrapolation technique yielded generally good results, but for certain tests the extrapolated values were obviously much too large. Examining these tests found that inconsistencies in the data such as two points almost at the same temperature, led to the erroneous results. These inconsistencies were due to experimental error. It was decided that it was not accurate to fit the first three data points to an exponential curve with disregard for experimental error.

The following curve fitting technique was arrived at after consultation with Rabinowicz. When an exponential is plotted on semi-log paper the result is a straight line. Fitting data points to the straight line that defines the exponential is usually accomplished by means of the least squares or extended differences methods. This curve fitting technique fit the first three data points to a straight line that was weighted towards the values of the first two data points. In detail, the procedure is as follows. First, the temperature at time equal to infinity, Θ_0, was determined by the same technique as described by Rabinowicz[19]. The first three data points were then plotted using,

$$\ln(\theta - \theta_0) = \ln(k) - at \qquad (3\text{-IV})$$

See Figure 11(a). Between the second and third plotted points a straight line was determined(Figure 11(b)). One-third of the distance away from the second plotted point was marked off(Figure 11(c)). This marked off point and the first plotted point defined the straight line that was used to find the constants, a and k (Figure 11(d)). If the three data points had fit an exponential curve perfectly, all three would have been on a single line in these plots. The closer the data is to an exponential, the closer the results from this technique will be to the previous curve fitting technique. When the data, because of experimental error and inconsistencies, varies from the exponential, this modified exponential curve fitting technique smooths out some of the inaccuracy. The extrapolate temperatures calculated using this method were very similar to the previous method's extrapolated temperatures, except that there were now no unreasonable values.

Table I lists the average surface temperatures found at time zero using the modified exponential extrapolation procedure. Figure 12 is a graph of these temperatures as a function of current squared.

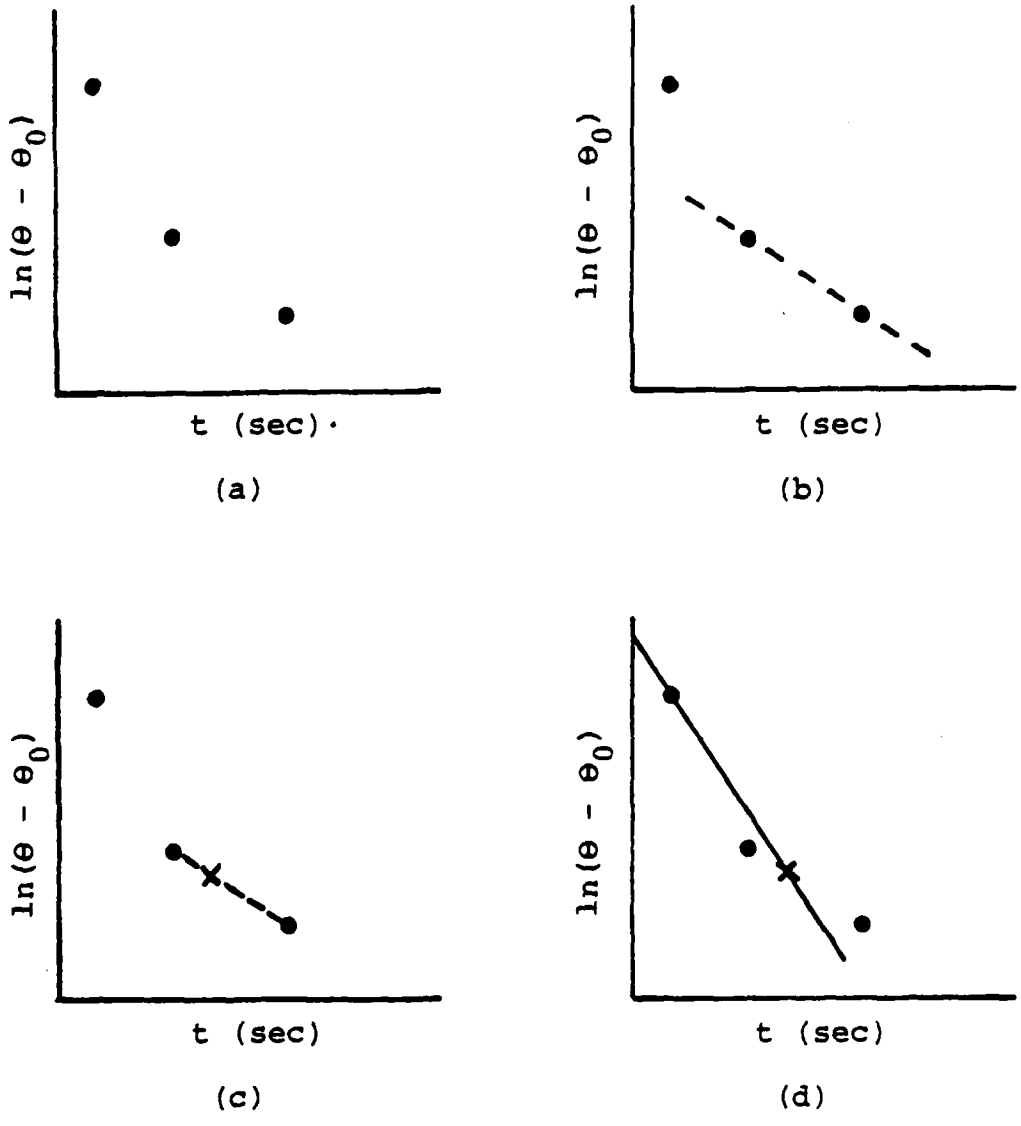

Figure 11. Modified exponential curve fitting technique.

Table I. Average temperature of the contact surface as determined from the experimental data, (°C).

v	0. m/s				1. m/s				10. m/s		
I \ W	.50	.75	1.0		.50	.75	1.0		.50	.75	1.0
0	-	-	-		49.	58. 57.	63.		101. 100.	83.	85.
10	54.	44.	36.		50.	76.	64.		99.	106.	125.
30	-	87.	66.		69.	75.	71.		110.	130.	116.
40	139.	115.	76.		75.	73.	72.		92.	94.	99.
45	154. 117.	129.	87.		74.	81.	74.		-	101.	96.
50	157.	147.	108.		82.	-	90.		99. 105.	101.	98. 134.
55	134.	137.	126.		-	89.	103.		87. 105.	100.	98.
60	187.	130. 136.	138.		-	95.	93.		123.	102.	137.
65	-	314.	181.		123.	102.	98.		173.	122.	-
70	-	-	153.		126.	131.	114.		-	-	-

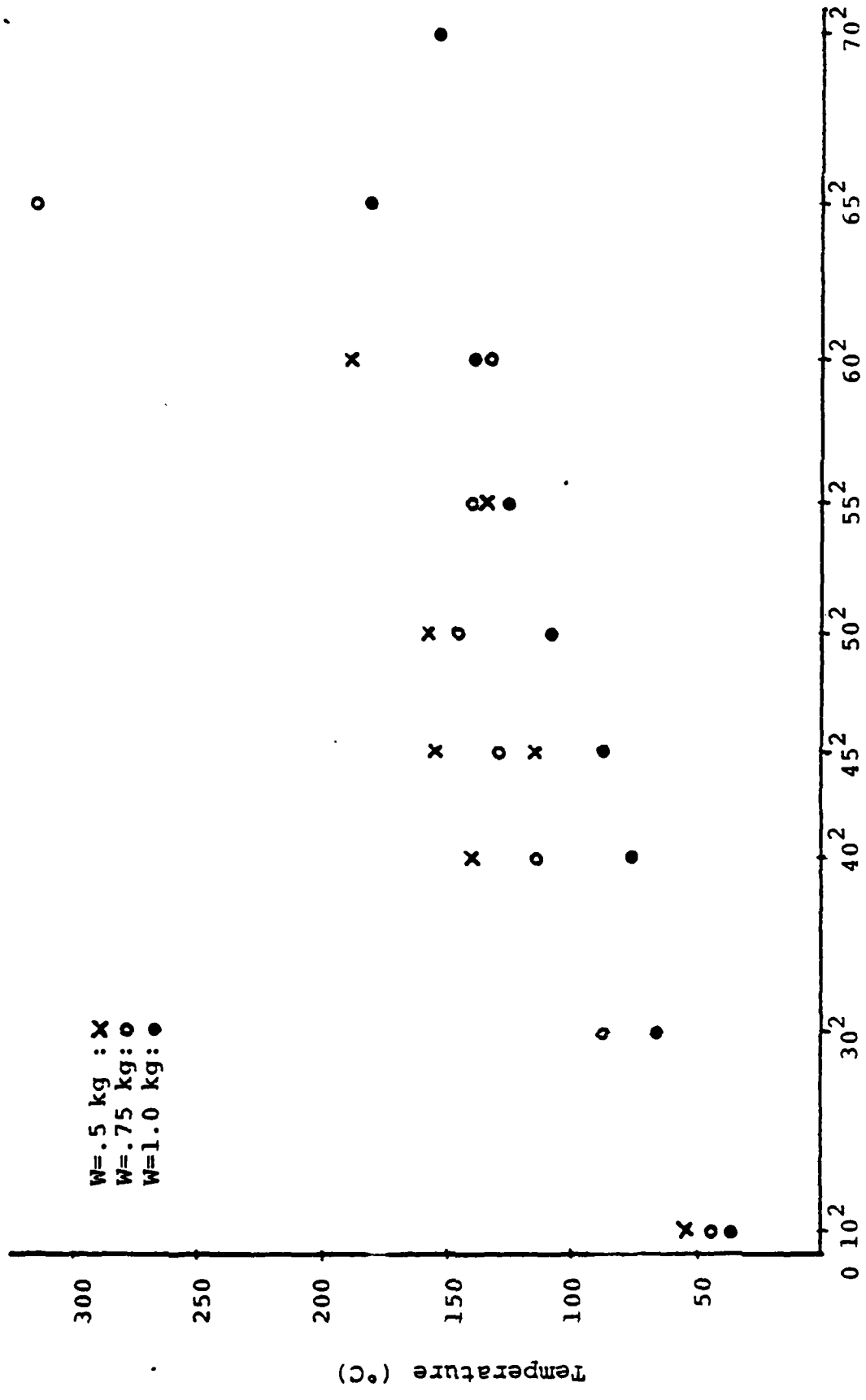

Figure 12(a). Average surface temperature vs. current squared at sliding speed of 0. m/s.

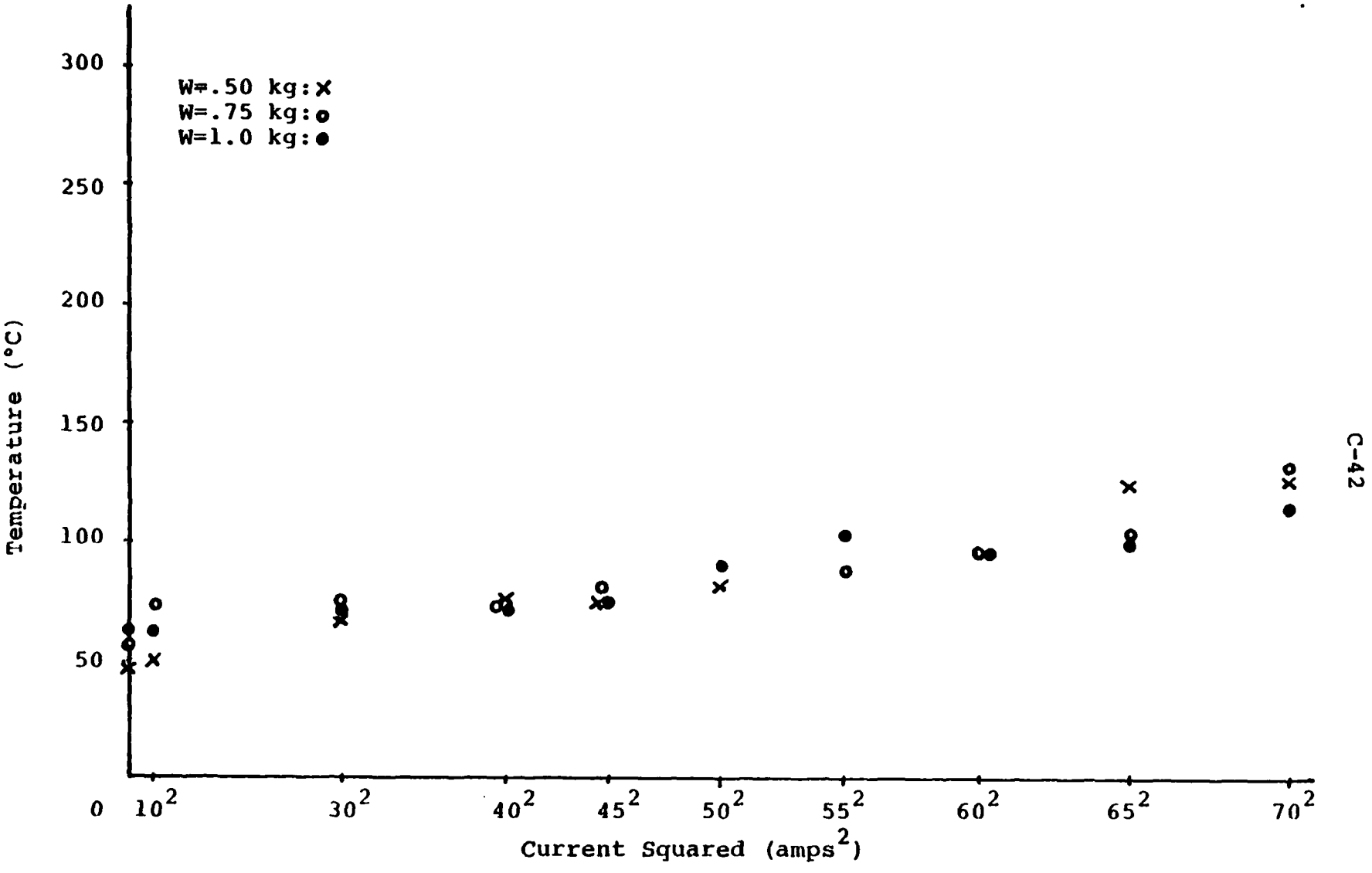

Figure 12(b). Average surface temperature vs. current squared at sliding speed of 1. m/s.

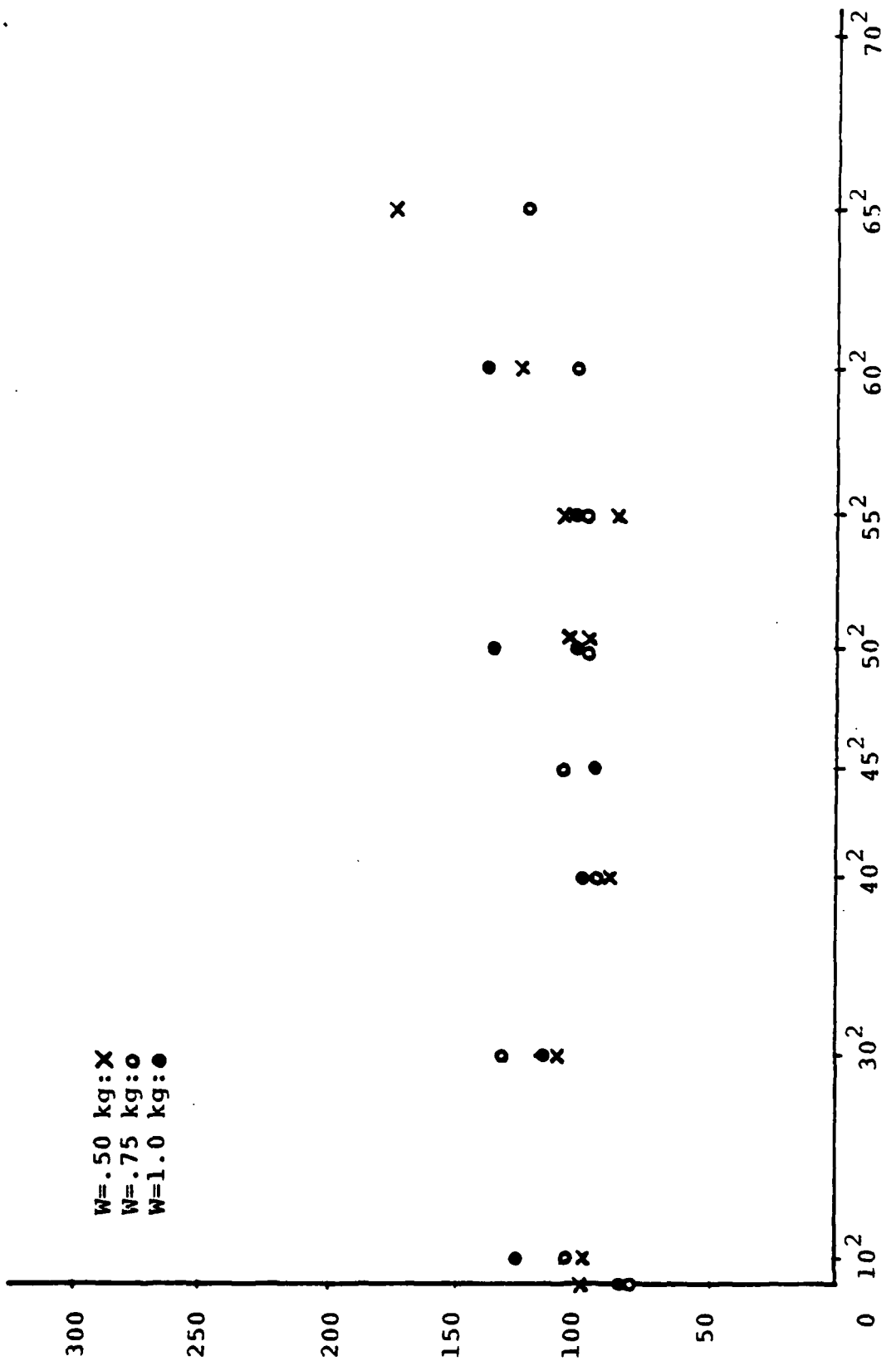

Figure 12(c). Average surface temperature vs. current squared at sliding speed of 10. m/s.

V. DISCUSSION

There are a few points that can be mentioned about the maximum average surface temperatures that were extrapolated from the experimental data. First, it can be seen that in general the temperatures are linearly proportional to the current squared. This is especially noticable of the tests run at 1 m/s(Figure 12(b)). Second, the effect of running the electrical contact at different loads is much more pronounced in the tests run with the copper disk stationary (Figure 12(a)) than in the tests run at 1 m/s and at 10 m/s. Third, the temperature range of the 0 m/s tests(Figure 12(a)) is greater than the ranges of the 1 m/s and 10 m/s tests. At a sliding speed of 0 m/s the temperatures range from less than 50°C to more than 175°C. At 1 m/s the temperatures range from about 50°C to 125°C, and at 10 m/s the temperatures mainly fall between 80°C to 140°C.

The fact that the surface temperatures are linearly proportional to the current squared is encouraging; the data confirms that the Joule effect is the major component contributing to the heating of the contact. The second and third observations confirm that spinning the copper disk has a large influence on the interfacial temperature, and that this influence is a moderating one. Finally, it is important to note as a general trend that the interfacial temperature of the tests running at 1 m/s are less than the temperatures of the tests running at 0 m/s and at 10 m/s under the same loads and currents.

Table II lists the values of Jaeger's dimensionless parameter 'L', defined in equation(3-II), for the various sliding situations tested during this study. Note that for the tests run at 1 m/s 'L' is less than 1.0 and therefore these tests were in the low speed regime. For the tests run at 10 m/s 'L' is close to 5.0, and therefore these tests were considered to be in the high speed regime. Jaeger's parameter was calculated by assuming a single circular contact and plastic deformation to determine 'b', the radius of the contact.

Theoretical calculations were carried out on the VAX 11/780 using Rabinowicz's equation,

$$(f W v + I^2 R)/ 4 J r (K_1 + K_2) \qquad (7\text{-II})$$

for the low speed regime and

$$(f W v + I^2 R)/ 3.6 J (r^3 K_2 \rho_2 c_2)^{1/2} \qquad (8\text{-II})$$

for the high speed regime. Table III lists the values of the parameters used in these calculations. The area of contact was determined on the basis of purely plastic deformation at the contact. Using these equations, four sets of calculations were run: i) first, a single circular contact was assumed, ii) three circular contacts were assumed, iii) five circular contacts were assumed, and then iv) ten contacts were assumed. See Appendix B for graphs of the theoretical calculations.

Upon examining the graphs of the theoretically determined temperatures in Appendix B, it is obvious that certain trends are followed as the number of contacts is increased. The first important observation is that the theoretical average surface temperature is a strong function of the number of con-

Table II. Jaeger's dimensionless parameter 'L' assuming 1 circular contact.

W \ v	0 m/s	1 m/s	10 m/s
.50	0	.42	4.2
.75	0	.59	5.9
1.0	0	.68	6.8

Table III. Values of the parameters used to calculate average surface temperatures.

Thermal coefficient of graphite	K_1=42. cal/m-s-°C
Thermal coefficient of copper	K_2=91. cal/m-s-°C
Friction coefficient	f=.2
Specific resistivity of copper	$\rho_2 c_2$=8.2*10^5 cal/m^3-°C
Hardness of graphite	p_1=1.47*10^8 kg/m^2
Constriction resistance	R=.015 watt/amp^2
Mechanical equivalent of heat	J=4.2 watt-s/cal
Sliding speed	v - m/s
Load	W - kg
Current	I - amps

tacts per brush. Second, as was expected, these theoretical temperatures are linearly proportional to the current squared. Third, as the number of contacts per brush increases, the positive slope of temperature vs current squared decreases and the temperature at zero current increases. In other words, the theoretical line connecting the temperatures rotates in a clockwise direction, causing magnitudes at low current to increase and magnitudes at high current to decrease. Fourth, because this theoretical line is rotating in a clockwise direction as the number of contacts increases, the temperature range also decreases as the contacts per brush increase. Fifth, when a single contact is assumed the theoretically determined temperatures show a definite dependence upon the load. This is evident by the spacing between the data points at the same sliding speed and current. When the number of contacts increases the spacing between temperatures at the same sliding speed and current decreases, i.e. the influence of different loads upon the temperature decreases.

From the graphs of the theoretically calculated average surface temperatures in Appendix B it can be seen that no one set of graphs, or no one number of contacts, accurately reflects the experimental data. The theoretically determined temperatures when one contact is assumed are obviously much too high, sometimes by as much as 800%. The temperatures when one contact is assumed should be recognized as the worst case temperatures and not necessarily the operating temperatures found in everyday situations. Upon closer examination of the

theoretical temperatures it is found that the best match for the 0 m/s experimental results(Figure 12(a)) is the theoretically determined results at 0 m/s when 3 contacts are assumed (Figure 13). For the experimental tests run at 1 m/s, the best match of the theoretical calculations is the graph at 1 m/s when 5 contacts are assumed(Figure 14). And for the experimental tests run at 10 m/s the best match is with the theoretically determined temperatures at a sliding speed of 10 m/s when 10 contacts are assumed(Figure 15). The best matches were determined on the basis of the actual magnitudes of the temperatures, the range of the temperatures, and the relative importance placed on the different loads. Based on these observations, one has to question if the number of contacts is related to the speed at which the brush slides.

There are several steps that could have incurred appreciable error in the data gathering and reduction. First, the equipment that was used to gather the data was fairly well worn. For instance, the drill press could have introduced errors into the data by not running smoothly and steadily. Second, the graphite pins were all from the same lot, so in terms of composition, they should have been the same. But it is possible that the number of contacts could have changed as the graphite pin wore down during testing, or that when the graphite pin broke and had to be replaced, the new pin had a different number of contacts. The high current tests when the sliding speed was 0 m/s and the tests run at 10 m/s seem to

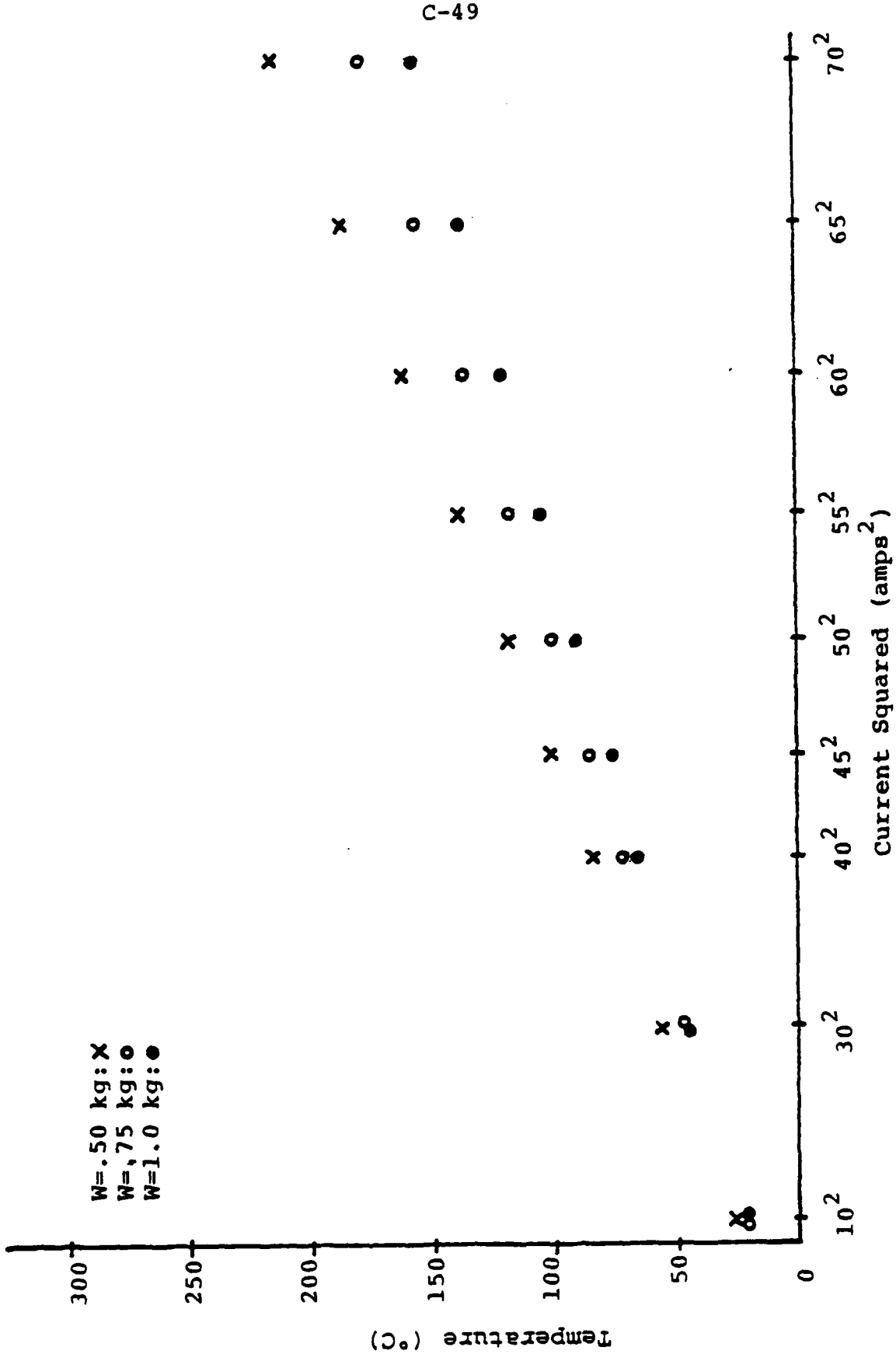

Figure 13. Average surface temperature vs. current squared at a sliding speed of 0. m/s, from equation (7-II) assuming 3 circular contacts.

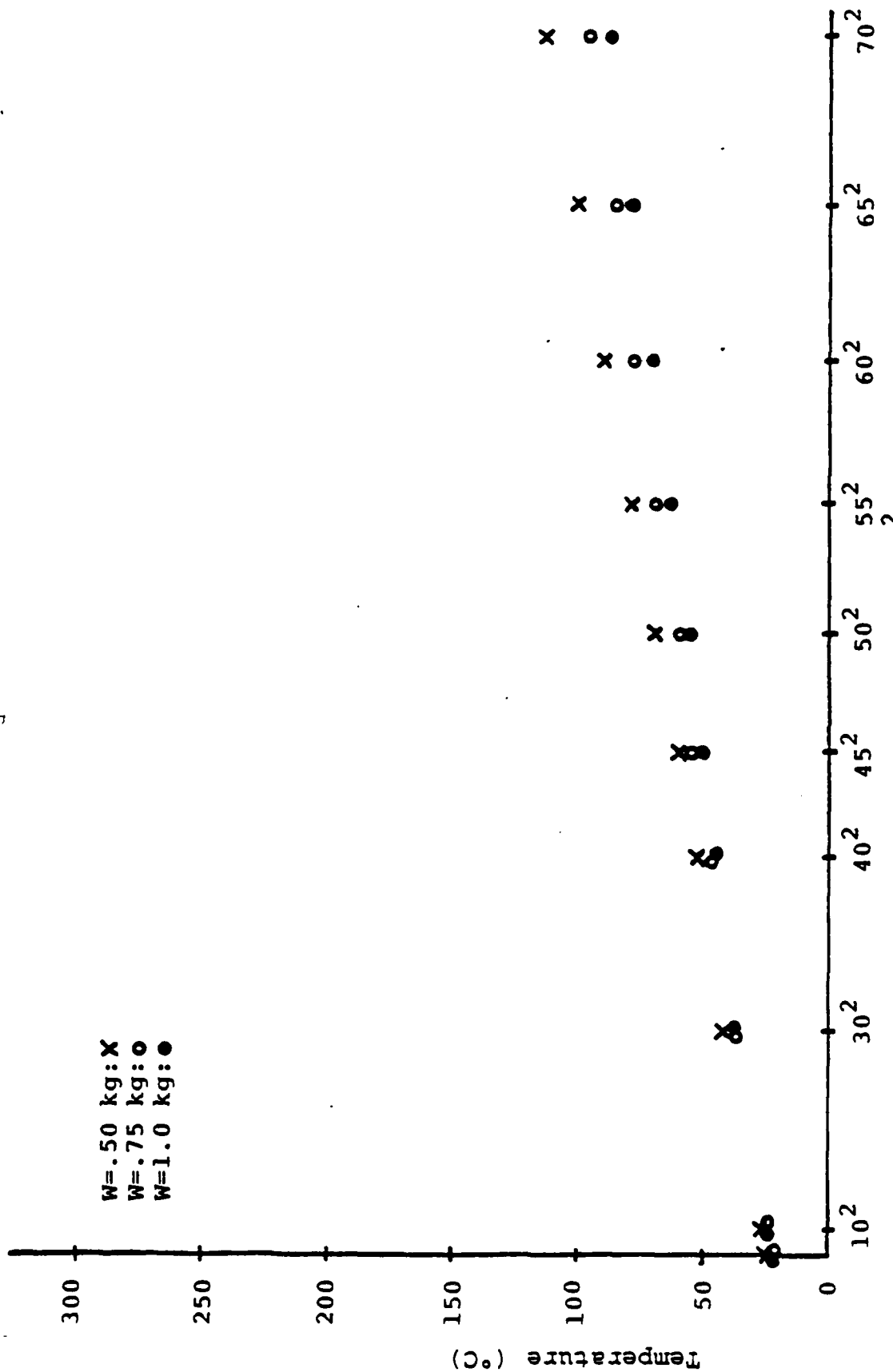

Figure 14. Average surface temperature vs. current squared at a sliding speed of 1. m/s, from equation (7-II) assuming 5 circular contacts.

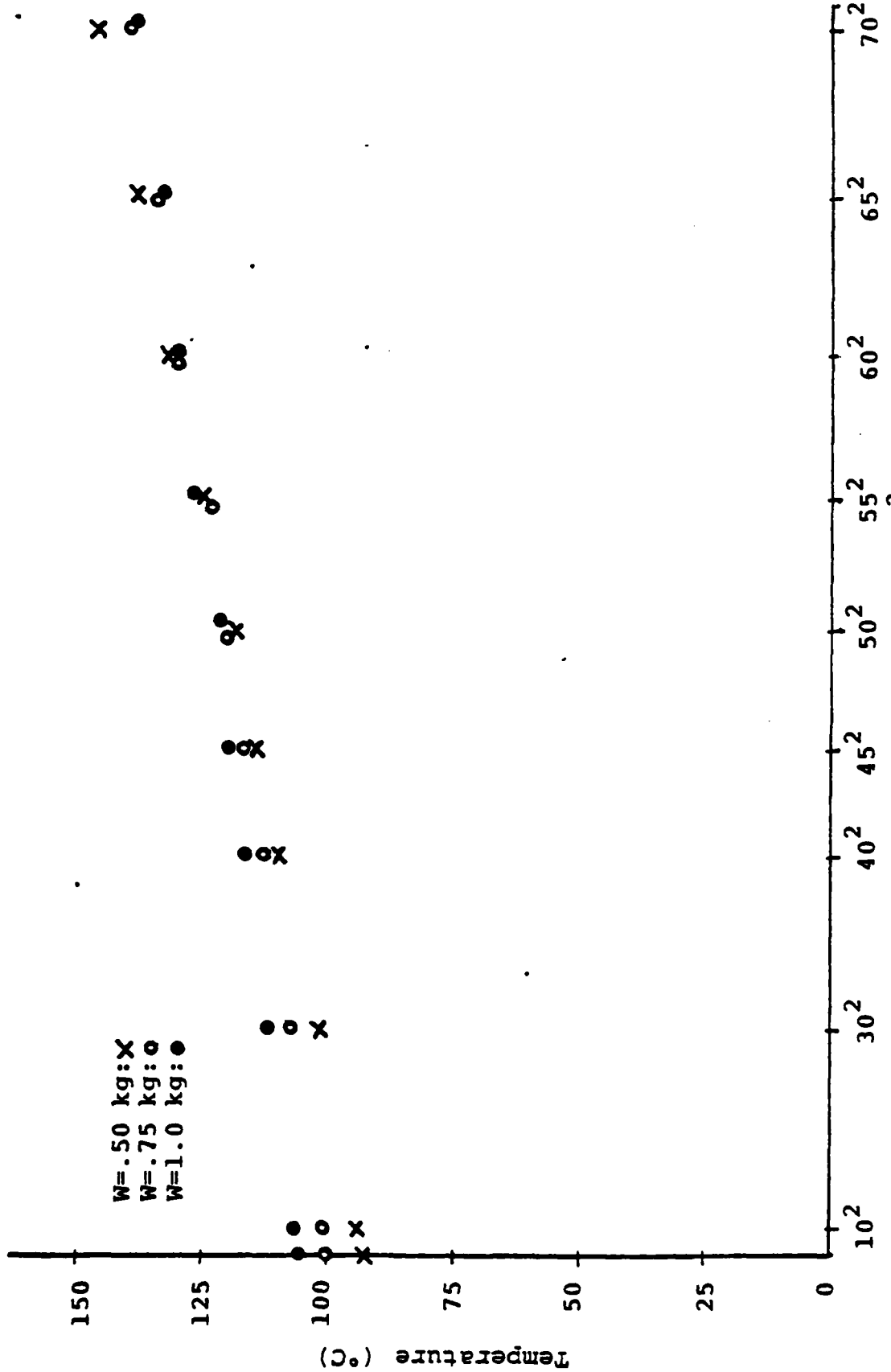

Figure 15. Average surface temperature vs. current squared at a sliding speed of 10. m/s, from equation (8-II) assuming 10 contacts.

have more scatter than the other data. One reason is that at the higher currents and speed the portion of the graphite pin that carried the large heat generating current could have undergone metallurgical changes. These changes would alter the thermocouple characteristics of the copper-graphite thermocouple and therefore introduce errors in the millivolt output of the thermocouple. Another possible source of error is due to the delay of the recorder's pen to respond to the thermocouple's signal; this delay was typically .6 seconds, but could have varied by $\pm$.1 seconds. This problem could have been overcome by measuring the data with a highly sensitive oscilloscope. Finally, the data gathered from the thermocouples had to be extrapolated back to time zero to find the operating average surface temperatures, and errors were introduced at this point. Although no estimate of the magnitude of the errors was formulated, there was one important point that instilled confidence in the experimentally determined temperatures. The tests that were conducted with zero current were monitored continuously during testing and therefore did not encounter the delay inherent of the recorder or experience errors due to extrapolation. These tests fit in very well with the data from the extrapolated tests as can be seen from Figures 12(b) and 12(c).

VI. CONCLUSION

In conclusion, the dynamic thermocouple has proven to be a valuable technique for measuring the interfacial temperature rise of sliding, electrical contacts. Good agreement between experimental data and theory was achieved depending upon the number of contacts assumed per brush. At this time there is no existing theoretical basis for predicting the number of contacts. Therefore, the theoretical formulations for predicting the interfacial temperature of sliding, electrical contacts are not sufficiently accurate enough for practical applications.

It is recommended that similar studies be conducted to extend the experimental range. Future research efforts should also be directed towards determining the number of contacts per brush under different operating conditions.

APPENDIX A: Problems with the Experimental Apparatus

Several problems involving the dynamic thermocouple were encountered prior to running the tests. The normal application for a dynamic thermocouple is to sliding contacts. When the sliding contact is also an electrical contact, the dynamic thermocouple technique cannot be used to measure the interfacial temperature when the current is flowing. Therefore in this study the sliding, electrical contact was monitored until the maximum temperature was reached, and then all power was cut off. The dynamic thermocouple technique was then used to measure the temperature decay curve of the contact. This method intoduced several problems such as grounding problems, switching difficulties, calibration and recording considerations.

The total emf generated by the dynamic thermocouple was recorded on a Fisher Recordall millivolt chart recorder. This recorder had a floating ground. The thermocouple circuit was then isolated from any other possible grounding. The power supply was completely cut out of the circuit by the solenoid switch. The Rockwell drill press that comprised the drive for the pin-on-disk wear tester was isolated from the circuit by placing a cylindrical piece of hard plastic between the shaft of the disk mount and the spindle jaws of the drill press.

When testing of the thermocouple circuit began, the response was not as expected. With only friction generating heat, the thermocouple measured the temperature rise from when the spindle first started rotating to when steady state was reached. When the spindle was stopped, the temperature

decayed down to ambient. This was as expected. The response of the thermocouple when current was generating the heat was surprising. When the heat generating current was flowing, the recorder measured the voltage drop across the interface due to this current and did not measure the emf generated by the dynamic thermocouple. This voltage drop was on the order of volts, while the recorder was set to measure millivolts. Therefore the signal from across the graphite-copper interface was off the scale of the recorder. When the power supply was cut out of the circuit the thermocouple's signal reflected the temperature decay at the graphite-copper interface. Unexpectedly, this signal increased rather than decreased as did the frictionally heated contact. By heating the graphite-copper contact point with a blowtorch it was ascertained that the response of the thermocouple during the frictionally heated tests was correct.

Several reasons for the thermocouple's response when the contact was electrically heated were put forth: i) the thermocouple was actually measuring the voltage decay of the circuit due to the large current that had been flowing, ii) the inductance from the solenoid switch was interfering with the circuit, iii) the cold junction might not remain at the reference temperature of 20°C and in addition, it might cool down faster than the hot junction, thereby causing the temperature difference between the hot and cold junctions to actually increase when the current was turned off, and iv) soldering the copper wire to the graphite was ineffective and

possibly adversely affecting the circuit.

Was the thermocouple circuit measuring the voltage decay of the power supply? When the leads of the power supply were reversed the response of the thermocouple remained unchanged. Furthermore, the voltage decay of the power supply was measured on a Tektronix oscilloscope and a typical time constant of the order of milliseconds was found. The chart recorder has a typical delay time of .6 seconds before the pen responds to the thermocouple's signal, and therefore was not recording the decay of the power supply.

The possibility of inductance from the solenoid switch interfering with the thermocouple's signal was then checked. The switch was operated manually, rather than electrically, and no change in the response was noted.

It was found that the cold junction of the graphite-copper dynamic thermocouple rose significantly above 20°C. A small glass bead was used to electrically isolate one end of a standard chromel-alumel thermocouple. This thermocouple was taped to the cold junction of the dynamic thermocouple, and its signal was fed into the second pen of the Fisher Recordall chart recorder. During some of the high current tests this cold junction temperature was as high as 80°C. Generally, the cold junction temperature did not decay faster than the hot junction temperature, and so this was not the solution to reversed temperature decay curve of the electrically heated tests.

Originally, the cold junction connection of the dynamic

thermocouple was formed by soldering the copper wire around the graphite pin.. It was decided that the electrical and thermal connection at this junction was inadequate. A uniform temperature might not have been maintained at the cold junction and therefore thermocouple effects between the solder and the copper or graphite could have caused the problem. The soldered junction was replaced by a strong copper clip securing the wire to the graphite. At this point, the temperature decay curve of the electrically heated contact righted itself. Now the thermocouple's signal decayed towards the ambient temperature, as in the frictionally heated tests.

As mentioned in the body of this report, the graphite-copper thermocouple was unique, and therefore had to be calibrated prior to testing. From Figure 6 it can be seen that a copper rod and copper wires were also a part of the thermocouple circuit. Because of the different coppers of the disk, rod, and wires it was necessary to determine if the junctions between the copper components would affect the thermoelectric signal. Simple tests were conducted to determine the thermal emf of the copper rod to copper disk junction, since this junction could heat up appreciably. At 200°C the disk to rod interface produced an emf of .1 mv, or less than 3% of the graphite-copper thermocouple at the same temperature. The junction of the copper rod and copper wire was also tested and found to have a very small output. Since this junction was considerably removed from the source of heat, it was not expected to heat up above room temperature and therefore

would have no effect. Thermocouple effects from junctions not within the thermocouple circuit also had to be considered. For example, the junction of the aluminum of the pin holder and the graphite pin or of the steel set screw contacting the graphite could interfere if they were part of a closed circuit. The experimental set-up was carefully examined to insure that the only closed circuit would be the dynamic thermocouple circuit when the temperature of the contact was measured.

Other problems that occurred during the course of the testing were oxide formation on the copper disk and breaking of the graphite pin at high loads, speeds, and currents. Below 55 amps oxide formation was not a major problem judging from the coloration of the disk. Above 55 amps the formation of oxide seemed to rapidly increase, causing the disk to turn dark orange, reddish-purple, and in some spots silver. When this stage of oxidation was reached the disk was removed and ground on 400 grade grinding paper to remove the oxide build-up. Gathering data at the higher loads, speeds, and currents was made much more difficult because the graphite pin broke quite often. An attempt was made to lessen this breakage by wrapping a portion of the graphite pin with carbon fibers; this did not help and was abandoned. The strong copper clip at the top of the graphite pin, i.e. at the cold junction of the dynamic thermocouple, seemed to reduce the amplitude of the vibrations at that end. This was probably due to the fact that the clip contained a spring which acted

as a damper. Later the length of the graphite pin was reduced from approximately 6 inches to 4 inches. A longer pin was preferred at it would help maintain a cooler temperature at the cold junction. But due to the amount of graphite breakage during the course of the testing, shorter pins were deemed acceptable.

Appendix B: Graphs of the Theoretically Determined Average Surface Temperatures

This appendix contains graphs of the theoretical calculations of the average interfacial temperatures versus current squared. Calculations were carried out assuming one, three, five, and ten circular contacts.

ONE CONTACT

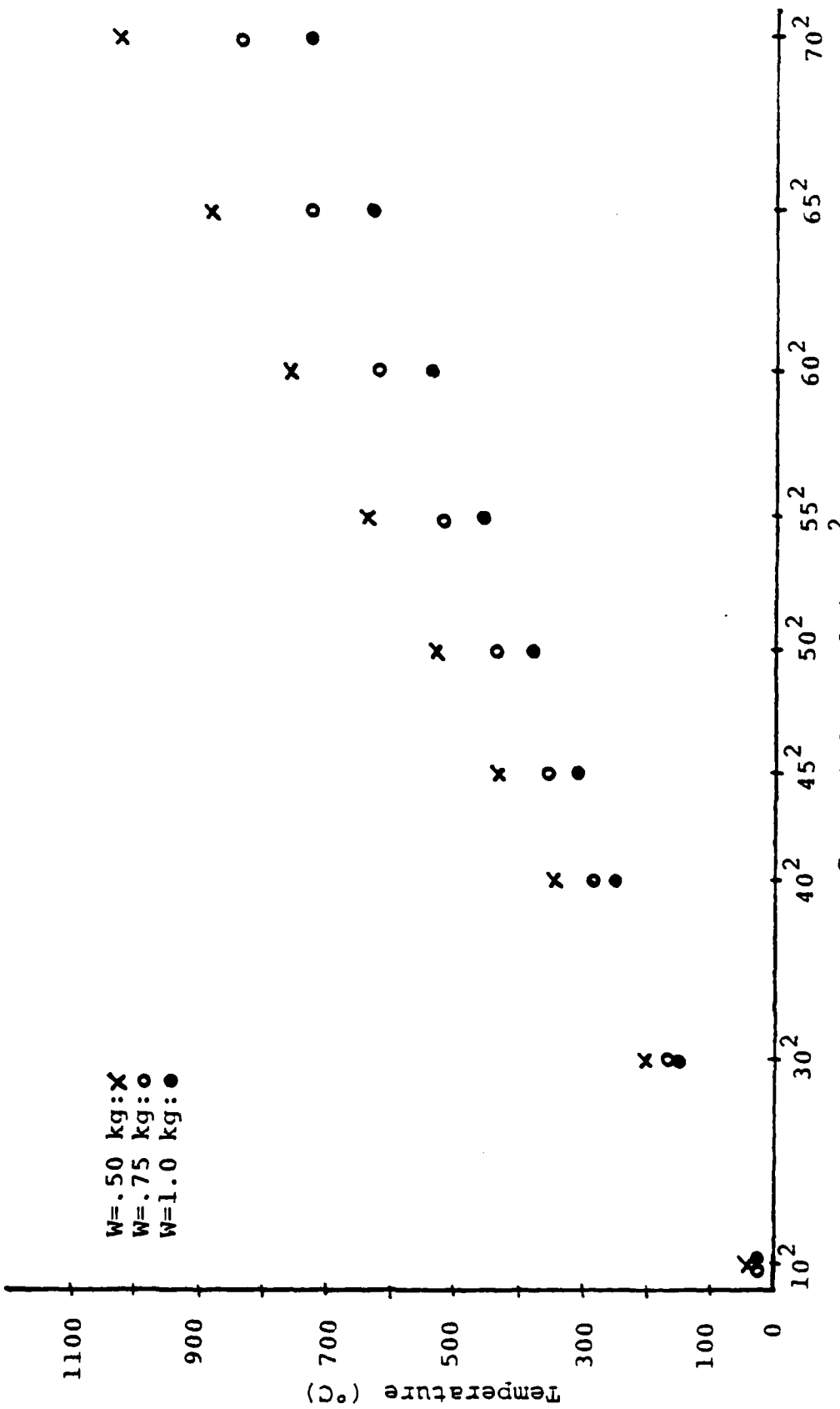

Figure 16(a). Average surface temperature vs. current squared at a sliding speed of 0. m/s, from equation (7-II) assuming 1 circular contact.

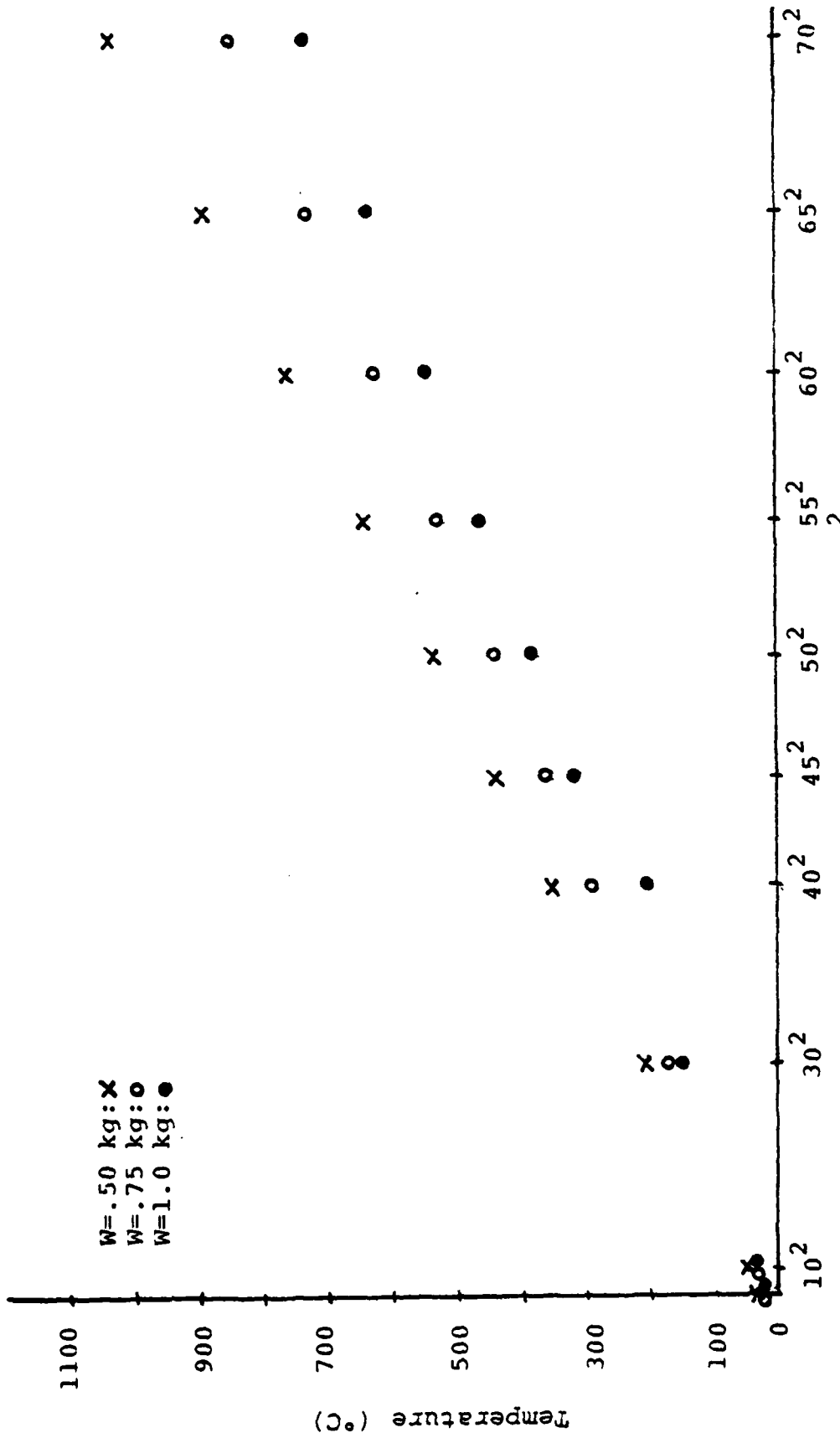

Figure 16(b). Average surface temperature vs. current squared at a sliding speed of 1. m/s, from equation (7-II) assuming 1 circular contact.

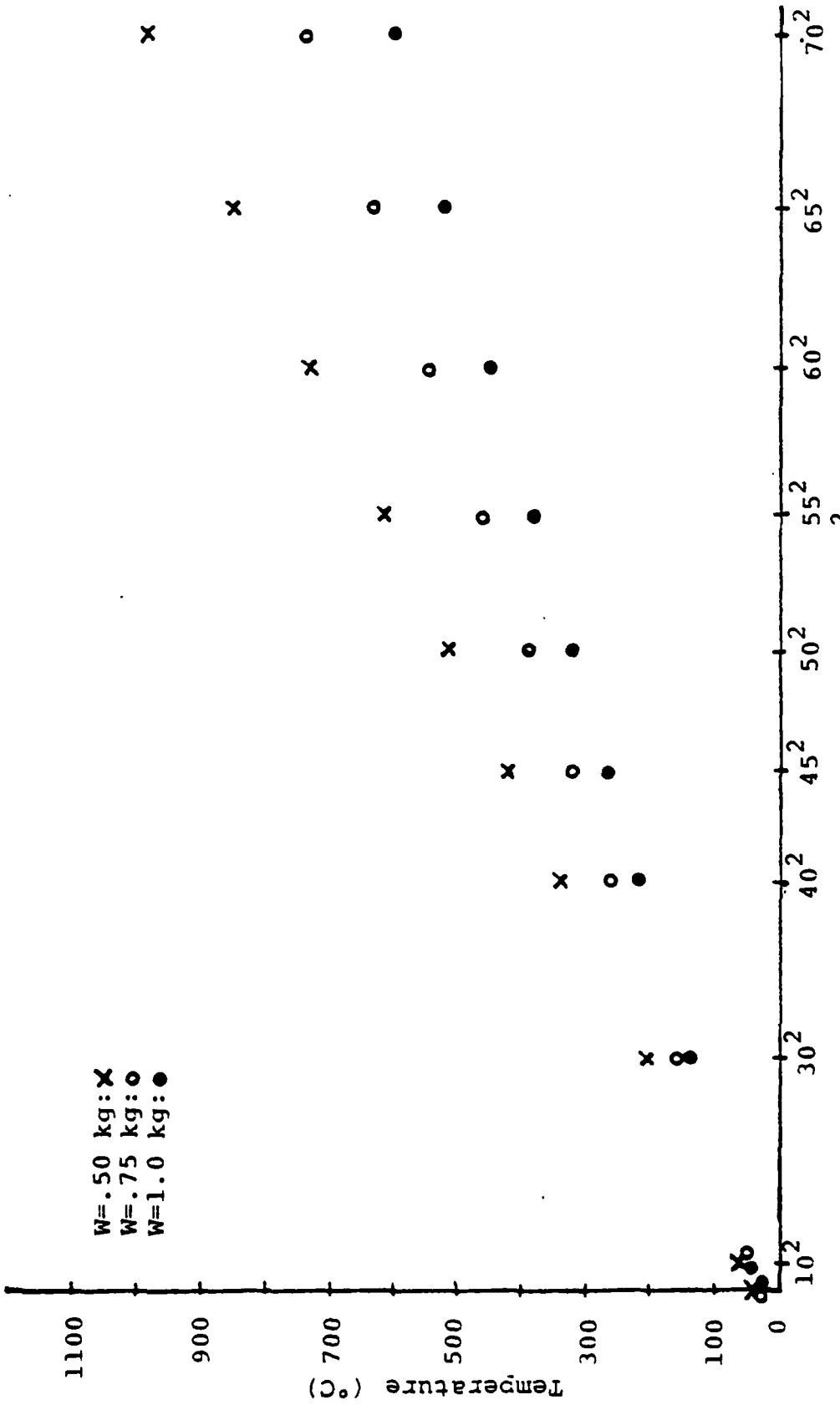

Figure 16(c). Average surface temperature vs. current squared at a sliding speed of 10. m/s, from equation (8-II) assuming 1 circular contact.

THREE CONTACTS

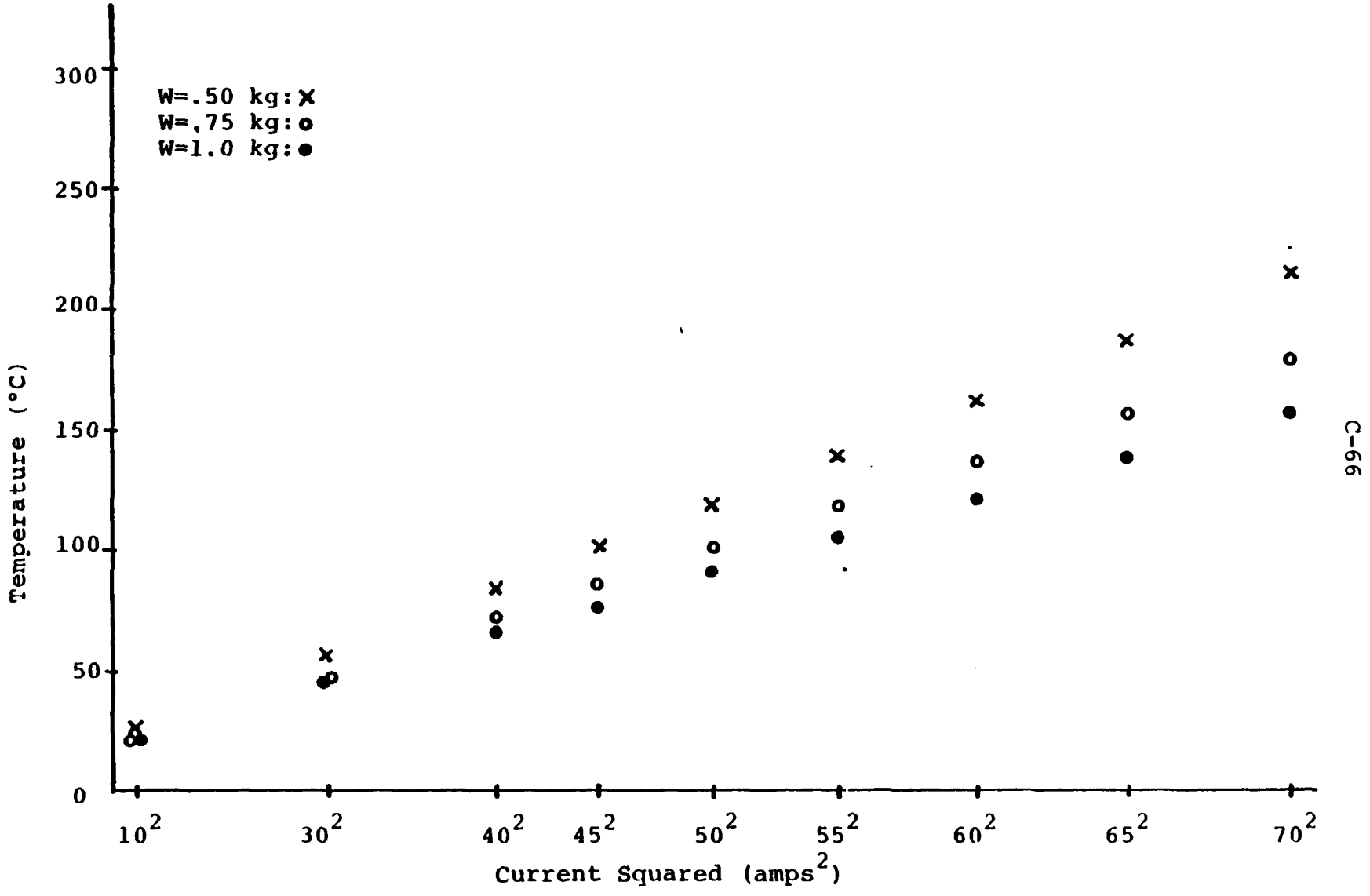

Figure 17(a). Average surface temperature vs. current squared at a sliding speed of 0. m/s, from equation (7-II) assuming 3 circular contacts.

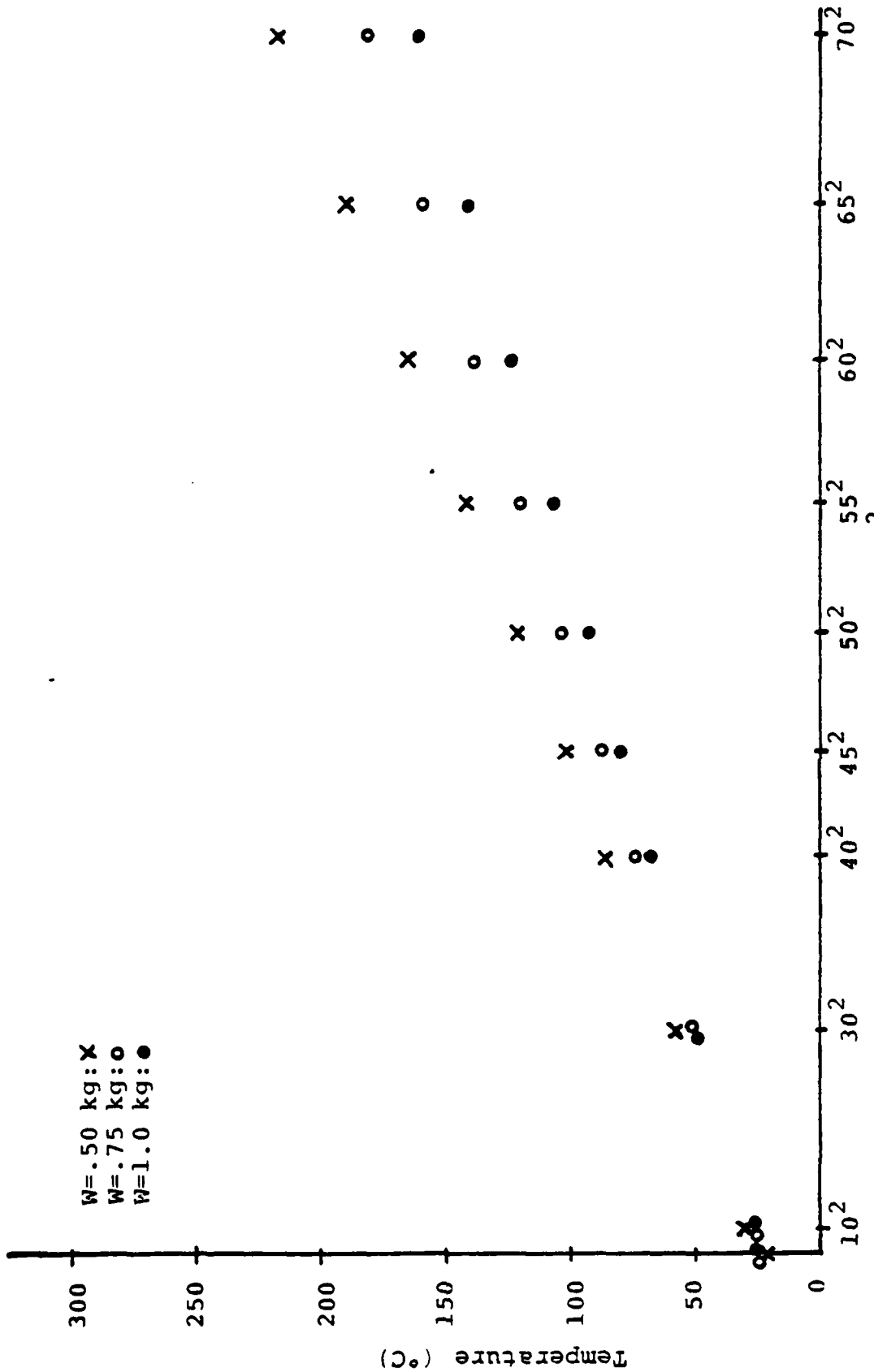

Figure 17(b). Average surface temperature vs. current squared at a sliding speed of 1. m/s, from equation (7-II) assuming 3 contacts.

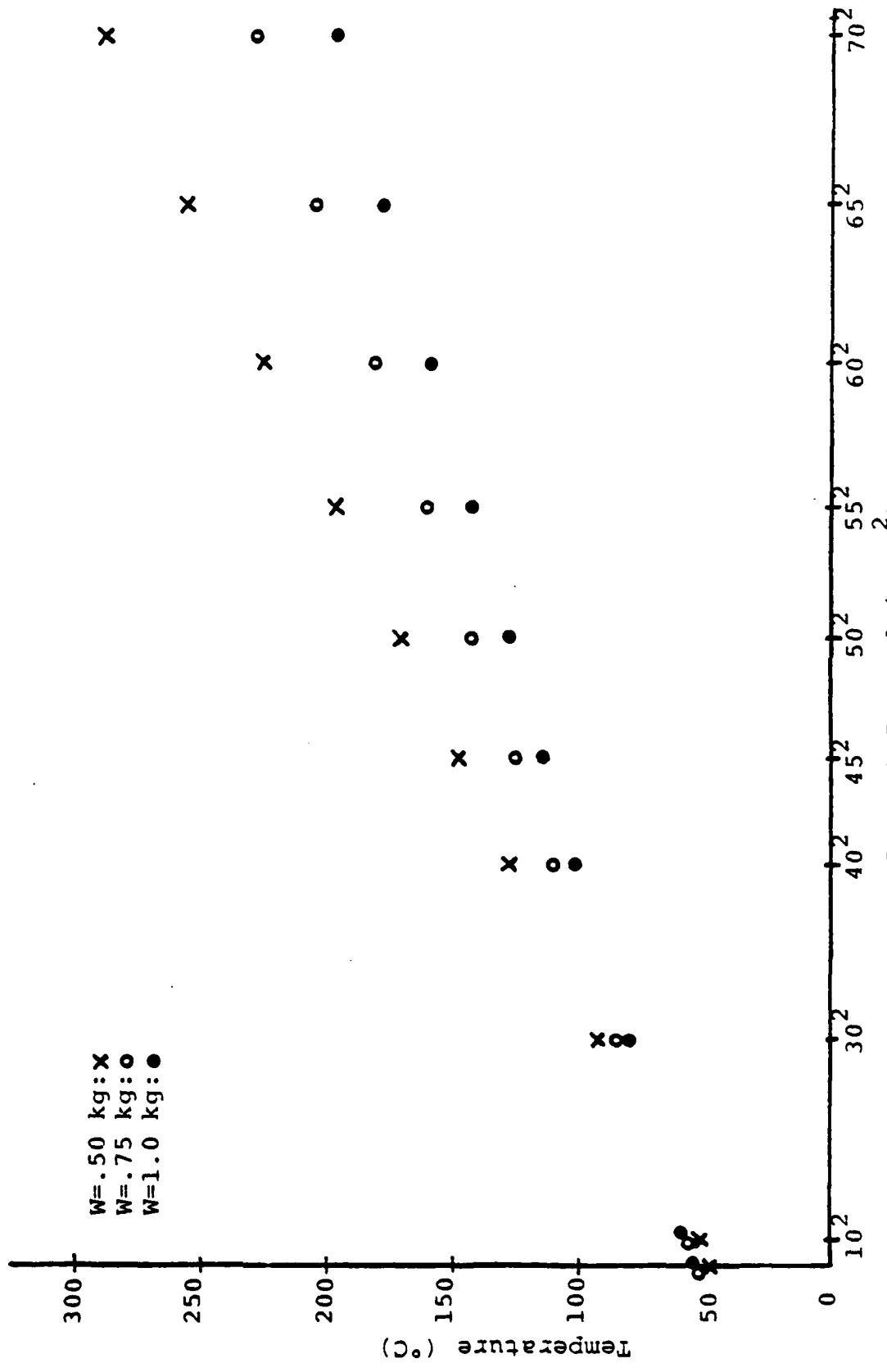

Figure 17(c). Average surface temperature vs. current squared at a sliding speed of 10. m/s, from equation (8-II) assuming 3 circular contacts.

FIVE CONTACTS

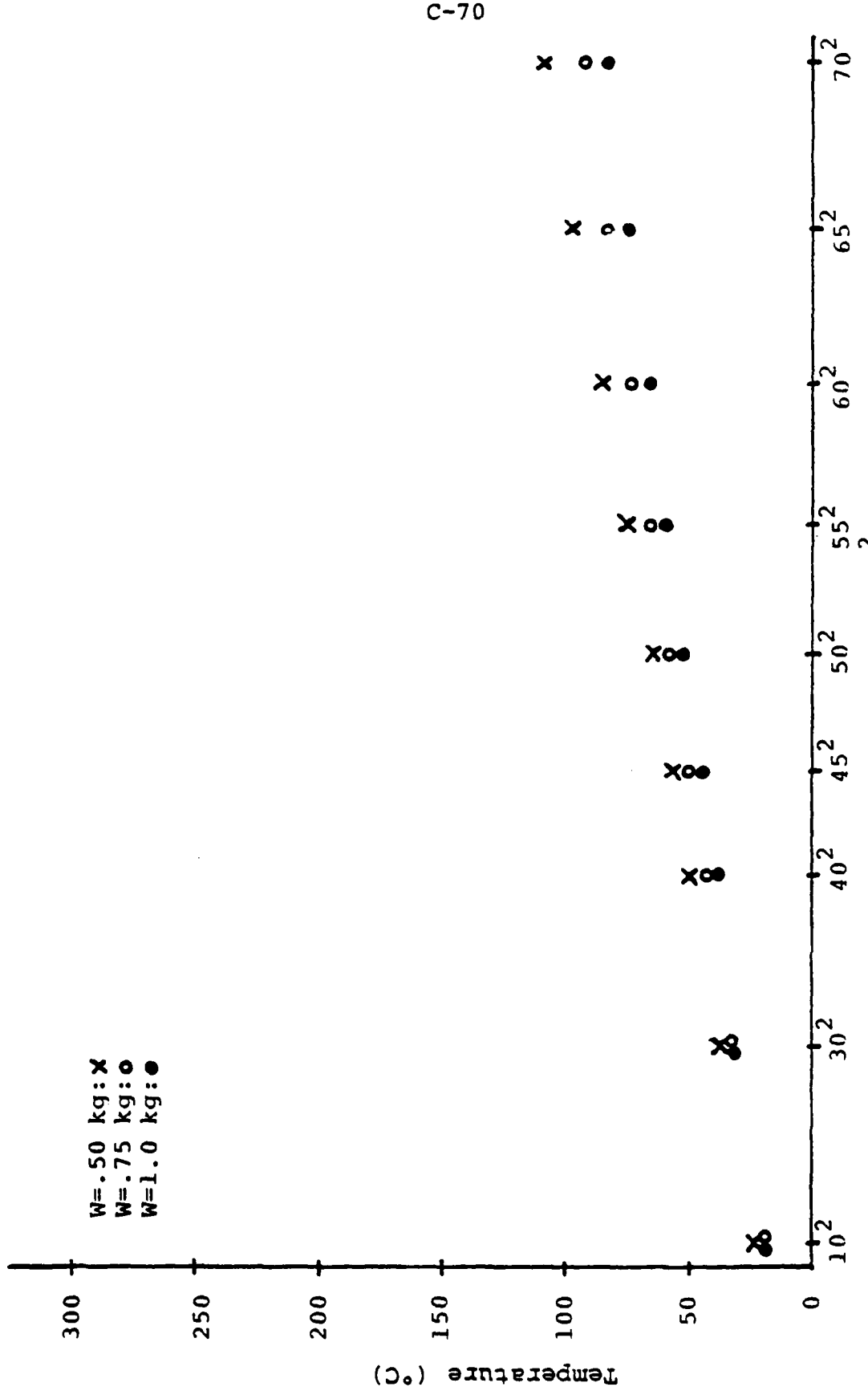

Figure 18(a). Average surface temperature vs. current squared at a sliding speed of 0. m/s, from equation (7-II) assuming 5 circular contacts.

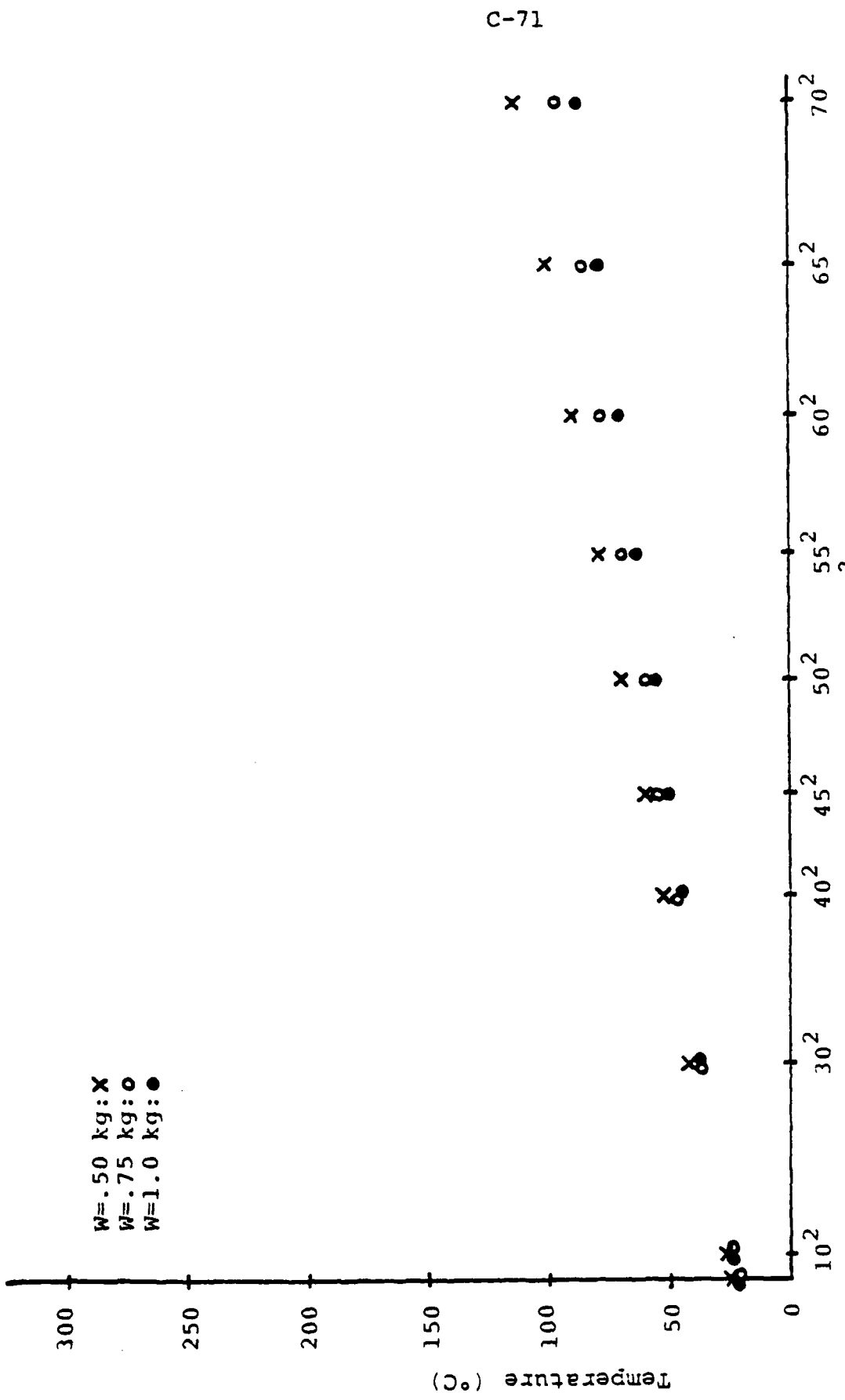

Figure 18(b). Average surface temperature vs. current squared at a sliding speed of 1. m/s, from equation (7-II) assuming 5 circular contacts.

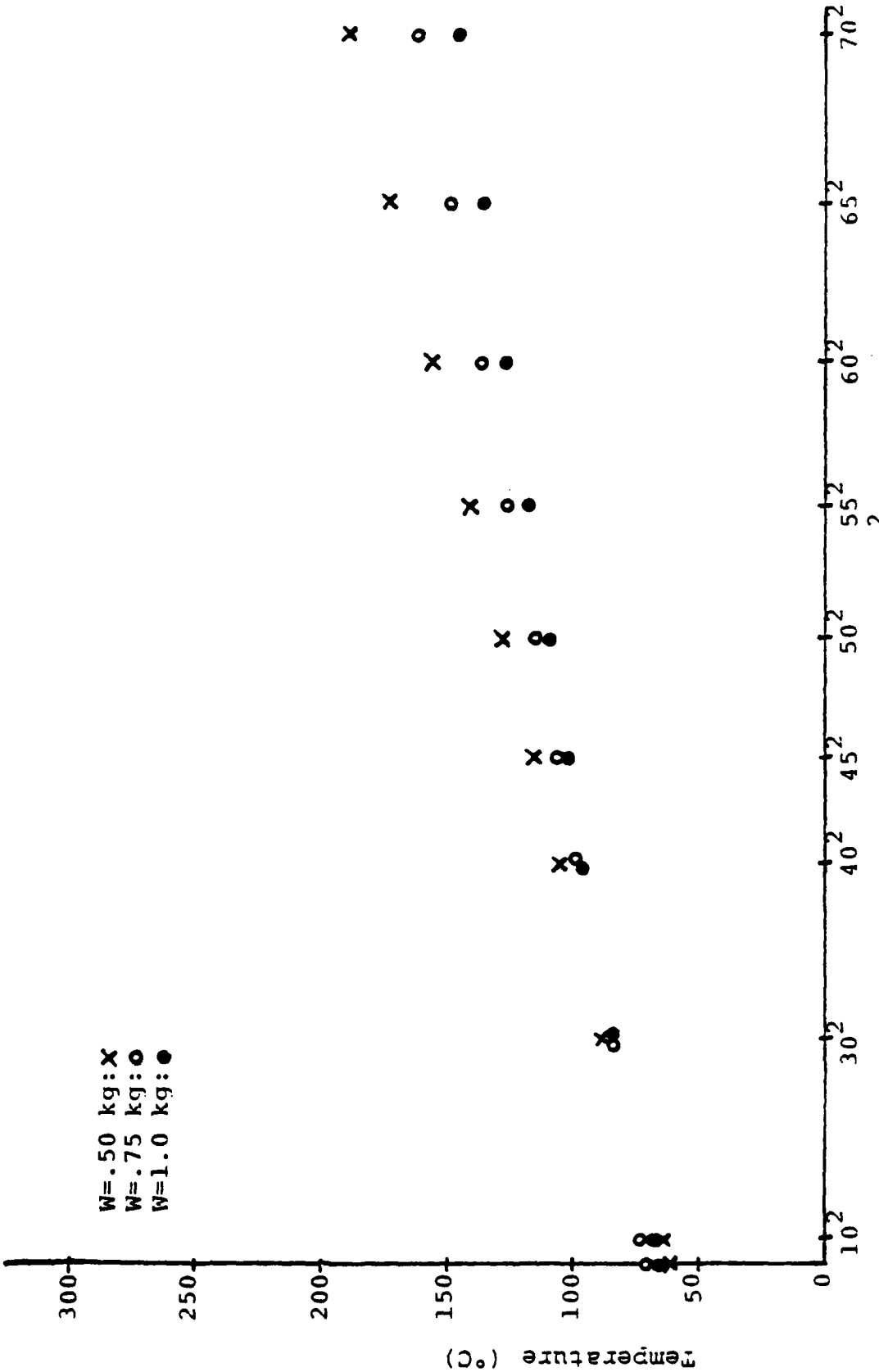

Figure 18(c). Average surface temperature vs. current squared at a sliding speed of 10. m/s, from equation (8-II) assuming 5 circular contacts.

TEN CONTACTS

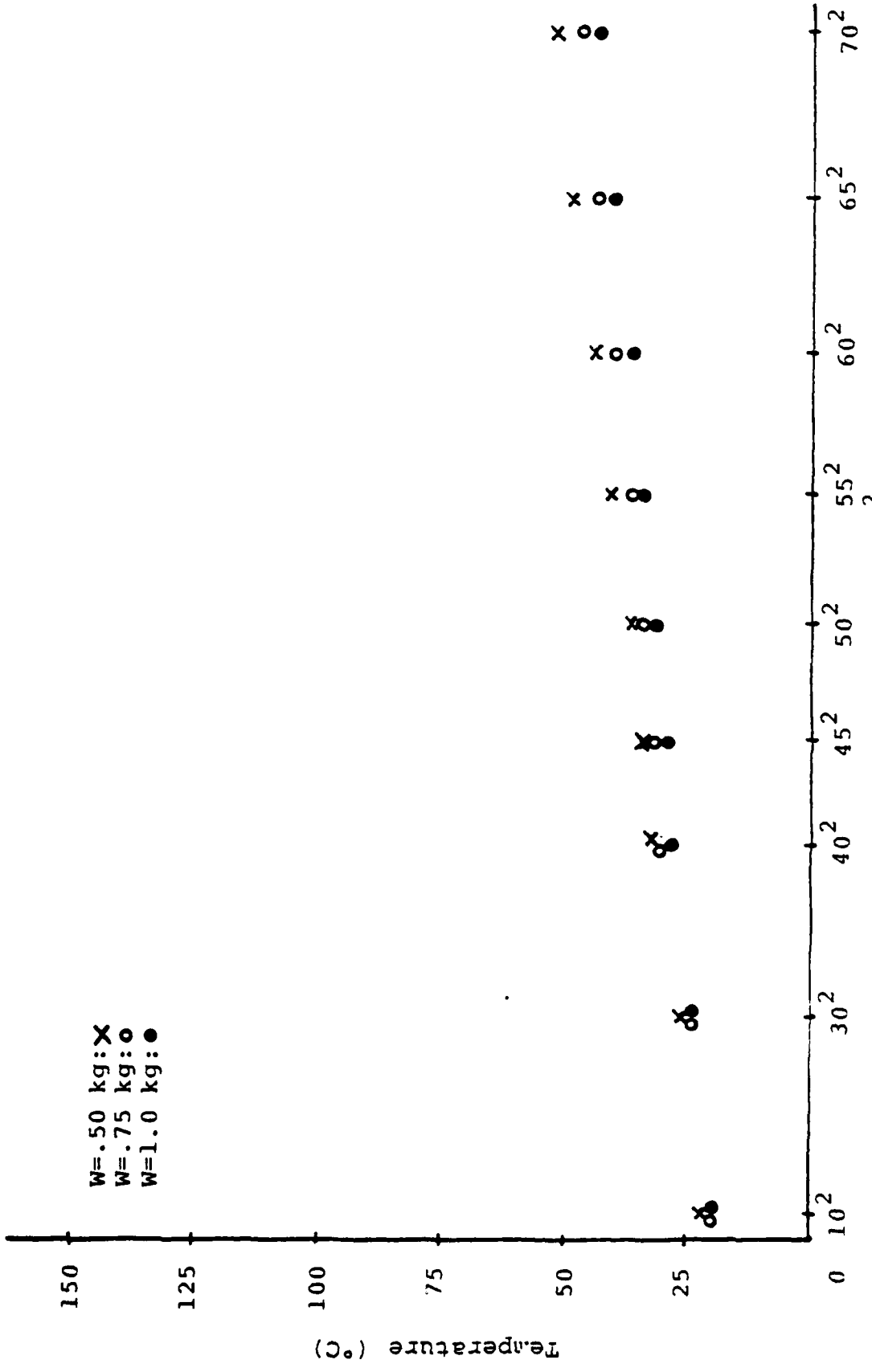

Figure 19(a). Average surface temperature vs. current squared at a sliding speed of 0. m/s, from equation 7-II) assuming 10 contacts.

AD-A121 456 MATERIAL OPTIMIZATION FOR HIGH-SPEED APPLICATIONS(U) MASSACHUSETTS INST OF TECH CAMBRIDGE DEPT OF MECHANICAL ENGIN..

UNCLASSIFIED E RABINOWICZ ET AL. 30 SEP 82 F/G 20/3 NL

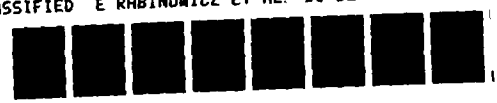

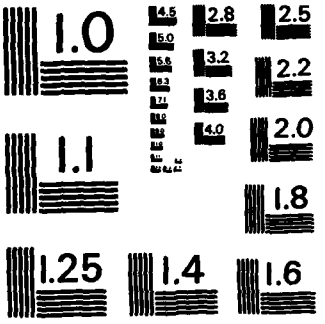

MICROCOPY RESOLUTION TEST CHART
NATIONAL BUREAU OF STANDARDS - 1963 - A

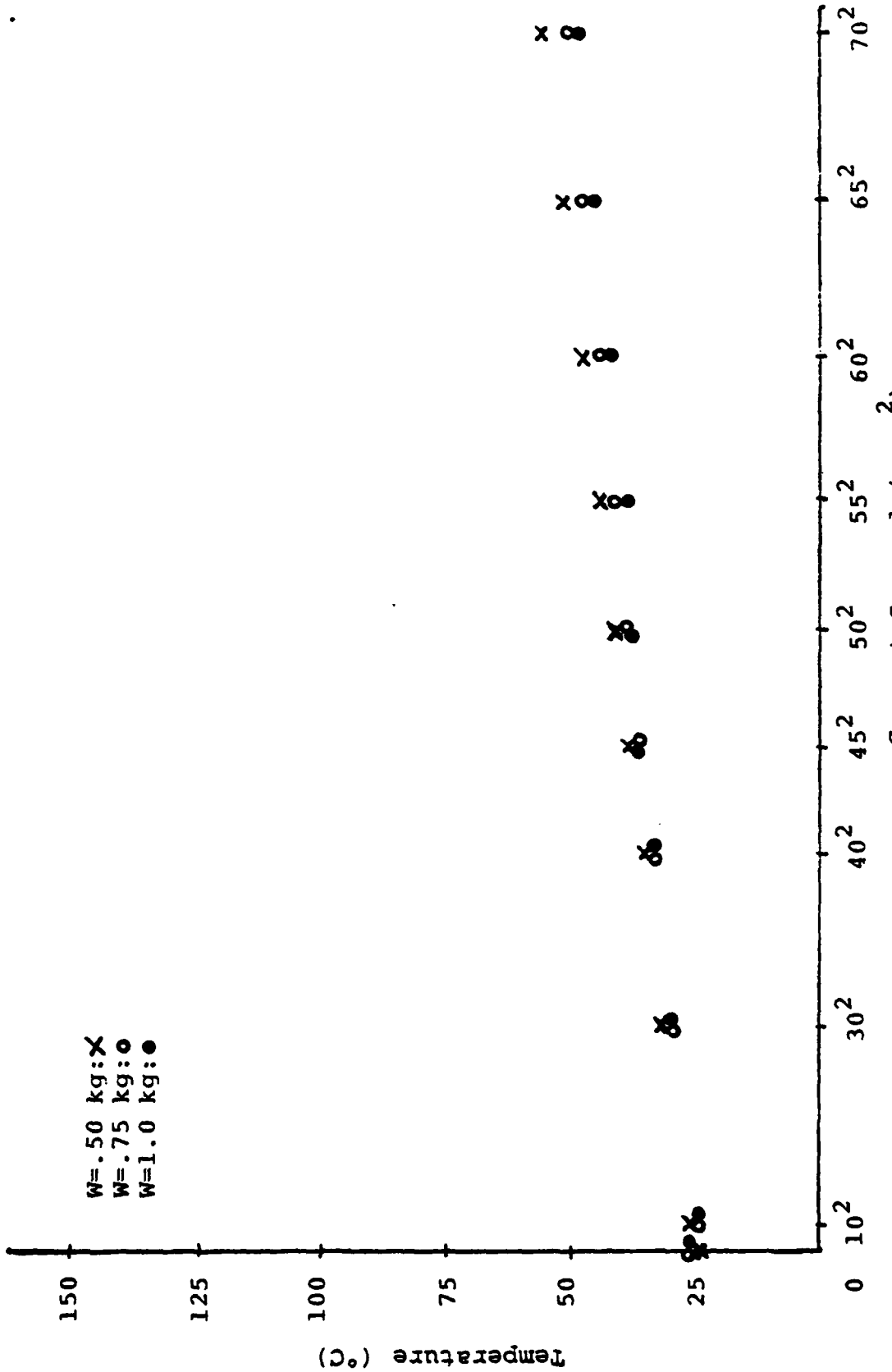

Figure 19(b). Average surface temperature vs. current squared at a sliding speed of 1. m/s, from equation (7-II) assuming 10 contacts.

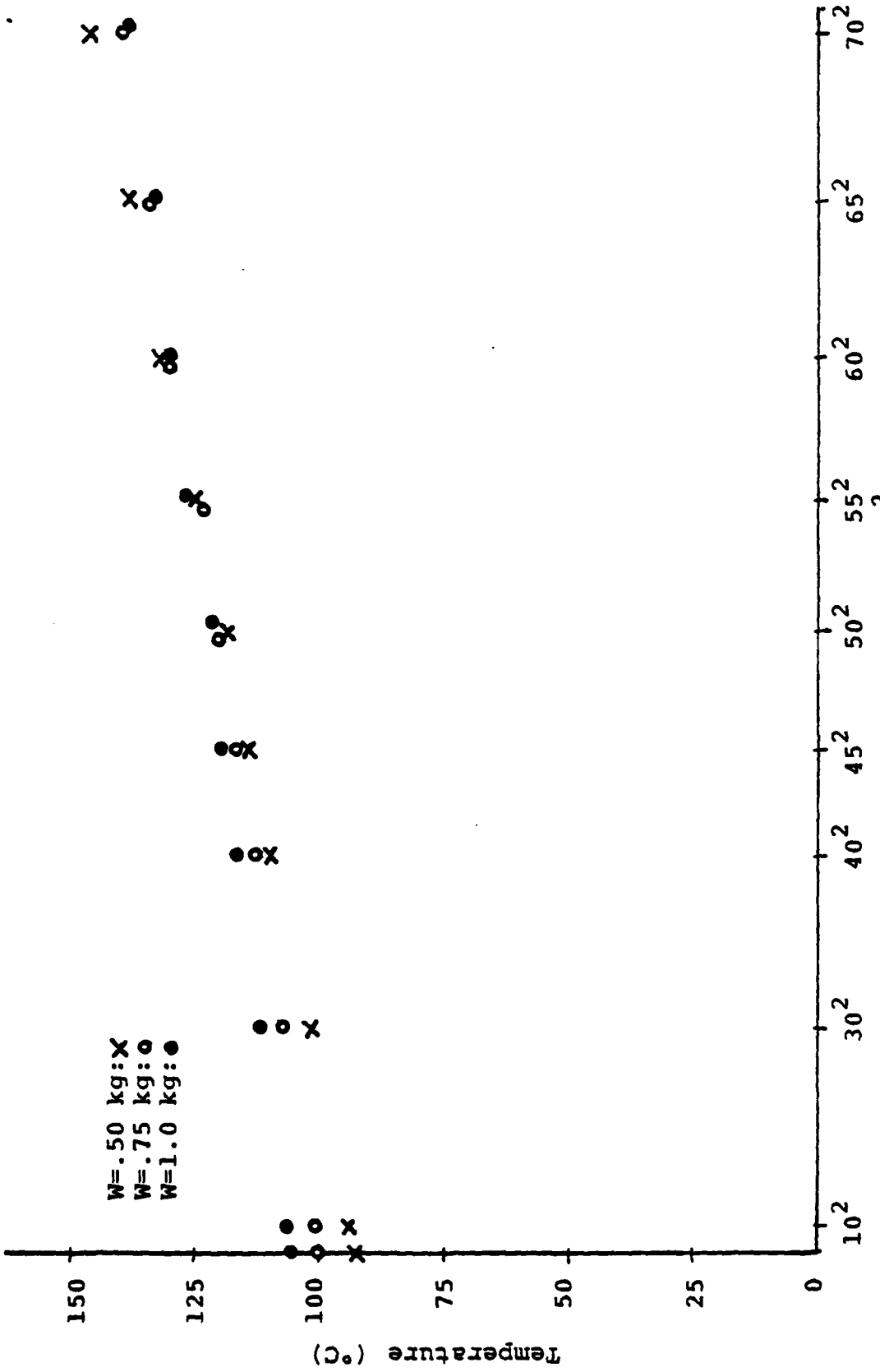

Figure 19(c). Average surface temperature vs. current squared at a sliding speed of 10. m/s, from equation (8-II) assuming 10 contacts.

APPENDIX C: Calculation of Time Constants

An attempt was made to determine the time constants of the temperature decay curves generated during this study. This was to compare the effects of the spinning disk to the stationary disk on the temperature decay curves' characteristics.

The time constant of interest for this comparison was not the overall time constant of the system; rather, it was the time constant for the decay of the interfacial contact temperature from its maximum to the disk temperature. For the purpose of calculating a single time constant to represent the temperature decay, the dynamics were assumed to be first order.

The tests were not originally intended to determine time constants. Therefore, the disk's bulk temperature was not measured. Yet, in order to properly calculate these time constants, the disk temperature would have needed to be measured. In order to attempt a time constant calculation, the following procedure was followed.

It was assumed that the disk temperature decayed much more slowly than the contact temperature while the contact temperature was higher than the disk temperature. For the purpose of this calculation the disk temperature was assumed to be at steady state. The computer generated temperature decay curves were used to find when the contact temperature became equal to the disk temperature. The first order time constant of this calculation is defined as the time at which

the temperature has decayed two thirds of the way from its maximum to the disk temperature.

Table IV shows the resulting calculations of the time constants for the tests run at 0 m/s, 1 m/s, and 10 m/s with a load of 0.75 kg. These time constants seem to be inconsistant because of their wide range and random nature. This is probably due to the inability to estimate when the contact temperature became equal to the disk temperature from the computer generated plots. Furthermore, the pseudo-steady state assumption for disk temperature may not have been correct. From the data collected it was not possible to calculate time constants accurately enough to make the attempted comparison.

Table IV. Time constant calculations (sec).

I	0. m/s .75 kg	1. m/s .75 kg	10.m/s .75 kg
0	-	1.10	1.85
10	.96	.88	1.07
30	.84	1.68	1.60
40	.79	3.57	1.81
45	5.94	1.83	1.49
50	2.73	-	1.28
55	3.59	3.78	1.25
60	1.74	6.11	1.09
65	6.74	4.94	1.24
70	-	2.60	-

REFERENCES

1) Burton, R.A., "Thermal Deformation in Frictionally Heated Contacts", Wear, 59 (1980) pp. 1-20.

2) McNab, I.R., "Recent Advances in Electrical Current Collection", Wear, 59 (1980) pp. 259-276.

3) Jaeger, J.C., "Moving Sources of Heat and the Temperature at Sliding Contacts", Proceedings of the Royal Society of New South Wales, v.56 (1942) pp. 203-224.

4) Holm, R., "Electric Contacts Handbook", H. Geber, Stockholm, Sweden (1946).

5) Schobert, E.I., "Carbon Brushes", Chapter 7, Chemical Publishing Co., New York (1965).

6) Rabinowicz, E., "The Temperature Rise at Sliding, Electrical Contacts", Unpublished work.

7) Blok, H., "Theoretical Study of Temperature Rise at Surfaces of Actual Contact Under Oiliness Lubricating Conditions", Inst. Mech. Eng., General Discussion of Lubrication, v.2 (1937) pp. 222-235.

8) Archard, J.F., "The Temperature of Rubbing Surfaces", Wear, 2 (1958/59) pp. 438-455.

9) Holm, R., "Calculation of the Temperature Development in a Contact Heated in the Contact Surface, and Application to the Problem of the Temperature Rise in a Sliding Contact", Journal of Applied Physics, v.19 (1948) pp. 361-366.

10) Holm, R., "Temperature Development in a Heated Contact with Application to Sliding Contacts", Journal of Applied Mechanics, Sept. 1952, pp. 369-374.

11) Uetz, H. and Sommer, K., "Investigations of the Effect of Surface Temperatures in Sliding Contact, Wear, 43 (1977) pp. 375-388.

12) Furey, M.J., "Surface Temperatures in Sliding Contact, ASLE Transactions, 7 (1964) pp. 133-146.

13) Dayson, C., "Surface Temperatures at Unlubricated Sliding Contacts", ASLE Transactions, 10 (1967) pp. 169-174.

14) Dow, T.A., Stockwell, R.D., Kannel, J.W., "Thermal and Thermomechanical Effects in Rolling/Sliding Contacts", Battelle Columbus Lab., Columbus, Ohio (1981) pp. 35-58.

15) Marshall, R.A., "The Mechanism of Current Transfer in High Current Sliding Contacts", Wear 37 (1976) pp. 233-240.

16) Dike, P.H., "Thermoelectric Thermometry", Chapter 1, Leeds and Northrup Co., Philadelphia, PA (1954).

17) Fenton, A.W., "The Travelling Gradient Approach to Thermocouple Research", Temperature, Its Measurement and Control in Science and Industry, v.4, part 3, ( ) pp. 1973-1990.

18) Rozenfeld, Z., "Tribological Properties of High Speed Slip Ring Systems", MS Thesis in Mechanical Engineering, MIT, June 1980.

19) Rabinowicz, E., "An Introduction to Experimentation", sect. 3-10, Addison-Wesley Publishing Co., Reading, MA (1970).